OCTOBER 1959 VOLUME 1 (1959) No. 3

JOURNAL OF NUCLEAR MATERIALS

JOURNAL DES MATERIAUX NUCLEAIRES

A JOURNAL ON METALLURGY, CERAMICS AND SOLID STATE PHYSICS IN THE NUCLEAR ENERGY INDUSTRY

CONTENTS

NORTH-HOLLAND PUBLISHING COMPANY – AMSTERDAM

Papers or letters should be sent to one of the Editors,

R. W. CAHN (Dept. of Metallurgy, University of Birmingham, Birmingham 15, England).
J. P. HOWE (Atomics International, P.O. Box 309, Canoga Park, California, U.S.A.).
P. LACOMBE (Centre de Recherches Métallurgiques de l'Ecole des Mines, Blvd. St. Michel 60, Paris VI, France)

either directly or through a member of the Editorial Advisory Board.

Papers or letters should be written in English, French or German, with a summary in the appropriate language. Translations of the summary into the two other languages will be added by the Editors.

Instructions to contributors will be found in Vol. 1, No. 1 (pp. 111–112).

Books for review should be sent to one of the Editors.

The Journal of Nuclear Materials will initially be published quarterly.

The subscription price of a volume of 360 pages is $ 18.00, 130 s., Gld. 68.50 per volume, post-free.

Subscriptions should be sent to the publishers, North-Holland Publishing Company. P.O. Box 103, Amsterdam or to any subscription-agent.

Les articles ou les lettres devront être envoyés à un des Rédacteurs-en-chef,

R. W. CAHN (Dept. of Metallurgy, University of Birmingham, Birmingham 15, England).
J. P. HOWE (Atomics International, P.O. Box 309, Canoga Park, California, U.S.A.).
P. LACOMBE (Centre de Recherches Métallurgiques de l'Ecole des Mines, 60 Bd. St. Michel, Paris VI, France)

ou directement ou par un membre du Conseil des Rédacteurs.

Les articles ou les lettres devront être rédigés en anglais, français ou allemand avec un résumé dans la langue correspondante. Les traductions du résumé dans les deux autres langues seront ajoutées par les éditeurs.

Les instructions aux auteurs se trouvent dans le Vol. 1, No. 2 (pp. 211–212).

Les Livres (exemplaires de presse) devront être envoyés à un des Rédacteurs-en-chef.

Le Journal des Matériaux Nucléaires paraîtra initialement tous les trois mois.

Prix de souscription par volume d'environ 360 pages: $ 18.00, 130 s., Gld. 68.50, franco.

Les abonnements devront être envoyés aux éditeurs, North-Holland Publishing Company, P.O. Box 103, Amsterdam, ou à votre librairie.

JOURNAL OF NUCLEAR MATERIALS - 3 (1959) 213–225 - NORTH-HOLLAND PUBLISHING CO., AMSTERDAM

OXYDATION A L'AIR DE DEUX ALLIAGES REFRACTAIRES (NICRAL D ET HASTELLOY X) A 900 ET 1100° C

J. SANNIER, R. DOMINGET et R. DARRAS

Centre d'Études Nucléaires de Saclay, Gif-sur-Yvette (S & O), France

Service de chimie des solides

Reçu le 10 Février 1959

Cette étude a porté sur l'oxydation dans l'air de deux alliages réfractaires, le Nicral D et l'Hastelloy X, à 900 et 1100° C, au moyen de thermobalances et d'examens micrographiques en coupe. Si, à 900° C, les vitesses d'oxydation superficielle sont sensiblement identiques pour les deux alliages, par contre à 1100° C le Nicral D s'oxyde plus rapidement que l'Hastelloy X. D'autre part, après 150 heures à 1100° C, le Nicral D présente également une oxydation intergranulaire et un peu d'oxydation interne, alors que l'Hastelloy X est surtout sensible à l'oxydation interne.

De plus, deux méthodes de désécaillage ont été comparées: une méthode électrolytique en bain de soude et carbonate de sodium qui s'est avérée satisfaisante pour les deux alliages, et une méthode chimique en bain de nitrate de sodium et peroxyde de sodium qui ne semble convenir que pour l'Hastelloy X.

The oxidation in air of two refractory alloys (Nicral D and Hastelloy X) has been studied at 900 and 1100° C, by means of recording thermobalances and microscopic cross section examination. At 900 °C, the surface oxidation rates of the two alloys are quite similar, but at 1100° C the alloy Nicral D oxidizes faster than the alloy Hastelloy X. On the other hand, after heating at 1100° C for 150 hours, Nicral D shows both intergranular oxidation and a small amount of internal oxidation, whereas Hastelloy X is especially subject to internal oxidation.

In addition, two descaling methods were compared: an electrolytic method, in a sodium hydroxide-sodium carbonate bath, and a chemical method using a sodium nitrate-sodium peroxide bath; the latter appears suitable only for Hastelloy X.

Die Luftoxydation zweier hitzebeständiger Legierunge (Nicral D und Hastelloy X) bei 900 und 1100° C wurde durch Thermowagen und mikroskopisch untersucht. Die Geschwindigkeit der Oberflächenoxydation bei 900° C ist bei beiden Legierungen ungefähr gleich; bei 1100° C Nicral D oxydiert schneller als Hastelloy X. Andrerseits, nach 150-stündigem Erhitzen auf 1100° C, zeigt Nicral D neben intergranularer auch ein wenig innerer Oxydation, während Hastelloy X sich als besonders empfindlich gegenüber innerer Oxydation zeigt.

Es wurden ferner zwei Methoden zur Entfernung der Zunderschicht verglichen: eine elektrolytische, in einem Natriumhydroxyd-Natriumcarbonat Bad, und eine chemische Methode mit einem Natriumnitrat-Natriumperoxyd Bad. Die chemische Methode scheint nur für Hastelloy X geeignet zu sein.

1. Introduction

Les publications traitant de l'oxydation des métaux et plus particulièrement des aciers et alliages inoxydables ou réfractaires à température élevée apparaissent très nombreuses, surtout depuis quelques années; en effet, indépendamment de l'intérêt du sujet au point de vue fondamental, les exigences accrues de la technique moderne en matériaux utilisables à des températures sans cesse croissantes expliquent largement l'étendue des recherches entreprises.

Pour ne parler que des alliages réfractaires, cette abondance se retrouve d'ailleurs dans la variété des nuances proposées au choix des utilisateurs par les divers fabricants; en effet, s'il s'agit toujours de compositions chimiques correspondant à quelques grandes catégories bien connues (25 Cr – 20 Ni; 20 Cr – 40 à 60 Ni; 20 Cr – 80 Ni notamment, le complément

étant évidemment du fer), il n'en reste pas moins que certaines additions secondaires ou impuretés (Al, Ti, Si, C), le mode d'élaboration, l'état métallurgique de chaque matérial particulier, peuvent avoir une influence parfois considérable sur la résistance à l'oxydation. Aussi, et peut-être plus encore que dans d'autres domaines de la corrosion, est-il donc nécessaire de réaliser une première sélection parmi les nuances envisageables pour une application déterminée, quitte à s'assurer ensuite du bon comportement, dans des conditions plus proches de l'utilisation, de celles ayant résisté à ces essais préliminaires, étant entendu que le facteur *temps* ne peut souvent pas être respecté, de toute façon.

Or on sait que, notamment dans le cas des aciers réfractaires, la méthode classique de la mesure des augmentations de poids en fonction du temps par pesées discontinues risque de donner des résultats fort erronés, car elle se heurte au phénomène "d'écaillage" de la couche d'oxyde formée; en outre il va de soi que cette cause d'erreur intervient d'autant plus que l'essai dure plus longtemps et surtout que les cycles de chauffage et refroidissement sont plus nombreux.

Dans le présent travail, nous nous sommes efforcés, en premier lieu, à propos de l'étude du cas de deux aciers particuliers, d'estimer la validité de l'essai en thermobalance gravimétrique pour effectuer une sélection préliminaire, ce qui fait appel à une méthode essentiellement reproductible. Mais vu l'impossibilité de disposer d'un grand nombre de thermobalances, cela conduirait à des essais peu nombreux. C'est pourquoi nous avons également cherché à déterminer dans quelle mesure est valable la méthode par pesées manuelles et détermination des pertes de poids, compte tenu d'un procédé de "désécaillage" satisfaisant, chacun des échantillons ne subissant dans cette hypothèse qu'un seul chauffage, un seul refroidissement et une seule pesée. Deux procédés de désécaillage ont précisément été comparés par leur application à des échantillons oxydés en thermobalance.

Concurremment il a été largement fait appel aux examens micrographiques.

Il convient enfin d'insister sur le but exact de ce travail, limité à la sélection comparative d'alliages réfractaires résistant à l'oxydation; la nécessité de la compléter ensuite par des essais plus proches des conditions réelles d'emploi n'est pas niée, mais sort du cadre que nous nous étions fixés.

2. Composition des Alliages Etudiés

L'étude a porté sur:

Un acier du type 25 Cr – 20 Ni: "Nicral D"†

Un alliage du type 20 Cr – 50 Ni: "Hastelloy X" ††, dont les compositions sont détaillées ci-dessous (voir tableau 1).

3. Préparation des Echantillons

Les échantillons sont découpés dans de la tôle de 1 mm d'épaisseur. Pour la commodité de l'étude en thermobalance et de l'observation micrographique en coupe, les dimensions suivantes ont été adoptées: longueur 30 mm, largeur 15 mm.

Ils sont polis mécaniquement sous eau, successivement aux papiers 240, 320 et 400. On procède ensuite au polissage électrolytique:

3.1. Nicral D

Le bain suivant est utilisé:

450 cm³ d'acide acétique glacial
40 cm³ d'acide perchlorique ($d = 1.60$)
15 cm³ d'eau.

† Dénomination Imphy.
†† Dénomination Union Carbide (USA).

Tableau 1

Alliage	C	Mn	Si	Ni	Cr	Fe	Mo	Ti
Nicral D (ND)	0.05	0.63	1.56	17	21.73	59		
Hastelloy X (HX)	0.04	0.76	0.71	48.09	21	17.3	8.20	0.23

Le polissage est effectué dans un bécher de 1000 cm³ refroidi extérieurement. La cathode, circulaire, est en acier inoxydable; l'anode, constituée par l'échantillon, tourne au centre du bain. La tension en circuit ouvert est de 40 volts. En circuit fermé, elle tombe à 25 volts pour une intensité d'environ 4 ampères. Le polissage dure 4 minutes.

Dans ces conditions, on obtient une surface brillante, les joints de grains étant très peu marqués (planche 1).

3.2. Hastelloy X

Le bain acéto-perchlorique semble moins satisfaisant, les échantillons polis laissant apparaître des traînées blanchâtres, faisant supposer un polissage irrégulier des constituants de l'alliage. L'essai du bain composé de:

850 cm³ de PO_4H_3 à 75 %
150 cm³ de SO_4H_2 à 66° B,

employé à 60° C avec anode fixe et agitation par air comprimé, n'a pas donné de meilleurs résultats.

L'examen micrographique de l'Hastelloy X dans l'état de livraison après polissage au Disa-Electropol (planche 1) permet d'expliquer ce polissage irrégulier: la structure de l'Hastelloy X n'est pas homogène et présente de nombreuses précipitations alignées dans une direction préférentielle, vraisemblablement dans le sens de laminage de la tôle. Par contre, le Nicral D présente une structure beaucoup plus homogène.

Finalement, pour le polissage de l'Hastelloy X, le bain acéto-perchlorique, utilisé dans les conditions suivantes, a été retenu:

La cathode est constituée par deux plaques d'acier inoxydable parallèles, distantes de 3 cm, l'échantillon formant anode étant placé au milieu, parallèlement aux plaques:

Tension en circuit ouvert: 20 volts;
Tension en circuit fermé: 16 volts;
Intensité: 1.25 ampère;
Densité de courant: 0.12 A/cm²;
Durée de polissage: 3 minutes.

4. Etude de l'Oxydation en Thermobalance

L'étude de l'oxydation du Nicral D et de l'Hastelloy X a été effectuée à 900 et 1100° C en thermobalance Adamel à enregistrement continu (fig. 1). Les variations de poids ΔP obtenues, converties en mg d'oxygène fixé par

PLANCHE 1

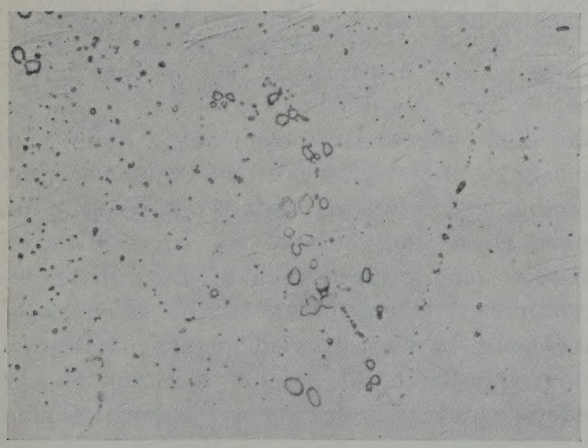

Hastelloy X. Etat initial. Polissage Disa-Electropol: 3 secondes, sans attaque. × 450.

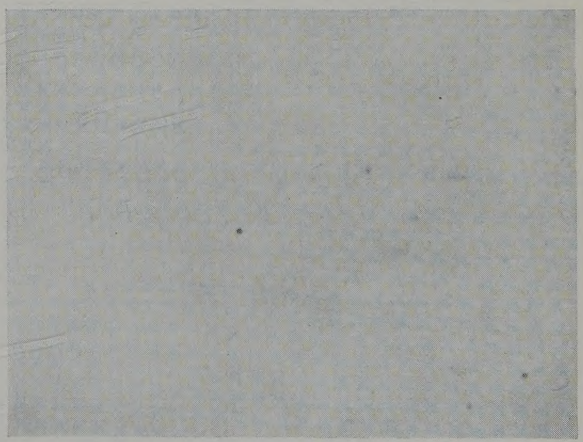

Nicral D. Etat initial. Polissage Disa-Electropol: 7 secondes, sans attaque. × 450.

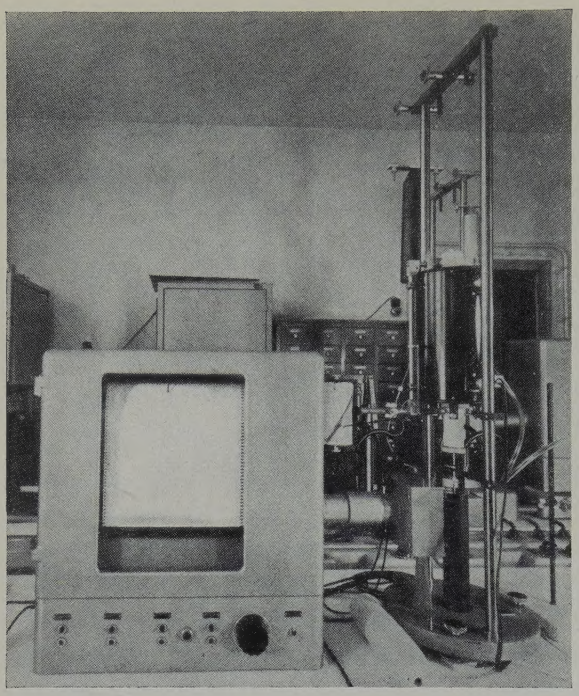

Fig. 1. Thermobalance ADAMEL à enregistrement continu.

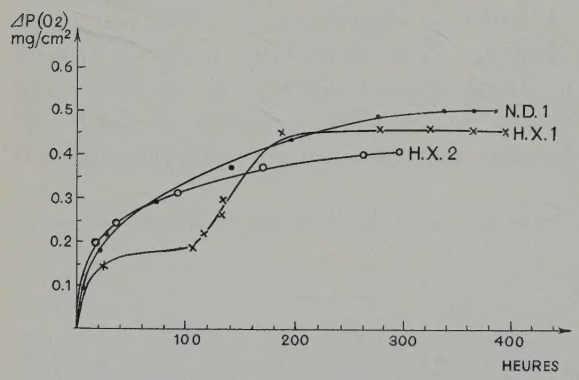

Fig. 2. Courbes de thermobalance à 900° C.

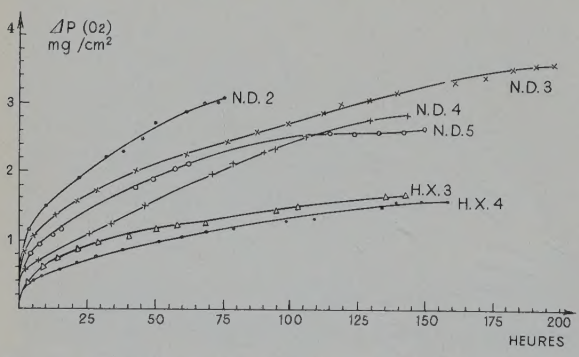

Fig. 3. Courbes entregistrées à le thermobalance à 1100° C. (Les points figurés sur les courbes représentent des pointés pour repérer l'échelle des temps.)

cm² de métal sont représentées par les figures 2 et 3.

L'observation des courbes conduit aux remarques suivantes:

4.1. Oxydation a 900° C

1. Pour le Nicral D comme pour l'Hastelloy X, la vitesse d'oxydation diminue avec le temps. On obtient même un palier horizontal au bout d'environ 300 heures avec les échantillons ND 1 et HX 1, ce qui laisse supposer la formation d'une couche d'oxyde protectrice. Il n'est évidemment pas exclu qu'au bout de temps plus longs, l'oxydation reprenne, par suite d'une détérioration de la couche d'oxyde.

2. Les augmentations de poids pour le Nicral D et l'Hastelloy X sont sensiblement équivalentes. On peut calculer l'épaisseur approchée de la couche d'oxyde correspondante † et 'épaisseur de métal transformé en oxyde (voir tableau 2).

3. On remarque encore sur la figure 2 que la courbe d'oxydation de l'échantillon HX 1 présente un premier palier horizontal entre 60 heures et 110 heures, alors que celle de l'autre échantillon HX 2 est beaucoup plus régulière. Comme les augmentations de poids pour les 2 échantillons redeviennent sensiblement identiques au bout de temps plus longs, on pourrait supposer qu'il s'agit, dans le cas d'HX 1, d'un retard à l'oxydation dû, soit à la formation d'une première couche empêchant la diffusion, cette couche disparaissant ensuite par interaction entre ses différents constituants, soit à un film superficiel préexistant, formé au polissage électrolytique et assurant une protection éphémère. Il s'agit d'ailleurs là d'un phénomène déjà observé au cours d'autres études, dans le cas de métaux assez divers et notamment le magnésium [6]). Des essais complémentaires seraient évidemment nécessaires pour approfondir son origine, mais comme son effet s'annule pour des durées d'exposition plus

† Dans ce calcul, on a supposé que la composition de l'oxyde est identique à celle de l'alliage. Cette hypothèse est discutée au paragraphe 6.

Tableau 2

Alliage	Augmentation de poids après 400 h	Epaisseur correspondante de la couche d'oxyde (calculée)	Epaisseur de métal oxydé (calculée)
Nicral D	0.5 mg/cm²	3.0 μ	1.7 μ
Hastelloy X	0.45 mg/cm²	2.8 μ	1.6 μ

longues, il présente peu d'intérêt dans cette étude.

4.2. Oxydation a 1100° C

La figure 3 représente les courbes d'oxydation à 1100° C de 4 échantillons en Nicral D et de 2 échantillons en Hastelloy X. L'échantillon ND 2 n'a pas subi de polissage électrolytique.

On peut faire les remarques suivantes:

1. L'oxydation de l'Hastelloy X est inférieure à celle du Nicral D.

2. Pour les deux alliages, il y a diminution de la vitesse d'oxydation avec le temps.

En se référant aux courbes d'oxydation de ND 3 et HX 3, on arrive à une loi d'oxydation du type logarithmique:

$$\Delta P = k \log (at+1).$$

Dans le cas de l'échantillon ND 3, il y a un bon accord entre la courbe expérimentale et la formule:

$$\Delta P_{mg} = 26 \log (0.12\ t_{heures}+1),$$

pour des temps compris entre 25 et 200 heures.

En ce qui concerne l'échantillon HX 3, la courbe d'oxydation peut être représentée par l'équation:

$$\Delta P_{mg} = 10 \log (0.3 t_{heures}+1),$$

pour des temps compris entre 5 et 150 heures.

3. L'échantillon ND 2, non poli électrolytiquement, présente une oxydation nettement plus importante que les autres éprouvettes de Nicral D.

Les augmentations de poids des échantillons polis électrolytiquement sont les suivantes, après 145 heures de chauffage:

	ΔP mg/cm²		ΔP mg/cm²
HX 3	1.7	ND 3	3.2
HX 4	1.6	ND 4	2.6
		ND 5	2.9

La dispersion des résultats est de 3 % pour l'Hastelloy X et de 10 % pour le Nicral D. En prenant les valeurs moyennes, on obtient les chiffres suivants: (voir tableau 3)

4. On observe sur les courbes de thermobalance relatives au Nicral D une brusque augmentation de poids après environ une demi-heure d'oxydation. Ceci semble mettre en évidence l'effet protecteur du polissage électrolytique au début de l'oxydation. Cette hypothèse est confirmée par le fait que l'échantillon non poli électrolytiquement n'a pas présenté cette particularité.

Par contre, ce phénomène n'a pas été observé avec l'Hastelloy X.

5. Il convient de noter qu'à la fin des essais, le refroidissement brusque occasionné par le

Tableau 3

Alliage	Augmentation de poids après 145 h	Epaisseur de la couche d'oxyde (calculée)	Epaisseur de métal oxydé (calculée)
Nicral D	2.9 mg/cm²	17 μ	10 μ
Hastelloy X	1.65 mg/cm²	10 μ	6 μ

relèvement du four provoque une sérieuse diminution de poids des échantillons de Nicral D par suite de l'écaillage (de l'ordre de 8 mg à 900° C pour un poids d'oxyde formé de 75 mg). Par contre, l'Hastelloy X ne présente pas ce phénomène, les diminutions de poids étant négligeables.

Le Nicral D semble donc beaucoup plus sensible à l'écaillage par choc thermique.

5. Etude Micrographique

L'étude a été effectuée en oxydant, dans un four horizontal, des échantillons suspendus à l'aide d'un fil de platine dans un berceau en acier réfractaire (fig. 4).

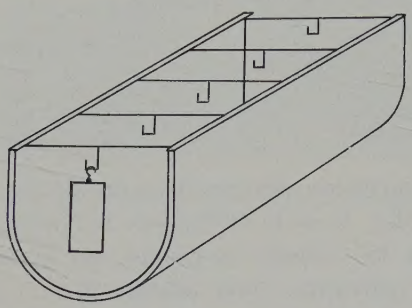

Fig. 4. Support des échantillons.

Les échantillons oxydés sont examinés en coupe. Pour pouvoir observer correctement la couche d'oxyde et l'interface métal-oxyde, il est nécessaire d'enrober la plaquette de métal dans une substance dure.

Nous avons utilisé la méthode préconisée par M. Moreau †, et qui évite tout chauffage notable. L'enrobage est effectué à l'aide d'une résine polyester 7302 ††. On mélange 50 g de résine et 1 cm³ de catalyseur C 20 †† en agitant pendant 20 minutes. On ajoute ensuite 50 g d'alumine – 12 heures — en poudre. Après agitation, on verse le mélange dans un moule en verre dans lequel se trouve l'échantillon et on porte 24 heures à l'étuve à 40–45° C. L'échantillon enrobé est tronçonné sous eau à l'aide d'un disque diamanté. On le polit également sous eau aux papiers 320, 400 et 600, puis on termine par un polissage à la pâte diamantée.

L'examen micrographique conduit alors aux remarques suivantes:

5.1. Oxydation a 900° C pendant 300 heures (planches 2 et 3)

En ce qui concerne le Nicral D, la pellicule d'oxyde apparaît très irrégulièrement répartie. A certains endroits, le métal est absolument à nu. Ceci est dû à l'écaillage par choc thermique, bien que le refroidissement dans le four ait été relativement lent.

Par contre, l'Hastelloy X présente une couche d'oxyde assez régulièrement répartie, mais morcelée. L'épaisseur de cette couche est nettement plus faible pour l'Hastelloy X que pour le Nicral D.

Dans les deux cas, on ne décèle aucune pénétration intergranulaire.

5.2. Oxydation a 1100° C pendant 150 heures

1. Le Nicral D (planche 4) présente à la fois un phénomène d'oxydation intergranulaire prononcé et un phénomène d'oxydation interne; ce dernier est absent dans la masse, ce qui rend effectivement improbable l'apparition d'une autre phase. L'oxydation interne a d'ailleurs déjà été observée dans des alliages tels que Cu-Si, Fe-Al ou Ni-Cr, par suite d'une dissolution de l'oxygène dans l'alliage [1]).

L'interface métal/oxyde est irrégulier. En outre, le polissage semble mettre en évidence deux phases distinctes superposées dans la couche d'oxyde, la phase sous-jacente ayant des prolongements intergranulaires. L'existence de traces d'une troisième phase serait même possible, en surface, sous forme d'ilôts plus clairs.

La zone intéressée par la pénétration intergranulaire est importante. Son épaisseur mesurée sur les micrographies est d'environ 60 μ; elle est donc bien supérieure à l'épaisseur de la couche d'oxyde, soit 17 μ, d'après l'étude en thermobalance pendant un temps identique, ce qui correspond à une pénétration dans le

† IRSID, St Germain en Laye, S. & O.

†† Fournisseur: Usines de Melle (Deux-Sèvres).

PLANCHE 2

Nicral D. Oxydation à 900° C. 300 heures. × 450.

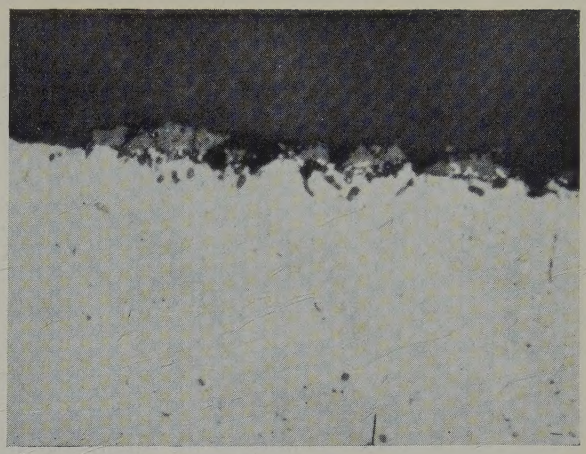

Nicral D. Oxydation à 900° C. 300 heures. × 450.

PLANCHE 3

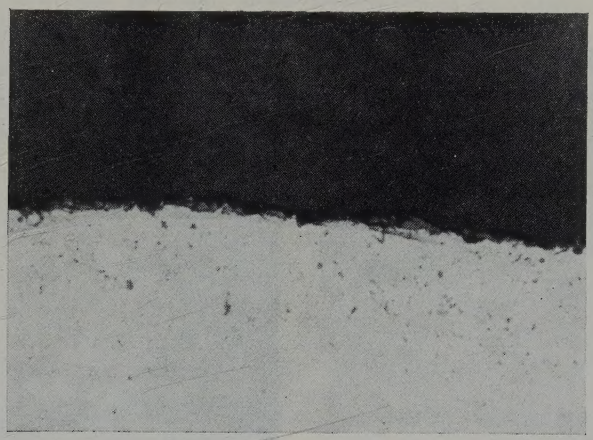

Hastelloy X. Oxydation à 900° C. 300 heures. × 450.

PLANCHE 4

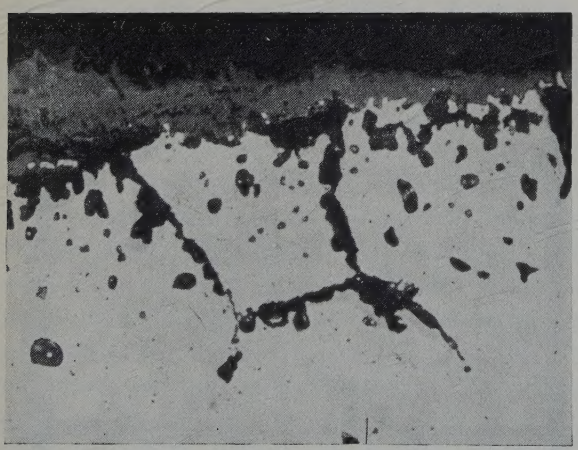

Nicral D. Oxydation à 1100° C. 150 heures. × 450.

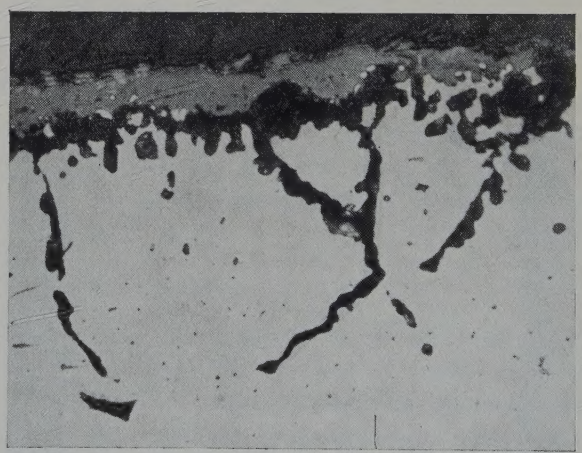

Nicral D. Oxydation à 1100° C. 150 heures. × 450.

PLANCHE 5

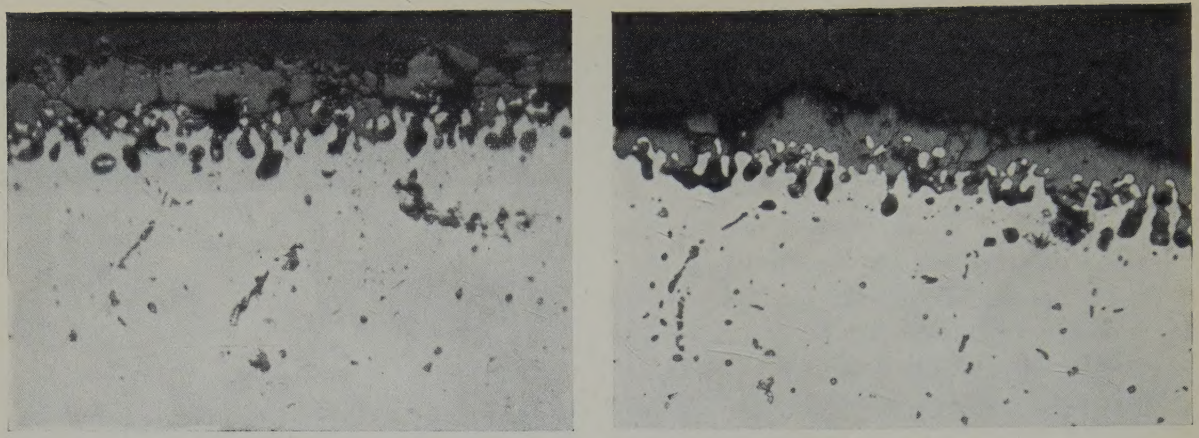

(a) (b)

Hastelloy X. Oxydation à 1100° C. 150 heures. × 450.

(a) Echantillon HX3 de la figure 3. (b) Echantillon HX4 de la figure 3.

PLANCHE 6

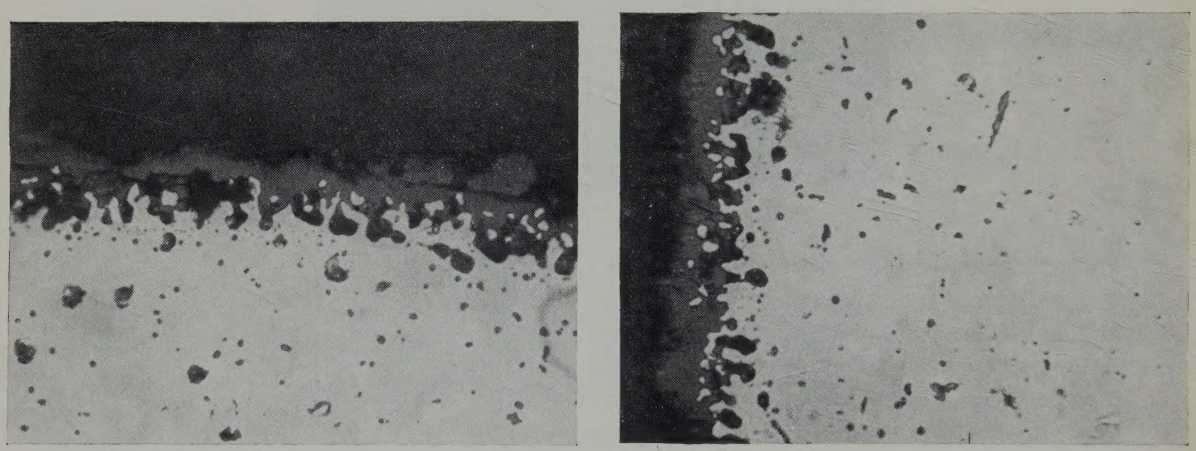

(a) (b)

Hastelloy X. Oxydation à 1100° C. 150 heures. × 450.

(a) Sous-couche d'oxyde au voisinage de l'interface.

(b) Coupe du même alliage à plus grande profondeur, montrant l'absence de phase intermétallique précipitée.

PLANCHE 7

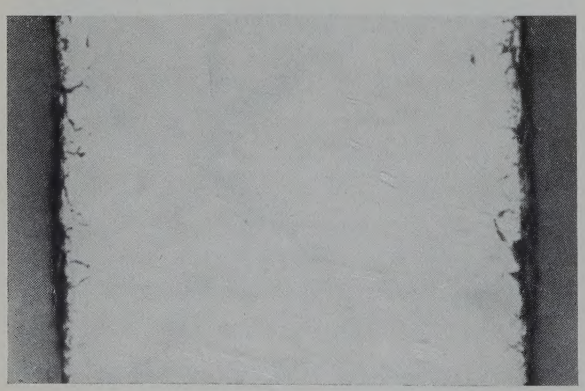

Nicral D. Oxydation à 1100° C. 150 heures. × 60.

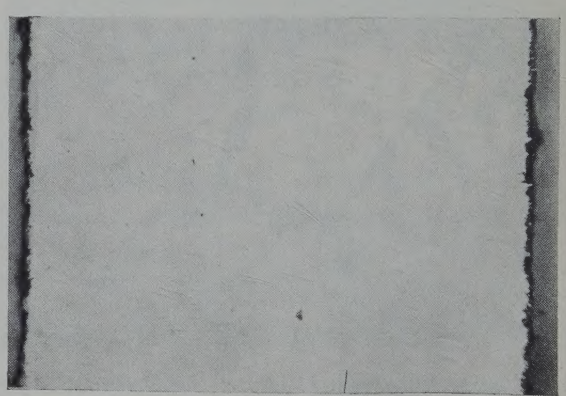

Hastelloy X. Oxydation à 1100° C. 150 heures. × 50.

métal de 10 μ. L'oxydation intergranulaire intéresse donc une épaisseur de métal six fois plus importante que l'oxydation en surface.

2. L'Hastelloy X (planches 5 et 6) présente surtout un phénomène d'oxydation interne, la corrosion intergranulaire n'apparaissant pas nettement. Ici encore, l'interface métal-oxyde est très irrégulier et l'oxyde comprendrait deux phases.

Cet oxyde apparaît très morcelé. Il y a en particulier de nombreuses fissures perpendiculaires à l'interface, qu'on peut attribuer à l'effet du refroidissement. Ainsi, bien que l'oxyde ne s'écaille pas au refroidissement, il peut cependant être sensible au choc thermique, l'oxydation reprenant aux endroits fissurés. Des essais avec cyclage thermique seraient nécessaires pour préciser ce point.

La zone intéressée par l'oxydation interne est d'une épaisseur sensiblement égale à celle de l'oxydation intergranulaire du Nicral D. Toutefois, la précipitation d'oxyde étant en général très fine et dispersée, les conséquences en ce qui concerne la tenue mécanique du métal sont sans doute moins fâcheuses.

La planche 7 montre les différences d'aspect entre les deux alliages oxydés, mises en évidence par deux micrographies effectuées sur *la totalité de la section* des échantillons. Cette technique peut d'ailleurs permettre d'apprécier rapidement l'épaisseur de métal resté sain, ce qui est plus judicieux que d'estimer l'épaisseur de la couche d'oxyde, en raison surtout de la possibilité d'un écaillage au cours du refroidissement. Deux difficultés apparaissent cependant. Tout d'abord, c'est la nécessité de connaître avec précision l'épaisseur du métal initial, donc de préparer des plaquettes d'épaisseur absolument uniforme (au moins au $^1/_{100}$ mm près); le polissage électrolytique provoque d'ailleurs une attaque plus prononcée sur les bords. D'autre part, la limite entre le métal sain et le métal oxydé intergranulairement est souvent mal définie ou du moins mal distinguée (planche 7), en raison du faible grossissement. Par contre, la méthode deviendrait très séduisante dans le cas d'échantillons plus minces (quelques dizièmes de mm).

6. Etude du "Désécaillage"

L'emploi d'une thermobalance pour l'étude de l'oxydation superficielle constitue une méthode très commode mais limite le nombre d'essais. Aussi, était-il indiqué d'examiner la possibilité de soumettre les éprouvettes oxydées à un désécaillage séparant l'oxyde *sans attaquer le métal*, afin de pouvoir se borner à une pesée manuelle. Deux méthodes de désécaillage ont été comparées:

Une méthode électrolytique en bain de soude et carbonate de sodium [2]).

Une méthode chimique en bain de nitrate de sodium et peroxyde de sodium [3]).

La méthode à l'hydrure de sodium [4]) n'a pas été retenue en raison des difficultés considérables de mise en œuvre.

6.1. Methode electrolytique

Le bain est constitué par un mélange de 60 % de NaOH et 40 % de CO_3Na_2, fondu à 450° C. L'électrolyse est effectuée en courant continu dans les conditions suivantes:

Tension en circuit fermé: 5 volts
Intensité: 4 ampères
Densité de courant: 0.4 A/cm^2.

L'anode est constituée par le bac à électrolyse en fer, l'échantillon tournant au centre du bain et formant cathode. Nous avons adopté le principe de l'anode tournante après avoir remarqué, au cours d'essais à blanc sur des éprouvettes immobiles, des attaques trop importantes du métal lui-même.

Après passage dans le bain, les échantillons sont lavés à l'eau puis plongés pendant 15 secondes dans une solution d'acide chlorhydrique à 50 %, saturée en As_2O_3 jouant le rôle d'inhibiteur.

1. *Essai à blanc*

Ces essais ont été effectués sur des éprouvettes de Nicral D et d'Hastelloy X polies électrolytiquement et non oxydées. La variation de poids au cours du traitement est déterminée par pesée des échantillons toutes les 5 minutes; les résultats sont rassemblés dans le tableau

suivant pour des échantillons ayant une surface totale voisine de 10 cm^2 et un poids d'environ 3 g:

Tableau 4

Temps de décapage en minutes	Diminution de poids en mg	
	Nicral D	Hastelloy X
5	0.4	0.1
10	0.5	0.4
15	0.65	0.55
20	0.80	0.70

Les variations de poids sont donc relativement faibles et prennent rapidement un caractère linéaire.

2. *Désécaillage d'échantillons oxydés*

Les essais ont été effectués sur des éprouvettes oxydées en thermobalance à 1100° C (figs. 5, 6 et 7) et à 900° C (fig. 8). Les quantités d'oxygène combiné étaient donc connues. Mais deux difficultés se présentent dans le calcul du poids de métal correspondant:

a) La composition globale de l'oxyde correspond-elle à la composition de l'alliage initial?

Les résultats de spectres de rayons X obtenus sur un alliage 25 Cr — 20 Ni chauffé 150 heures à 1100° C [5]) ne permettent pas de répondre à la question: les auteurs ont identifié des phases dont les paramètres correspondent à des spinelles, mais, pour un paramètre donné, il y aurait deux formules possibles de spinelles, d'où une indétermination sur la composition de l'oxyde.

Aussi, faute de données expérimentales plus précises, nous admettrons pour l'oxyde une composition identique à celle de l'alliage, étant donné la durée assez importante de l'oxydation.

b) Sous quelle forme s'oxydent les constituants de l'alliage?

Il n'y a pas de problème pour Ni et Cr qui ne donnent naissance qu'à un seul oxyde. Par contre, le fer peut conduire à FeO ou Fe_2O_3. Dans la couche externe, l'oxyde de fer est sous la forme Fe_2O_3. Mais dans la couche interne, le fer peut intervenir dans la formation de spinelles ($MO.M'_2O_3$), sous forme de FeO. Les deux oxydes doivent donc coexister.

Quoi qu'il en soit, il convient de remarquer que l'erreur possible est limitée par le fait que les métaux Fe, Cr et Ni ont des masses atomiques très voisines et que pour un même poids d'oxygène fixé, le poids d'alliage correspondant ne diffère pas considérablement dans les deux hypothèses où l'oxyde de fer est, soit à l'état de FeO, soit à l'état de Fe_2O_3.

Nous avons ainsi calculé les quantités de métal correspondant à 1 mg d'oxygène fixé, dans ces deux hypothèses (la forme Fe_3O_4 serait également possible, mais se situe entre FeO et Fe_2O_3):

Nicral D: 1 mg O_2 correspond à 2.46 mg d'alliage, si l'on considère les oxydes Fe_2O_3, Cr_2O_3 et NiO; et 3.05 mg d'alliage, si l'on considère les oxydes FeO, Cr_2O_3 et NiO.

Hastelloy X: 1 mg O_2 correspond à 2.8 mg d'alliage, si l'on considère les oxydes Fe_2O_3, Cr_2O_3 et NiO; et à 3.02 mg d'alliage, si l'on considère les oxydes FeO, Cr_2O_3 et NiO.

Sur les courbes de désécaillage, nous avons alors tracé deux droites en pointillé, déterminant la zone dans laquelle devrait théoriquement se terminer le désécaillage.

Le tableau suivant groupe les résultats des différents essais (voir tableau 5)

On peut faire les remarques suivantes:

Echantillons oxydés à 1100° C (figs. 5, 6 et 7).

Aussi bien pour le Nicral D que pour l'Hastelloy X, il y a une diminution très marquée des pertes de poids au bout de 5 minutes de désécaillage.

Cependant, pour le Nicral D, il semble que le désécaillage doive être effectué plus longtemps que ne l'indiquait la littérature [2]): 20 à 30 minutes au lieu de 5 minutes. De plus l'attaque semble se poursuivre légèrement et d'une façon régulière, même après des temps de désécaillage très importants. Ceci peut s'expliquer par l'importante oxydation intergranulaire du Nicral D: l'oxyde contenu dans les fissures ne doit être extrait qu'assez lentement. On peut encore remarquer qu'il n'y a pas de différence dans l'allure des courbes de désécaillage pour les

TABLEAU 5

Echantillon : Nature et Repère	Température d'oxydation (° C)	Durée d'oxydation (h)	Poids d'oxygène combiné (mg)	Poids initial de l'échantillon (g)	Temps de désécaillage (min)	P_1 Poids après désécaillage (g)	P_2 Poids théorique après désécaillage (g)	P_2—P_1 (mg)
Nicral D (a)	1100	50	20	3.3372	30	3.287	3.282 ± 0.006	+ 5
Nicral D (b)	1100	150	26	3.0544	30	2.990	2.982 ± 0.008	+ 8
Nicral D (c)	1100	150	31.5	2.8873	30	2.818	2.801 ± 0.009	+17
Hast. X (a)	1100	165	16.4	4.4068	10	4.364	4.359 ± 0.002	+ 5
Hast. X (b)	1100	150	19.5	4.6131	10	4.561	4.556 ± 0.002	+ 5
Nicral D (d)	900	380	4.5	4.7634	10	4.750	4.750 ± 0.002	0
Hast. X (c)	900	400	5	4.5516	10	4.540	4.538 ± 0.001	+ 2

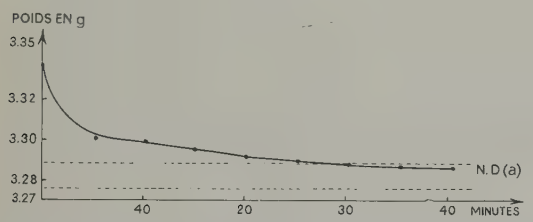

Fig. 5. *Nicral D.* Désécaillage électrolytique après oxydation à 1100° C.

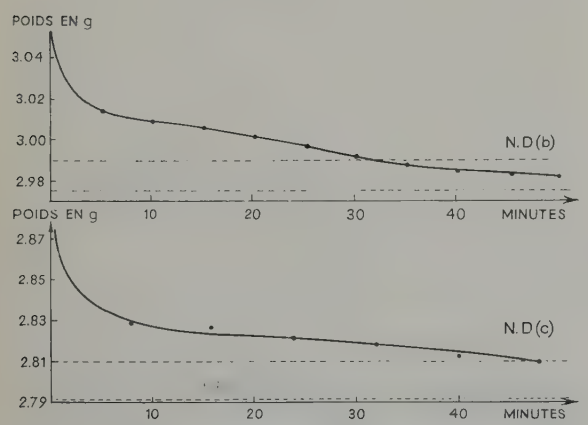

Fig. 6. *Nicral D.* Désécaillage électrolytique après oxydation à 1100° C.

temps d'oxydation de 50 heures et 150 heures.

Pour l'Hastelloy X, *le désécaillage semble achevé après* 10 *minutes d'attaque*, les pertes de poids devenant ensuite négligeables. Pourtant, contrairement au Nicral D, les courbes de diminution de poids de l'Hastelloy X ne pénètrent pas dans la zone de désécaillage théorique. Ceci peut s'expliquer par l'oxydation interne plutôt qu'intergranulaire de l'alliage, l'oxyde situé au sein du métal ne pouvant évidemment être attaqué par le bain.

De toute façon, exiger une trop grande précision serait illusoire; par exemple, une

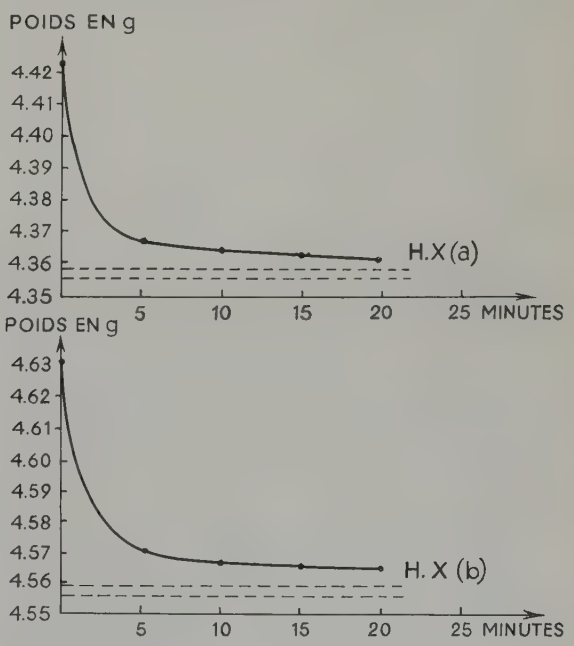

Fig. 7. *Hastelloy X.* Désécaillage électrolytique après oxydation à 1100° C.

différence de 5 mg entre la valeur trouvée par désécaillage et la valeur théorique moyenne, correspond à un poids d'oxygène combiné de 2 mg. Ceci est nettement inférieur à la dispersion des courbes d'oxydation: à 1100° C, après 150 heures d'oxydation, les poids de O_2 combiné varient de 26 à 32 mg pour le Nicral D.

Echantillons oxydés à 900° C (fig. 8)

Aussi bien pour le Nicral D que pour l'Hastelloy X, les résultats sont très satisfaisants:

Le désécaillage est terminé au bout de 10 minutes, l'attaque ne se poursuivant pratiquement plus au-delà de ce temps.

La précision est excellente.

A la vue de ces différents résultats, on peut conclure que le désécaillage par la méthode électrolytique est satisfaisant et donne des renseignements acceptables sur la quantité d'oxyde formé. De plus, le métal lui-même semble peu attaqué, puisque le poids réel après désécaillage est toujours supérieur ou au moins égal au poids calculé.

6.2. Methode chimique au nitrate

Le bain est constitué par un mélange de 85 % de NO_3Na et 15 % de Na_2O_2, fondu à 500° C.

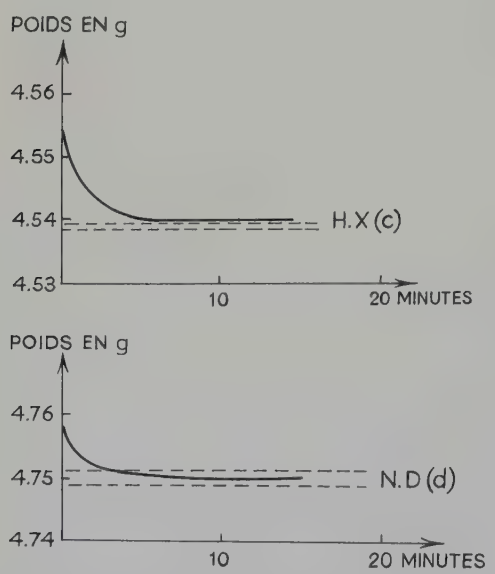

Fig. 8. Désécaillage électrolytique après oxydation à 900° C.

Après passage dans le bain, les échantillons sont lavés à l'eau puis plongés durant 15 secondes dans une solution d'acide chlorhydrique à 50 %, saturée en As_2O_3.

1. *Essais à blanc*

Ces essais ont été effectués sur des éprouvettes de Nicral D et d'Hastelloy X polies électrolytiquement. Le désécaillage est contrôlé par pesée des échantillons toutes les 4 minutes:

Tableau 6

Temps de désécaillage en minutes	Diminution de poids (mg)	
	Nicral D	Hastelloy X
4	10.1	0.35
8	13.3	0.45
12	16.4	0.55
16	19	0.60

Le Nicral D est donc assez profondément attaqué par ce bain. Par contre l'Hastelloy X résiste très bien.

2. *Désécaillage d'échantillons oxydés*

Le désécaillage a été pratiqué sur deux échantillons oxydés pendant 150 heures à 1100° C, un échantillon de Nicral D et un échantillon d'Hastelloy X (fig. 9).

L'observation des courbes montre, en ce qui concerne l'Hastelloy X, un bon désécaillage comparable au désécaillage électrolytique. Par contre, cette méthode ne convient pas pour le Nicral D, l'attaque ne se ralentissant pratiquement pas en fonction du temps. Ceci était d'ailleurs à prévoir d'après l'essai à blanc.

Le bain au nitrate et peroxyde apparaît donc plus réactif vis à vis du métal que le bain électrolytique soude-carbonate et son application semble devoir être contrôlée soigneusement par des essais témoins.

7. Conclusions

Cette étude a permis de mettre en évidence les points suivants:

1. La vitesse d'oxydation augmente très sensiblement entre 900 et 1100° C pour le

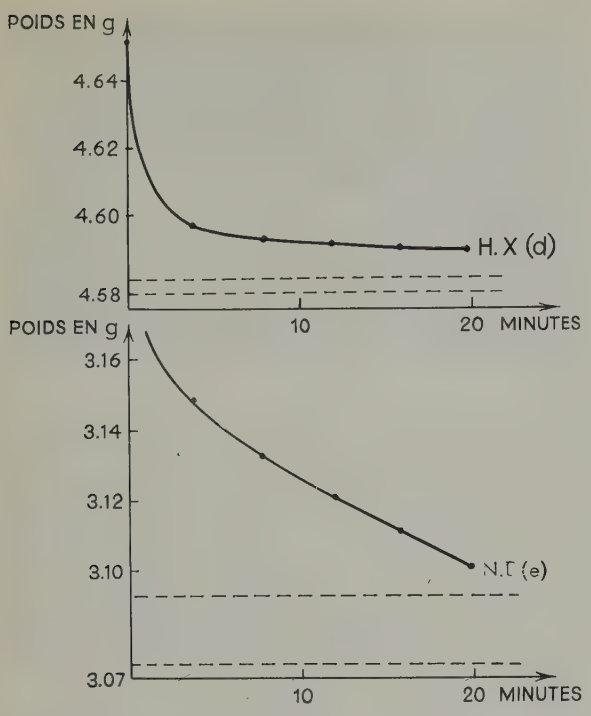

Fig. 9. Désécaillage chimique après oxydation à 1100° C.

Nicral D; cette vitesse, calculée sur un test de 200 heures, passe de 2.2×10^{-3} mg/cm^2· h pour 900° C à 1.8×10^{-2} mg/cm^2· h pour 1100° C.

2. Si les oxydations en surface du Nicral D et de l'Hastelloy X sont sensiblement identiques à 900° C, par contre à 1100° C le Nicral D s'oxyde davantage.

3. Le Nicral D est très sensible à l'écaillage par choc thermique.

4. L'examen micrographique à 1100° C montre une pénétration intergranulaire importante dans le Nicral D et une oxydation interne dans l'Hastelloy X, n'ayant pas nettement le caractère intergranulaire.

5. L'étude des deux méthodes de désécaillage montre qu'elles sont susceptibles de donner des résultats valables, avec toutefois une restriction pour la méthode au nitrate dans le cas du Nicral D.

6. Finalement, l'association du désécaillage et de l'examen micrographique en coupe permettant d'obtenir, chacun plus particulièrement, des renseignements sur l'oxydation superficielle d'une part, et sur l'oxydation interne ou intergranulaire d'autre part, doit constituer une méthode précise d'étude de la résistance à l'oxydation des alliages réfractaires à haute température. L'emploi de la thermobalance serait plutôt réservé à des essais relativement courts et peu nombreux d'étalonnage ou de contrôle des autres techniques employées.

Bien entendu, quand la pénétration intergranulaire devient très prononcée, ou d'importance beaucoup plus grande que l'oxydation superficielle, l'utilisation du désécaillage perd de son intérêt. Il est d'ailleurs probable que, dans le cas d'une zone métallique trop perturbée par l'oxyde, le bain de désécaillage attaque non seulement la couche d'oxyde mais désagrège aussi le métal lui-même. La micrographie, effectuée notamment sur la totalité de la section considérée, doit alors donner des renseignements suffisants.

Bibliographie

[1]) J. Bénard, Métaux-Corrosion **31** (1956) 306

[2]) A. S. Brasunas, J. T. Gow et O. E. Harder, ASTM, Proceedings **46** (1946) 871

[3]) L. Colombier et J. Hochmann, Aciers Inoxydables, Aciers Réfractaires (Dunod, Paris, 1955)

[4]) W. F. S. Taylor, Metal Treatment and Drop Forging (nov. 1956) p. 465

[5]) H. J. Yearian, H. E. Boren et R. E. Warr, Corrosion USA (nov. 1956) p. 45

[6]) R. Caillat et R. Darras, Deuxième Conférence de Genève (1958) 15P/1146, p. 22

JOURNAL OF NUCLEAR MATERIALS - 3 (1959) 226–232 - NORTH-HOLLAND PUBLISHING CO., AMSTERDAM

DISPERSIONS OF URANIUM CARBIDES IN ALUMINUM FOR PLATE-TYPE FUEL ELEMENTS REQUIRING HIGH-URANIUM CONCENTRATIONS †

W. C. THURBER and R. J. BEAVER

Metallurgy Division, Oak Ridge National Laboratory ††

Received 15 April 1959

Uranium carbides are potential fissile dispersoids for aluminum-base fuel elements in which the isotopic enrichment in U^{235} is limited to 20 %. Uranium dicarbide appears to be wholly compatible with aluminum at 600° C. Uranium monocarbide, on the other hand, is chemically active under the same conditions and is converted to the uranium-aluminum intermetallic compounds UAl_3 and UAl_4. Plate-type fuel elements containing dispersions of UC_2 in aluminum can be manufactured using established procedures with the exception that the cores must be vacuum degassed prior to rolling into fuel plates. Corrosion testing in 60° C water indicates that UC_2-Al dispersions will corrode catastrophically if the fuel-bearing section is inadvertently exposed to reactor process water.

On peut envisager l'emploi des carbures d'uranium comme produits fissiles susceptibles d'être mis en dispersion dans le cas des éléments combustibles à base d'aluminium où l'enrichissement isotopique en ^{235}U est limité à 20 %. Le dicarbure d'uranium semble tout à fait compatible avec l'aluminium à 600° C. Par contre, le monocarbure d'uranium, dans les mêmes conditions, est chimiquement actif et est transformé en composés intermétalliques entre uranium et aluminium UAl_3 et UAl_4. Des éléments combustibles en forme de plaques à base de dispersions de UC_2 dans l'aluminium peuvent être usinés avec les procédés courants, mais le cœur doit être dégazé sous vide avant le laminage en plaques. Les essais de corrosion par l'eau à 60° C montrent que la corrosion des dispersions UC_2-Al sera catastrophique si la section contenant le combustible est exposée à l'eau du réacteur par inadvertance.

Die Karbide des Urans kommen als disperse, spaltungsfähige Bestandteile für solche Brennstoffelemente in Betracht, in denen der angereicherte Gehalt an ^{235}U auf 20 % begrenzt sein soll. UC_2 scheint mit Aluminium bei 600° C nicht zu reagieren, aber UC ist unter diesen Umständen chemisch aktiv, wobei die Verbindungen UAl_3 und UAl_4 entstehen. Brennstoffplatten aus Aluminium mit feinverteiltem UC_2 können mittels bekannter Methoden hergestellt werden, nur muss der Brennstoffkern vor dem Auswalzen unter Vakuum entgast werden. Korrosionsversuche in Wasser bei 60° C zeigten, dass UC_2-Al-Mischungen katastrophal angegriffen werden, falls sie etwa direkt mit dem Reaktorwasser in Berührung kommen sollten.

1. Introduction

Under the Atoms-For-Peace Plan, foreign countries are presently designing and constructing research reactors quite similar to the Materials Testing Reactor (MTR) at Arco, Idaho, and the Bulk Shielding Reactor (BSR) at Oak Ridge, Tennessee, which utilize uranium supplied by the United States and incorporated into aluminum plate-type fuel elements. Although the technology of manufacturing such fuel elements for domestic use is generally well developed, problems are created with elements for export due to the limited U^{235} isotopic enrichment of uranium leased under the plan. The 20 % maximum enrichment coupled with the desire to retain the proven BSR fuel element design, shown in fig. 1, results in approximately a five-fold increase in uranium content of fuel elements for foreign application. This, in turn, leads to fabrication difficulties and higher costs when

† Paper presented at the American Nuclear Society Meeting, Hotel Statler, Los Angeles, California, June 2, 3, 4 and 5, 1958.

†† Operated for the US Atomic Energy Commission by the Union Carbide Corporation.

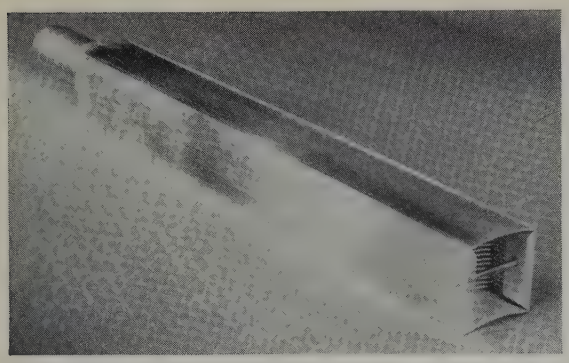

Fig. 1. Bulk Shielding Reactor Fuel Element. This element consists of 18 roll-clad composite plates with a fuel section of a 14 wt % U-Al alloy 20 mils thick clad on both sides with 20 mils of 1100 aluminum. The plates are assembled into an integral unit by brazing, using an aluminum-silicon eutectic composition alloy.

the conventional uranium-aluminum alloy is used as the fuel material [1, 2]). Since the problem of fabrication is intimately associated with the volume fraction of the fuel alloy occupied by the brittle, low-density, uranium-aluminum compounds, an obvious approach is to substitute a fissile compound of higher density. Powder metallurgy procedures are particularly convenient for incorporating high-density fuel compounds into base metals and generally consist simply of weighing the component powders, blending to obtain a homogeneous mixture, pressing at room temperature and sintering into compacts of the required shape.

This paper describes studies conducted at the Oak Ridge National Laboratory directed toward the incorporation of uranium carbides into aluminum for applications requiring high concentrations of uranium. The general approach to the problem was to adhere as closely as possible to existing aluminum plate-type fuel element manufacturing procedures [3]).

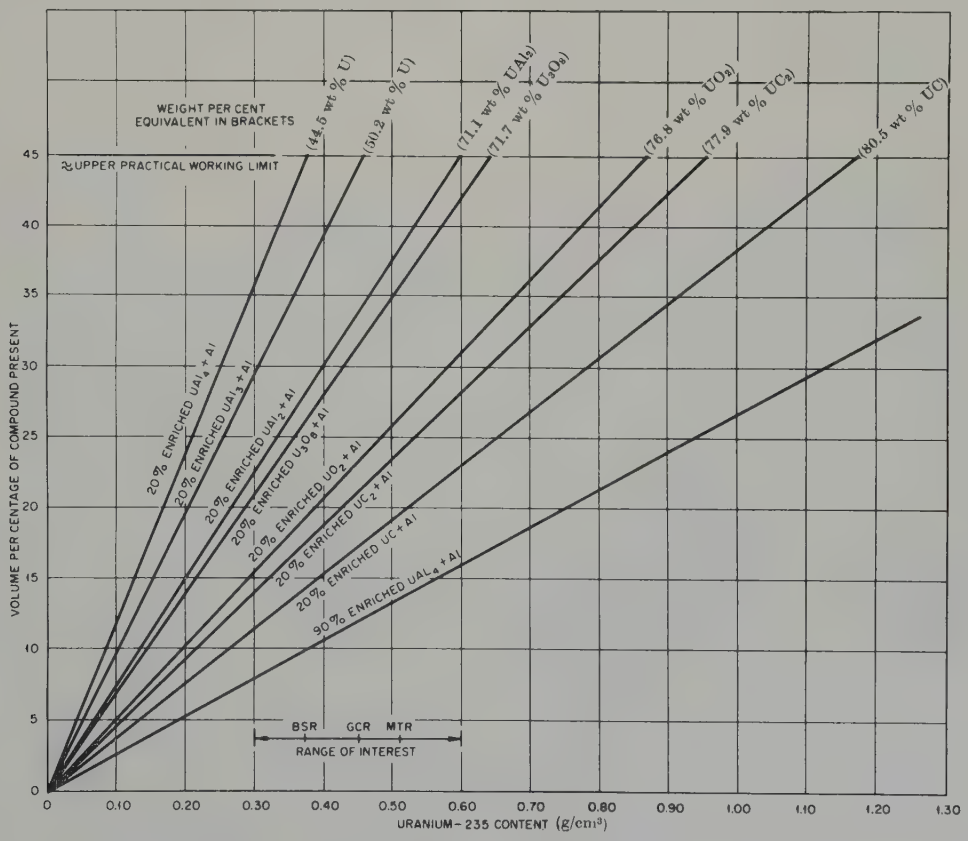

Fig. 2. Variation in U^{235} content with volume per cent compound present for several fuel-bearing material combinations.

2. Materials Selection

The relationship between the volume of intermetallic compound and the uranium loading for various fuel compounds which might be dispersed in aluminum is shown in fig. 2. The estimated upper working limit, based on fabrication considerations, is 45 vol % of fuel compound. In this figure, the "concentration range of interest" representing the fuel loading for several operational reactors lies between 0.3 and 0.6 g of U^{235} per cc. It is obvious that uranium-aluminum alloys containing highly enriched uranium are most suitable. Of the 20 % enriched materials, the carbides of uranium, UC and UC_2, appear to be very attractive, since in the "range of interest" the volume occupied by either compound lies well below the 45 vol % limit. As might be predicted from density considerations, UO_2 also appears promising, followed by U_3O_8, and finally the highly concentrated U-Al alloy in decreasing order of preference. The high density of the uranium carbides has stimulated an investigation to determine their suitability for aluminum fuel element applications.

3. Compound Preparation

Uranium carbides used in studies of compatibility with aluminum were prepared by arc-melting uranium and carbon in an argon atmosphere [4]). Most of the dicarbide used in fabrication of composite fuel plates, however, was prepared by the reaction of UO_2 with carbon at 2400° C. In either case, the materials were milled under argon to 100-mesh because of their pyrophoric nature. Subsequent handling of the material could be conducted in air.

4. Compatibility Studies

Since these fuel elements are conventionally joined by brazing at 605° C, it is necessary for the uranium carbides to be stable with aluminum at temperatures of this magnitude to avoid any deleterious volume changes, warpage, or correlative effects in composite plates during processing. To determine the compatibility of selected carbides of uranium with aluminum, a series of uranium carbides, ranging from 4.46 % C to 9.24 % C were produced by the arc-melting method. This range of compositions bracketed carbides from sub-stoichiometric UC to super-stoichiometric UC_2 as indicated in fig. 3. Mixtures containing 50 wt % of the specific carbide in aluminum were blended, cold-pressed into small compacts, and heat-treated in a vacuum of less than 0.1 μ for extended periods of time at both 580 and 620° C. Reaction was observed by dimensional measurements, as well as X-ray diffraction and metallographic examination of the compacts.

Data presented in table 1 demonstrate that uranium carbides in the vicinity of the monocarbide concentration react rapidly with aluminum at 620° C. In fact, the dispersion containing the 4.46 % C uranium carbide disintegrated after 10 h. As the carbon concentration increases, the carbide becomes increasingly more stable. It should be noted that dispersions approximating the dicarbide composition (9.16

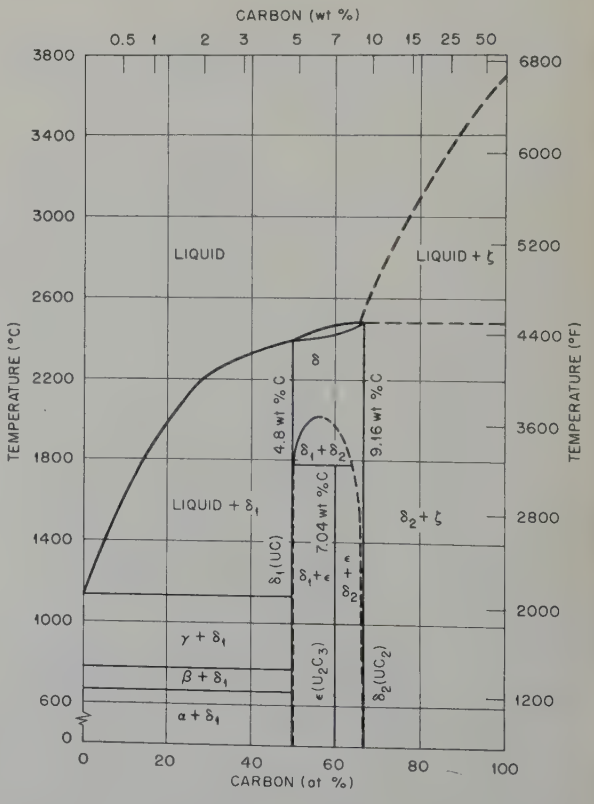

Fig. 3. Uranium-carbon constitution diagram.

TABLE 1

Compatibility of arc melted uranium carbides and aluminum in compacts containing equi-weights of carbides and aluminum

Hours at 620° C	% C in uranium carbide						
	9.20 %	8.24 %	7.98 %	6.96 %	5.75 %	4.86 %	4.46 %
4	NG			NG	NG	NG	ΔV=1.2 %
10	NG			NG	ΔV=70.8 %	ΔV=87.1 %	disintegrate
16	NG (no U–Al)			NG (no U–Al)			
24	NG (no U–Al)	NG	NG	ΔV = 4.6 % (5 % UAl_4)			
48	NG	NG (5 % UAl_3)	ΔV = 0.6 % 1 % UAl_4 (1 % UAl_3)				
72	NG	NG (5 % UAl_3)					
96	NG (4 % UAl_4)	NG (5 % UAl_3)					

Key

ΔV = Volume Expansion
NG = No growth
( ) = Amount of U–Al intermetallic

wt % C) contain no reaction products after 24 h, although products began to appear after the 48-h treatment. This may be attributed to monocarbide impurity in the dicarbide. However, no volume changes were observed in these compacts after as much as 96 h at temperature. A similar trend was observed on the same series of carbides heat-treated at 580° C.

Since it has been established that uranium carbides hydrolize [5]) rapidly in water and that hydrogen is readily soluble in aluminum, it is reasonable to expect that hydrogen from either or both of these sources could influence the reaction of uranium carbides with aluminum. Several experiments were conducted to validate this thesis. In the first of these experiments, a pressed compact of a dispersion containing 50 wt % uranium monocarbide in aluminum and a similar compact of uranium dicarbide in aluminum were sealed under vacuum in separate quartz tubes and heat-treated for 24 h at 620° C. The solid and gaseous products of reaction were identified by X-ray diffraction and mass spectrometric techniques, respectively. As shown in table 2, the UC_2-Al dispersion reacted to form 3 % UAl_3 with the release of about 90 % methane. On the other hand, the UC-Al dispersion reacted to form 65 % intermetallic with the release of 99.9 % hydrogen. Figure 4

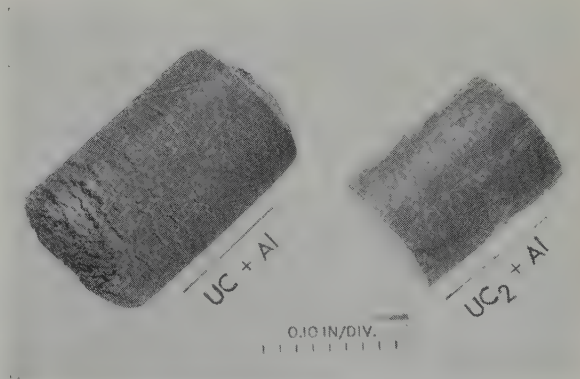

Fig. 4. Appearance of compacts of UC-Al and UC_2-Al after identical heat treatments of 24 h at 620° C in vacuum. Effects of UC-Al reaction are obvious.

TABLE 2

Role of gases in reaction of uranium carbides and aluminum

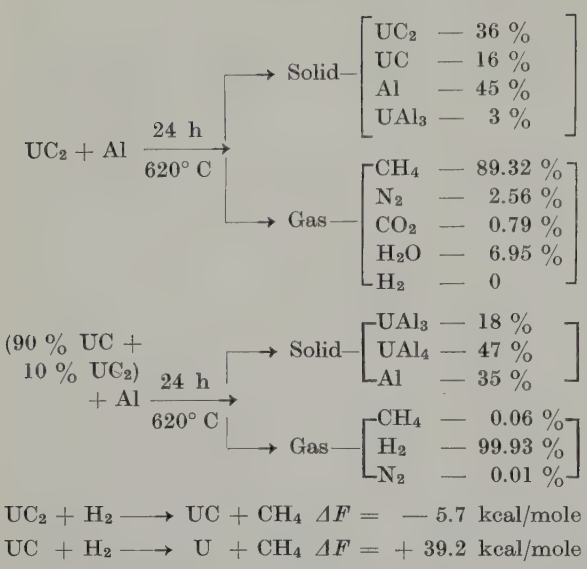

compares the dimensional changes of these two compacts. The effect of the reaction on the UC-Al compact is most pronounced.

From these observations it was postulated that hydrogen released from the component powders in the compact is responsible for the formation of methane and UC in the UC_2-Al dispersion. The UC which is thus formed subsequently reacts with aluminum to produce UAl_3 or UAl_4. The thermodynamic feasibility of the former reaction was established as indicated in table 2. Uranium monocarbide, however, does not react with hydrogen.

To further substantiate this proposal, two identical compacts containing the UC_2-Al dispersion were heat-treated at 620° C for 24 h in dynamic vacuum and in hydrogen, respectively. As indicated in the lower portion of table 2, the compact heat-treated in vacuum exhibited no significant reaction and no growth, whereas the compact heat-treated in hydrogen contained 23 % UAl_4 as a reaction product, and increased 1.4 % in volume.

Further investigations revealed that approximately 0.5 wt % H_2O could be removed from UC_2 powder at 300° C. Aluminum powder, on the other hand, appeared to contain only 0.15 wt % H_2O under the same conditions. These observations suggest that UC_2, per se, will not react with aluminum at a significant rate unless water or H_2 is present.

5. Fuel Plate Fabrication

Experimental fabrication of full-size composite plates revealed that during fabrication and subsequent heat treatments, the plates blistered severely. Fig. 5 illustrates the type of blisters observed on the surfaces. Fig. 6 shows that the blisters actually initiate in the fuel material. Analysis of the gas contained in the blisters indicated that more than 50 % of the gases were hydrocarbons. Vacuum degassification of the pressed compacts for 3 h at 600° C,

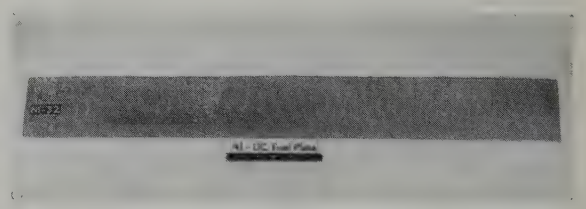

Fig. 5. Blistering on the surface of composite aluminum fuel plate with UC_2-Al core.

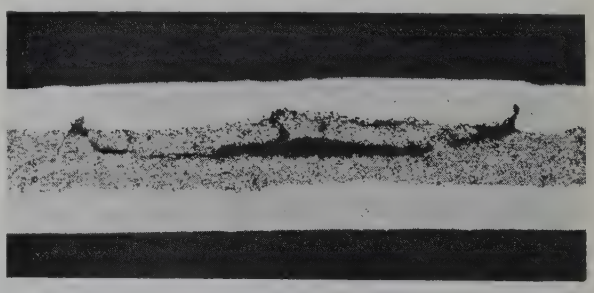

Fig. 6. Cross section through blister of type shown in fig. 5 illustrating that the source of the defect is within the fuel core rather than at the core-clad interface.

prior to insertion in the aluminum picture frame, appeared to eliminate the blistering problem in the subsequently manufactured and heat-treated fuel plate.

6. Fuel Element Assembly

In joining fuel plates by brazing, it is important that the plates do not "grow" significantly, otherwise plate buckling and warping will occur. Testing of full-size fabricated plates at a temperature of 605° C for a period of 16 h, which is far in excess of the time at temperature required during manufacturing, revealed that an elongation of only 0.1 % occurred. A 1 % value is considered significant. Several full-size fuel elements have been produced, demonstrating that MTR-type elements, containing a 60 wt % dispersion of UC_2 can be manufactured utilizing conventional "picture frame" procedures with the exception that the pressed compacts must be degassed prior to the roll-bonding operation.

7. Corrosion Testing

Corrosion testing of unclad specimens of the fabricated dispersion, as well as composite samples deliberately defected, revealed that in 60° C static, distilled water, catastrophic corrosion occurred within 24 h. The appearance of typical specimens after testing is shown in figs. 7 and 8. The virtual disintegration of the unclad sample and severe attack of the perimeter of the clad sample are apparent. Although uranium carbide-aluminum dispersions are questionable for use in water-cooled reactors, preliminary corrosion data [6, 7] indicate that these dispersions may be suitable in organic-cooled systems.

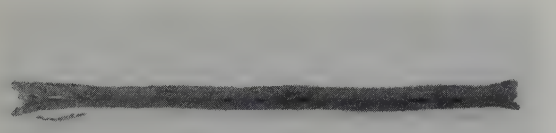

Fig. 7. Appearance of section from composite UC_2-Al fuel plate after exposure in static distilled water at 60° C for 24 h. Catastrophic attack along exposed perimeter is obvious.

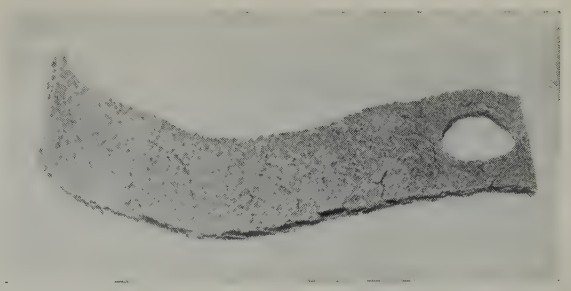

Fig. 8. Appearance of unclad, fabricated UC_2-Al dispersion after exposure in static distilled water at 60° C for 48 h indicating severity of attack.

8. Irradiation Performance

To evaluate the in-pile performance of UC_2-Al dispersions, a series of miniature composite fuel plates are currently being irradiated in the MTR process water in "leaky rabbit" capsules to anticipated burnups of 20, 40, 60, and 80 % of the U^{235} atoms present [8]). These composite fuel plates, which are 15 cm long, 1.9 cm wide × 0.013 cm thick contain an active core of 60 wt % UC_2 (enriched 20 % in the U^{235} isotope) in aluminum. Manufacturing techniques were identical to those developed for full-size, composite plates. No results have been obtained to date on these irradiations.

9. Summary

It is concluded that in manufacture of aluminum fuel elements in which conventional processing is utilized:

1. Uranium carbides approximating the monocarbide composition react drastically with aluminum within 10 h at temperatures between 580° C and 620° C.

2. Uranium carbides approximating the dicarbide composition show insignificant reaction with aluminum and no growth, after as long as 96 h at a temperature of 620° C.

3. Gaseous hydrocarbons are released during 600° C heat treatment of dispersions of UC_2

in aluminum, causing blistering in composite plates. Vacuum degasification of fuel compacts eliminates this defect.

4. Dispersions of UC_2 in aluminum will corrode catastrophically in quiescent 60° C water in the event of an inadvertent defect in the cladding.

Acknowledgements

The writers gratefully acknowledge the assistance of C. F. Leitten Jr, W. J. Kucera, H. J. Wallace, J. B. Flynn and G. E. Angel in this work.

References

[1]) W. C. Thurber and R. J. Beaver, Oak Ridge (USA) Report, ORNL-2476 (1958)

[2]) W. C. Thurber, J. H. Erwin and R. J. Beaver, Oak Ridge (USA) Report, ORNL-2351 (1958)

[3]) J. E. Cunningham and E. J. Boyle, Proceedings of the first Geneva Conference 9 (1955) 203

[4]) R. J. Gray, W. C. Thurber and C. K. H. DuBose, Oak Ridge (USA) Report, ORNL-2446 (1957)

[5]) L. M. Litz, Uranium Carbides - Their Preparation, Structure and Hydrolysis, USAEC Document NP-1453 (1948)

[6]) Private communication, 57AT-5780 from M. H. Binstock, Atomics International (dated September 1957)

[7]) A. Boettcher and G. Schneider, Second Geneva Conference (1958) 15/P/964

[8]) C. F. Leitten and W. C. Thurber, Oak Ridge (USA) Report, ORNL-CF-58-10-20 (1958)

JOURNAL OF NUCLEAR MATERIALS - 3 (1959) 233–243 - NORTH-HOLLAND PUBLISHING CO., AMSTERDAM

THE PLUTONIUM - URANIUM SYSTEM †

F. H. ELLINGER, R. O. ELLIOTT and E. M. CRAMER

University of California, Los Alamos Scientific Laboratory, Los Alamos, New Mexico

Received 23 April 1959

The plutonium-uranium phase diagram has been constructed from thermal, dilatometric, metallographic and X-ray diffraction data. All alloys solidify as a body-centered cubic solid solution, the phase resulting from the complete mutual solid solubility of epsilon plutonium and gamma uranium. Epsilon plutonium is the only plutonium allotrope in which uranium is appreciably soluble, whereas alpha uranium dissolves a maximum of 15 at % plutonium, and beta uranium dissolves about 20 at % plutonium. Two intermediate phases, both having wide homogeneity ranges, exist in this alloy system, and one of them is stable at elevated temperatures only.

Un diagramme de phase uranium-plutonium a été établi à partir des données thermiques, dilatométriques, métallographiques et des études de diffraction aux rayons X.

Tous les alliages se solidifient sous forme de solution solide cubique centrée, la phase résultant de la solubilité multuelle complète des solides Pu epsilon et U gamma. Le plutonium epsilon est la seule forme allotropique du plutonium dans laquelle l'uranium est soluble en quantité appréciable tandis que l'uranium α dissout un maximum de 15 at % de plutonium et l'uranium β dissout environ 20 at % de plutonium.

On trouve dans ce système deux phases intermédiaires avec un grand domaine d'homogénéité, l'une de ces phases étant stable à haute température seulement.

Das Zustandsdiagramm Plutonium-Uran wurde mit Hilfe von thermischen, dilatometrischen, metallographischen und Röntgen-kristallographischen Methoden bestimmt. Alle Legierungen erstarren als innenzentrierter kubischer Mischkristall als Resultat der vollständigen gegenseitigen Mischbarkeit von Epsilon-Plutonium und Gamma-Uran. ε-Plutonium ist die einzige allotrope Modifikation in der Uran in nennenswertem Masse löslich ist, während α-Uran ein Maximum von 15 At % Plutonium, und β-Uran ungefähr 20 % Plutonium löst. Zwei Zwischenphasen, beide mit weiten Homogenitätsbereichen bestehen in diesem Legierungssystem von denen eine nur bei hohen Temperaturen beständig ist.

1. Introduction

The investigation of plutonium-uranium alloys was undertaken at Los Alamos Scientific Laboratory as part of a program to establish the phase diagrams of plutonium in order to provide basic information useful in reactor technology. Although the plutonium-uranium phase diagram has appeared earlier in review articles, a detailed description of the work has not been published heretofore.

Recently, at the Second United Nations International Conference on the Peaceful Uses of Atomic Energy, Bochvar [1]) *et al.* presented a plutonium-uranium phase diagram which differs considerably in phase-boundary details from those reported in the present paper.

2. Experimental

2.1. Materials

The purity of the plutonium used in preparing most of the alloys was about 99.8 wt % ††. The main impurities were aluminum, silicon, iron, nickel, carbon and oxygen. Higher grade

† Work done under the auspices of the U.S. Atomic Energy Commission.

†† In this report the symbols wt % and at % are used to represent weight per cent and atomic per cent, respectively.

plutonium (99.9 wt %) was used for the alloys studied with the high-temperature diffractometer. The uranium was purer than 99.95 wt %.

2.2 Preparation of the alloys

The alloys were induction melted in degassed magnesia crucibles in vacua at pressures less than 0.1 micron Hg. All of the alloys were solidified in the crucibles. The weight of the alloy ingots varied between 3 and 40 gram, the larger ingots being used for dilatometric and thermal-analysis specimens, and the smaller ones for X-ray and metallographic studies.

2.3. Chemical analysis

The plutonium and uranium for each alloy were weighed to the nearest 0.0001 g; however, the uranium content of most of the alloys was checked by a polarographic method [2]). The analytical compositions differed from the as-weighed compositions only by amounts within the accuracy of the polarographic method, hence the as-weighed compositions were considered to be reliable.

2.4. Heat treatment

All alloys used for X-ray and metallographic studies were given a preliminary homogenization at either 600 or 700° C for about 300 h prior to equilibration heat treatments at selected temperatures. The specimens were heat treated in evacuated clear-silica capsules placed in muffle-type furnaces having automatic temperature control, and were quenched by immersing the capsules in cold tap-water after the heat treatment.

2.5. Thermal analysis

The thermal analysis furnace consisted essentially of a molybdenum-wound alundum tube having a 2-inch inside diameter, and which was mounted in a water-cooled brass vacuum chamber. D.C. power was supplied by a motor-generator set, and the furnace power input was regulated by means of an electronic program controller. A magnesia crucible, having a re-entrant thermocouple well integral with the bottom of the crucible, was supported within the heater tube. Temperatures were measured with a platinum/platinum-10 % rhodium calibrated thermocouple. The inverse-rate (fixed temperature increment) type of data was taken, using heating and cooling rates of approximately 3° C/min.

2.6. Dilatometry

A strain-gage autographic dilatometer [3]) was employed in this investigation. Basically, this apparatus determines the amount of expansion (or contraction) of the specimen (0.25 inch diameter by 0.5 to 1 inch long) by measuring the differential movement between an outer silica tube containing the cylindrical specimen and an inner silica rod resting on the specimen. The differential movement is detected by means of four resistance strain-gages that are fastened to a cantilever beam that moves in response to the change in length of the specimen. The change in resistance of the strain-gages (the result of expansion or contraction of the specimen) is recorded as dilation in inches on the X-axis of an X–Y recorder while the temperature is being recorded in millivolts on the Y-axis. Thus, an autographic plot of dilation vs. temperature is produced. The dilatometer furnace temperature is regulated by an automatic program controller providing a heating rate of 2–3 °C/min. A pressure of 10^{-5} mm Hg is maintained in the dilatometer during a run.

2.7. X-ray diffraction

Filings of the alloys for X-ray diffraction samples were prepared in glove boxes having either an argon or helium atmosphere. The filings were placed in thin-walled, clear-silica capillaries which were then evacuated to 10^{-5} mm Hg and sealed. The use of silica capillaries allowed successive heat treatments and quenches to be made upon the same sample. Diffraction patterns were obtained with 114.6 mm diameter cameras (Straumanis film mounting) at room temperature, and with Unicam 19 cm diameter high-temperature cameras at elevated temperatures. A high-temperature diffractometer [4])

was also utilized to determine the complex plutonium-rich end of the phase diagram. The great advantage of this latter equipment lies in its ability to record phase transitions almost continuously during heating or cooling of the specimen. Phase identification of metallographic samples was accomplished with a diffractometer fitted with a sample holder [5]) to accommodate the 1-inch diameter sample mounts. Filtered copper X-radiation was used for all the diffraction work except for the back-reflection focusing patterns of alpha uranium. Iron X-radiation was used for the latter work.

2.8. Density measurements

The density of the alloys was determined by the liquid displacement method, using bromobenzene as the displaced liquid.

2.9. Metallography

Standard methods of mechanical polishing were used in this investigation except that carbon tetrachloride rather than water was used for wet polishing. All polishing was done in glove boxes having a laboratory air atmosphere. The etching was done electrolytically in a fume hood. Etching reagents and procedure are given in table 1.

The microhardnesses of the phases were measured with a 136° diamond indenter (Vickers) and a 25-gram load.

Lineal analysis of 2-phase microstructures was made by utilizing a Hurlbut counter coupled to the microscope stage.

3. The Phase Diagram

3.1. Liquidus and solidus

The liquidus and solidus were located by means of thermal-analysis data, supplemented by observations of incipient melting in the microstructures. These data have been interpreted as defining a continuous liquid-plus-solid region between epsilon plutonium and gamma uranium, broken by a minimum at about 12 at % uranium and 610° C.

As may be seen in fig. 1, the course of the

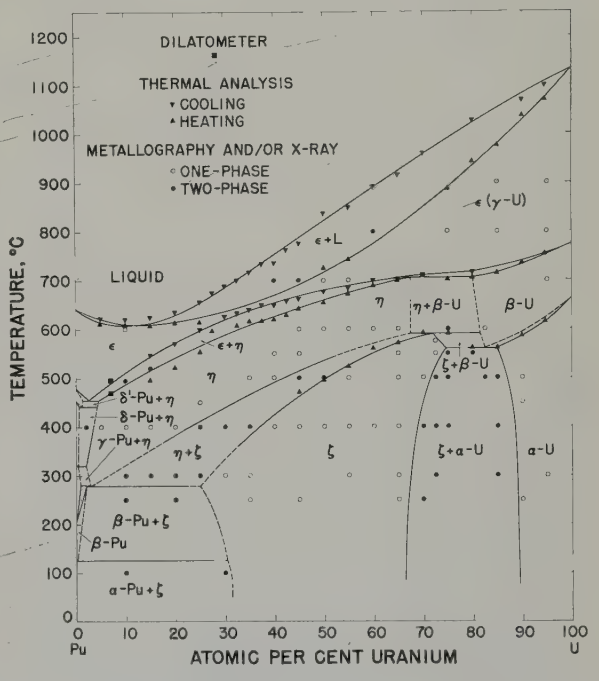

Fig. 1. Phase diagram of the plutonium-uranium system.

Table 1

Data on electrolytic etching of plutonium-uranium alloys

Composition (at % U)	Etchant †	Voltage (volts)	Current Density (mA/cm²)	Time (seconds)
Pu	A	6 —10	180—200	5— 15
1—75	A	7.5—15	150—250	10— 20
80—95	A	3 —10	100—200	10— 60
85—95	B	1 — 2	15	60—120
100	C	5 —10	60	10— 60

† A. Tetraphosphoric acid 7 ml; 2-ethoxyethanol 57 ml; Water 36 ml
B. Citric acid 10 g; Nitric acid 2.5 ml; Water 490 ml
C. Chromic acid 25 g; Acetic acid 300 ml; Water 30 ml

liquidus is defined over most compositions by the thermal arrests obtained on cooling. The course of the solidus is not as well defined by thermal data except at its plutonium-rich and uranium-rich ends. Throughout the intermediate composition range, the thermal-analysis curves obtained on heating showed few positive arrests that could be attributed to the start of melting. However, the solidus was judged to be continuous, based on the following observations: (1) the presence of liquid in a 45 at % uranium alloy and its absence in a 50 at % uranium alloy, both quenched from 700° C, placed a solidus point between these compositions at 700° C; (2) the smooth sequence of thermal arrests that marked the upper boundary of the $\varepsilon+\eta$ field does not indicate the presence of a horizontal as would be expected if the solidus intersected this field.

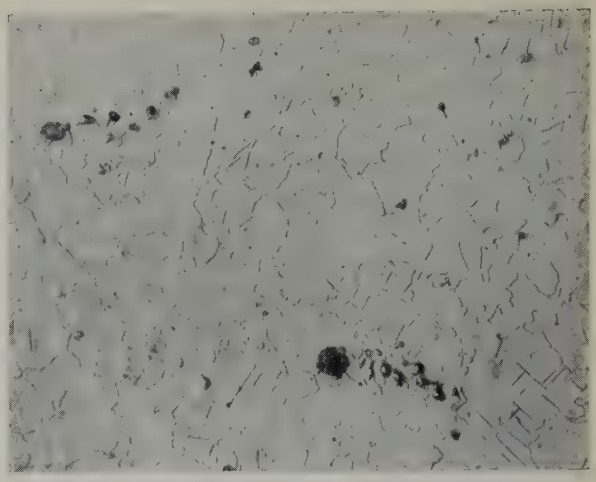

Fig. 2. Pu-30 at % U alloy, heat treated at 600° C for 284 h and quenched, and at 400° C for 255 h and quenched. The matrix is zeta that transformed from eta; the minor phase (in relief) is zeta that was stable at 400° C. Tetraphosphoric acid etch; oblique illumination. X 500.

3.2. The intermediate phases

The two intermediate phases, designated eta (η) and zeta (ζ), that exist in this alloy system have wide homogeneity ranges. The eta phase is stable at elevated temperatures only. It is formed, as indicated by thermal data, by a peritectoid reaction between the epsilon (gamma uranium) and beta-uranium phases at approximately 70 at % uranium and 705° C. Its homogeneity range extends across the diagram to 2 at % uranium at 320° C, and it decomposes eutectoidally into beta plutonium and zeta at about 3 at % uranium and 278° C.

The $\eta/(\eta+\varepsilon)$ boundary was defined by the combined data from thermal analysis, dilatometric and high-temperature X-ray diffraction work. The $\eta/(\eta+\zeta)$ boundary was located chiefly by metallographic examination of heat treated and quenched alloys. The microstructures of some alloys that were quenched from the $\eta+\zeta$ region were suitable for lineal and areal analysis. The eta phase in $\eta+\zeta$ structures usually transformed to zeta on quenching, but etching readily distinguished the transformed eta from the zeta that was stable at temperature. A typical microstructure is shown in fig. 2.

The X-ray powder pattern of eta is complex; however, it was indexed on the basis of a tetragonal unit cell with $a=10.57$ and $c=10.76$ Å for the 25 at % uranium alloy quenched from 500° C. This unit cell contains 52 atoms as calculated from 17.3 g/cm^3, the density of eta deduced from dilatometric data. This solution of the powder pattern is considered highly uncertain. The diffraction data, up to $\sin^2\theta=0.3604$, of the eta phase at room temperature are given in table 2.

The intermediate phase (zeta), stable at room temperature, forms by a peritectoid reaction between the eta and beta-uranium phases at approximately 72 at % uranium and 590° C. With decreasing temperature the zeta field widens rapidly toward plutonium-rich compositions, reaching a maximum width at 75 at % plutonium and 278° C. Below 278° C the zeta field narrows to about 69 at % plutonium, as determined by microscopic examination of a series of α-Pu$+\zeta$ alloys treated at 100° C for 3 years.

The microstructure of the zeta phase containing 32.5 at % uranium as it appeared in a slowly cooled thermal-analysis ingot is shown in fig. 3. After a somewhat faster cool, the structure of a 30 at % uranium alloy appeared

TABLE 2

X-ray powder data for the eta (η) phase (25 at % U) at room temperature

Observed				Calculated					
				Eta		PuO		Pu_2O_3—Pu_4O_7	
No.	Int.	d(Å)	$\sin^2\theta$	hkl	$\sin^2\theta$	hkl	$\sin^2\theta$	hkl	$\sin^2\theta$
1	W	3.164	0.0593					222	0.0589
2	M	2.840	0.0737	312	0.0737	111	0.0730		
				321	0.0742				
3	VW	2.738	0.0793					400	0.0786
4	VW	2.643	0.0850	400	0.0850				
5	M—	2.563	0.0905	401	0.0901				
				410	0.0904				
6	M	2.535	0.0925	114	0.0927				
7	M	2.500	0.0950	411	0.0955				
				330	0.0957				
8	W	2.464	0.0979			200	0.0973		
9	W	2.397	0.1034	204	0.1034				
10	W	2.364	0.1063	402	0.1055				
				420	0.1063				
11	W	2.314	0.1110	412	0.1111				
				421	0.1114				
12	W—	2.090	0.1360	314	0.1353				
				413	0.1366				
13	W	1.944	0.1573					440	0.1572
14	M	1.746	0.1949	116	0.1953	220	0.1946		
15	W+	1.658	0.2161	443	0.2163			622	0.2161
16	Trace	1.593	0.2340	425	0.2345			444	0.2357
17	W+	1.516	0.2585	623	0.2588				
18	M+	1.490	0.2677			311	0.2676		
19	W+	1.469	0.2755	416	0.2751				
20	W+	1.450	0.2825	641	0.2815				
				720	0.2817				
				525	0.2823				
21	VW	1.427	0.2920			222	0.2920		
22	W—	1.405	0.3012	544	0.3000				
				722	0.3022				
23	VW	1.291	0.3566	218	0.3550				
				427	0.3577				
				644	0.3585				
24	VW—	1.284	0.3604	802	0.3607				
				820	0.3614				

as shown in fig. 4. The banded pattern of the grains is thought to result from slow cooling through the $\eta+\zeta$ region. A photomicrograph of the zeta phase containing 50 at % uranium, but more rapidly cooled than the above alloys may be seen in fig. 5. The microcracks are characteristic of zeta in alloys containing about 40 at % uranium and greater.

The course of the $\zeta/(\zeta+\alpha\text{-U})$ boundary was located by means of heat treating/quenching experiments made chiefly with X-ray specimens. Microstructural evidence was difficult to obtain in this composition range because of rapid intergranular oxidation, as shown in fig. 6. However, this oxidation behavior seemed to be erratic, and it was successfully shown that a 65 at %

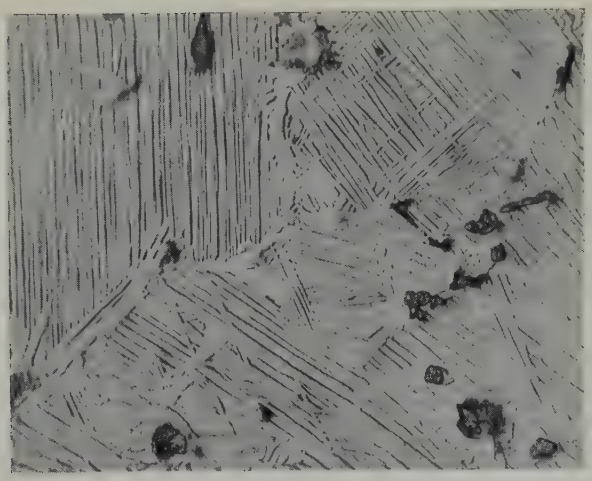

Fig. 3. Pu-32.5 at % U alloy, cooled slowly to room temperature, showing the zeta phase and oxide. Tetraphosphoric acid etch; oblique illumination. × 500.

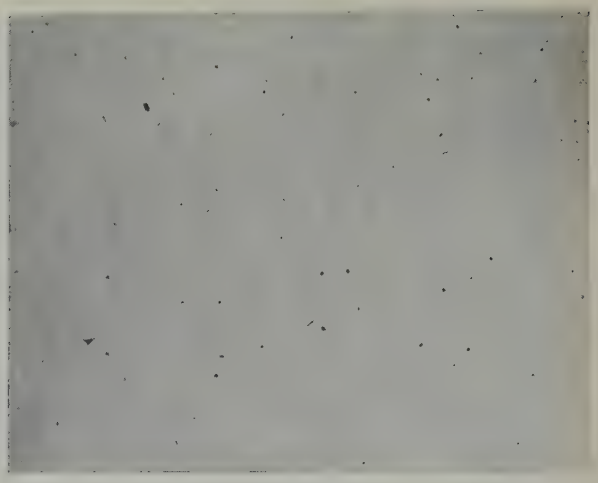

Fig. 5. Pu-50 at % U alloy, in the as-cast condition, showing the microcracks in the zeta phase. Tetraphosphoric acid etch. × 100.

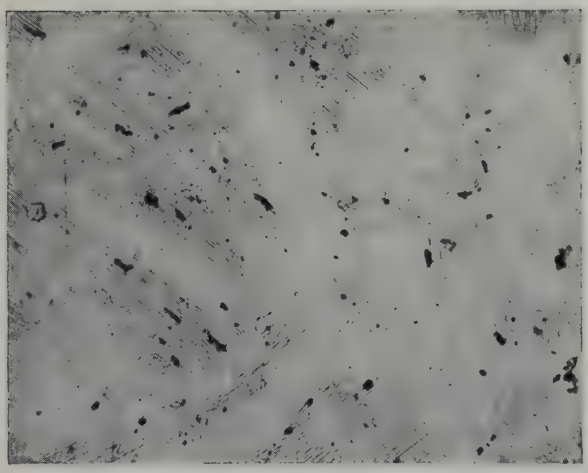

Fig. 4. Pu-30 at % U alloy, in the as-cast condition, showing the zeta phase. Tetraphosphoric acid etch. × 500.

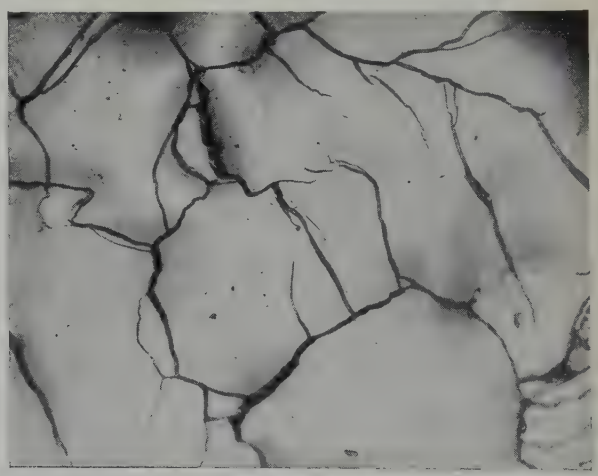

Fig. 6. Pu-70 at % U alloy, showing the intergranular oxidation of the zeta phase. Tetraphosphoric acid etch. × 250.

uranium alloy soaked at 250° C for 890 h consisted entirely of the zeta phase.

The X-ray powder pattern of zeta was indexed on the basis of a primitive cubic unit cell. The lattice constant was found to decrease from $a = 10.692$ Å at 35 at % uranium to $a = 10.651$ Å at 70 at % uranium (fig. 7). The number of atoms in this unit cell approximates 58, as calculated from the observed density of 18.5 to 18.8 g/cm^3. High-temperature X-ray work revealed, however, that zeta expands anisotropically with a symmetry tentatively identified as tetragonal. Hence, the crystal structure of zeta may be tetragonal with an axial ratio of unity at room temperature. The powder diffraction data, up to $\sin^2\theta = 0.3084$,

of the zeta phase at room temperature are listed in table 3.

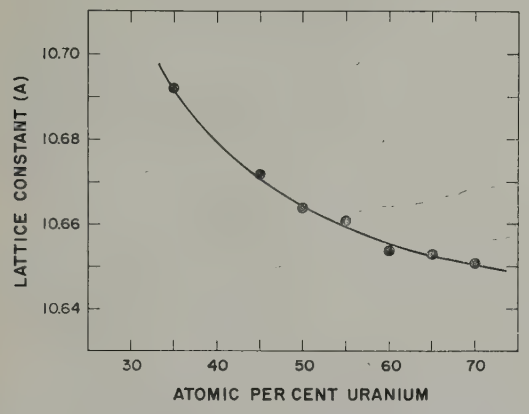

Fig. 7. Lattice constant vs. composition of the zeta phase.

3.3. Plutonium-rich phases

High-purity plutonium metal exists in six allotropic forms. The crystal structures and densities of the six modifications are listed in table 4.

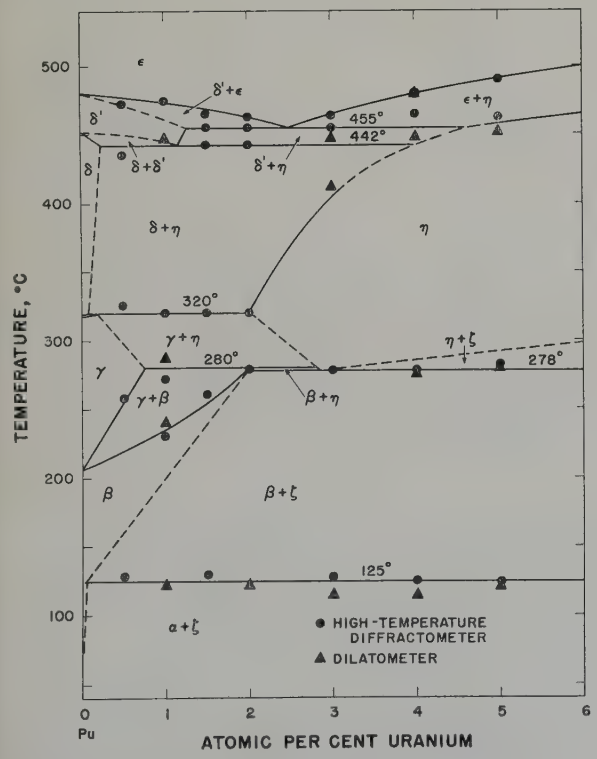

Fig. 8. Plutonium-rich end of the plutonium-uranium phase diagram.

The phase diagram of alloys containing up to 5 at % uranium, as constructed chiefly from high-temperature diffractometer data, is shown in fig. 8. The solubility of uranium in the allotropes of plutonium is quite limited, apart from that in epsilon plutonium. The latter forms a continuous solid solution with gamma uranium.

The $\beta+\eta$ field is the only one for which no direct experimental evidence was obtained. The $\gamma+\eta \rightleftharpoons \beta$ peritectoid horizontal falls very nearly at the same temperature as the $\eta \rightleftharpoons \beta+\zeta$ eutectoid horizontal. It was concluded, however, that the β peritectoid horizontal was at the higher temperature because, on heating at less than 0.5°/min, the $\beta \rightarrow \eta$ transition of alloys containing 3 or more at % uranium was sharp and rapid, and there was no evidence obtained for the formation of gamma plutonium. Thus, the existence of the very narrow $\beta+\eta$ field is indicated. Also, the $\gamma+\eta$ region could not extend beyond 3 at % uranium.

3.4. Uranium-rich phases

The crystal structures and densities of the three allotropic forms of pure uranium are shown in table 5. The lattice constants and densities are quoted from the work of Chiotti, Klepfer and White [10]). The lattice constants of the uranium stock used in the present work were found to be

$$a = 2.8542 \pm 0.0008 \text{ Å} \quad (26 \pm 2^\circ \text{ C})$$
$$b = 5.8667 \pm 0.0002$$
$$c = 4.9540 \pm 0.0009$$
$$\text{X-ray density} = 19.06 \text{ g/cm}^3,$$

as determined from back-reflection focusing patterns evaluated by Cohen's analytical extrapolation method.

Thermal analysis revealed that the α-U$\rightarrow\beta$-U transformation is lowered to 560° C by the solution of plutonium, at which temperature alpha uranium dissolves about 15 at % plutonium. Below 560° C the solubility decreases somewhat, reaching about 11 at % plutonium at 250° C. The microstructure of a 15 at %

TABLE 3

X-ray powder data for the zeta (ζ) phase (55 at % U) at room temperature

Observed				Calculated					
				Zeta		PuO		Pu_2O_3—Pu_4O_7	
No.	Int.	d(Å)	$\sin^2\theta$	hkl	$\sin^2\theta$	hkl	$\sin^2\theta$	hkl	$\sin^2\theta$
1	W	3.152	0.0598					222	0.0590
2	VW	3.077	0.0627	222	0.0631				
3	W	2.834	0.0740	321	0.0736	111	0.0731		
4	VW	2.740	0.0791					400	0.0787
5	MW	2.565	0.0903	410, 322	0.0894				
6	S	2.496	0.0953	411, 330	0.0947				
7	W—	2.463	0.0979			200	0.0975		
8	W	2.434	0.1003	331	0.1000				
9	W	2.311	0.1113	421	0.1105				
10	MW	2.264	0.1160	332	0.1157				
11	VW	2.159	0.1274	422	0.1263				
12	MW	2.123	0.1318	500, 430	0.1315				
13	W—	2.081	0.1372	510, 431	0.1368				
14	W	2.045	0.1421	511, 333	0.1420				
15	W—	1.969	0.1532	520, 432	0.1526				
16	W	1.940	0.1580	521	0.1578			440	0.1574
17	VW	1.851	0.1736	522, 441	0.1736				
18	Trace	1.823	0.1789	530, 433	0.1789				
19	Trace	1.793	0.1850	531	0.1841				
20	VW	1.768	0.1901	600, 442	0.1894				
21	W	1.744	0.1952	610	0.1946	200	0.1950		
22	VW	1.726	0.1994	611, 532	0.1999				
23	W+	1.657	0.2164	621, 540, 443	0.2157			622	0.2165
24	Trace	1.604	0.2310	622	0.2315				
25	VW	1.585	0.2366	630, 542	0.2367			444	0.2362
26	Trace	1.564	0.2429	631	0.2420				
27	W+	1.532	0.2531	444	0.2525				
28	W	1.519	0.2577	700, 632	0.2578				
29	W+	1.503	0.2630	710, 550, 543	0.2630				
30	W+	1.488	0.2684	711, 551	0.2683	311	0.2681		
31	VW	1.462	0.2782	720, 641	0.2788				
32	M	1.446	0.2841	721, 633, 552	0.2841				
33	W	1.426	0.2924			222	0.2924		
34	MW	1.410	0.2992	722, 544	0.2999				
35	VW	1.388	0.3084	731, 553	0.3104				

plutonium alloy, consisting of the alpha-uranium and zeta phases, is shown in fig. 9.

Beta uranium will dissolve a somewhat greater proportion of plutonium than alpha uranium, the maximum being about 20 at % plutonium at 705° C. Below 705° C the solubility decreases to about 18 at % plutonium at 560° C where beta uranium decomposes eutectoidally into alpha uranium and zeta. Beta uranium that contains at least 10 at % plutonium in solution can be retained at room temperature by water-quenching from the beta-uranium region. The lattice constants of the tetragonal unit cell of beta uranium containing 15 at % plutonium were found to be $a=10.61$ and $c=5.605$ Å at room temperature. The calculated density is 18.78 g/cm³.

The solution of plutonium in gamma uranium

TABLE 4

Crystal structures of the plutonium allotropes

Allotrope	Range of stability (° C)	Space lattice and space group	Unit cell dimensions (Å)	Atoms per unit cell	X-ray density (g/cm³)
Alpha[6]	Below 122	Monoclinic $P2_1/m$	$a = 6.1835 \pm 0.0005$ (21° C) $b = 4.8244 \pm 0.0005$ $c = 10.973 \pm 0.001$ $101.80 \pm 0.02°$	16	19.82
Beta[7]	122 to 206	Monoclinic	$a = 9.284 \pm 0.003$ (190° C) $b = 10.463 \pm 0.004$ $c = 7.859 \pm 0.003$ $92.13 \pm 0.03°$	34	17.70
Gamma[8]	206 to 319	Orthorhombic face-centered $Fddd$	$a = 3.1587 \pm 0.0004$ (235° C) $b = 5.7682 \pm 0.0004$ $c = 10.162 \pm 0.002$	8	17.14
Delta[9]	319 to 452	Cubic face-centered $Fm3m$	$a = 4.6371 \pm 0.0004$ (320° C)	4	15.92
Delta-Prime[9]	452 to 480	Tetragonal body-centered $I4/mmm$	$a = 3.327 \pm 0.003$ (465° C) $c = 4.482 \pm 0.007$	2	16.00
Epsilon[9]	480 to 640	Cubic-body-centered $Im3m$	$a = 3.6361 \pm 0.0004$ (490° C)	2	16.51

TABLE 5

Crystal structures of the uranium allotropes

Allotrope	Range of Stability (° C)	Space lattice and space group	Unit cell Dimensions (Å)	Atoms per unit cell	X-ray density (g/cm³)
Alpha[11]	Up to 662	Orthorhombic $Cmcm$	$a = 2.852$ (25° C) $b = 5.865$ $c = 4.952$	4	19.07
Beta[12]	662 to 772	Tetragonal $P4/mnm$ or $P4/nm$	$a = 10.744$ (662° C) $c = 5.652$	30	18.17
Gamma[13]	772 to 1133	Cubic body-centered $Im3m$	$a = 3.532$ (772° C)	2	17.94

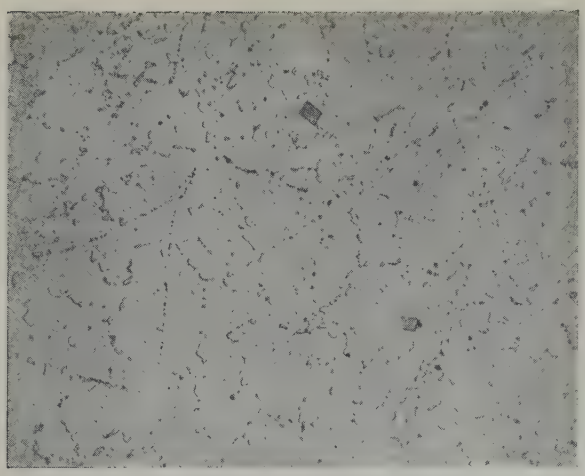

Fig. 9. Pu-85 at % U alloy, heat treated at 800° C for 8 h and quenched, and at 300° C for 1000 h and quenched, showing zeta phase in a matrix of alpha-uranium solid solution. Tetraphosphoric acid etch. × 500.

lowers the β-U→γ-U transformation to 705° C, the temperature of the γ-U + β-U⇌η peritectoid reaction. As already described, gamma uranium and epsilon plutonium form an unbroken series of solid solutions. It is interesting to note that, whereas an 85 at % uranium alloy quenched from the beta-uranium field is retained as beta uranium at room temperature, the same composition quenched from the gamma-uranium field will transform to alpha uranium.

4. Properties of Plutonium-Uranium Alloys

4.1. Microhardnesses of the phases

In the course of examining microstructures, the microhardnesses of the plutonium-uranium phases were measured in order to aid in identifying the phases. The range of hardness that was observed for each phase is listed in table 6.

4.2. Density of plutonium-uranium alloys

The density of plutonium-uranium alloys in the as-cast condition is shown graphically in fig. 10. The dip in the curve at the plutonium-rich compositions is attributed to the retention of beta plutonium, as indicated by the observation that a plutonium-10 at % uranium alloy

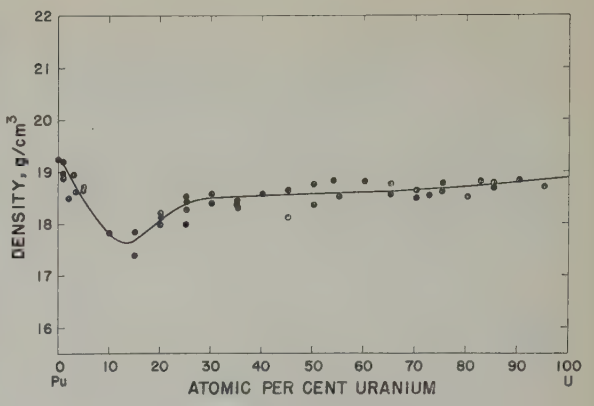

Fig. 10. The density of plutonium-uranium alloys in the as-cast condition

quenched from 300° C was composed of the alpha-plutonium and zeta phases, and had a density of 18.55 g/cm³, whereas the same composition quenched from 250° C was composed of the beta-plutonium and zeta phases, and had a density of 17.94 g/cm³.

Table 6

Microhardnesses of plutonium-uranium phases

Phase	Alloy composition (at % U)	Diamond pyramid hardness number, (25 g load)
Alpha plutonium	0— 5	200—240
Beta plutonium	10— 25	140—165
Zeta, as-cast	40— 75	275—450
Zeta, heat treated	30— 85	200—300
Beta uranium	75— 90	195—300
Alpha uranium	82—100	160—210

4.3. Fabricability of plutonium-uranium alloys

J. H. Kittel and L. R. Kelman [14]) report the successful preparation of cast and extruded uranium-rich alloys. Irradiation samples having diameters of 0.140 inch and larger were made by casting into copper molds. Castings having 3/8 inch diameters were extruded to 0.185 inch diameters at temperatures between 450 and 525° C. The castings were jacketed in copper as a lubricant, and required pressures in the range of 80 000 to 120 000 psi for extrusion.

Acknowledgments

The authors wish to thank all of the members of CMF-5, Los Alamos Scientific Laboratory, who contributed to this investigation, and wish to acknowledge in particular the work done by V. O. Struebing in preparing most of the alloys.

References

[1]) A. A. Bochvar, S. T. Konobeevsky, V. I. Kutaitsev, I. S. Menshikova, and N. T. Chebotarev, Second Geneva Conference, (1958) P/2197

[2]) M. E. Smith, Los Alamos (USA) Report LA-1249 (1951)

[3]) R. O. Elliott and W. N. Miner, Los Alamos (USA) Report LA-2175 (1958)

[4]) R. O. Elliott, Ph. D. Dissertation, University of California, Berkeley (1958)

[5]) C. K. Stambaugh and D. D. Whyte, Los Alamos (USA) Report LA-1385 (1952)

[6]) W. H. Zachariasen and F. H. Ellinger, J. Chem. Phys. **27** (1957) 811

[7]) W. H. Zachariasen and F. H. Ellinger, (1958) Unpublished

[8]) W. H. Zachariasen and F. H. Ellinger, Acta Cryst. **8** (1955) 431

[9]) F. H. Ellinger, J. Metals, AIME **8** (1956) 1256

[10]) P. Chiotti, H. H. Klepfer and R. W. White, (1958) ASM Preprint No. 83.

[11]) C. W. Jacob and B. E. Warren, J. Amer. Chem. Soc. **59** (1937) 2588

[12]) C. W. Tucker, Jr., P. Senio, J. Thewlis and N. Steeple, Acta Cryst. **9** (1956) 472

[13]) A. S. Wilson and R. E. Rundle, Acta Cryst. **2** (1949) 126

[14]) J. H. Kittel and L. R. Kelman, Argonne (USA) Report ANL-5706 (1958)

JOURNAL OF NUCLEAR MATERIALS - 3 (1959) 244-248 - NORTH-HOLLAND PUBLISHING CO., AMSTERDAM

THE EFFECT OF INCLUSIONS ON THE ARCING BEHAVIOUR OF METALS

P. C. L. PFEIL and L. B. GRIFFITHS

UKAEA *Research Group, Atomic Energy Research Establishment, Harwell, Didcot, Berks, UK*

Received 19 May 1959

Metallographically prepared specimens of commercial and laboratory-made stainless steel and copper have been made the negative electrode of a small spark gap in a low pressure hydrogen atmosphere, with the ultimate aim of predicting the suitability of these materials as components of thermo-nuclear apparatus. Microscopical examination, subsequent to sparking in the experimental tube, revealed that surface damage of the specimens had occurred around certain types of inclusion in the metals the remainder of the surface being unaffected. A correlation has been established between the resistivity of inclusions and their effectiveness as arc-initiators.

Des échantillons d'acier inoxydable ou de cuivre provenant du commerce ou préparés au laboratoire, et ayant subi un traitement métallographique ont été utilisés comme électrode négative d'un générateur d'étincelles sous atmosphère d'hydrogène à faible pression. Le but de ces essais est de déterminer si ces matériaux peuvent être utilisés dans des appareils thermonucléaires. Après l'étincelage dans le tube expérimental, l'examen microscopique révèle qu'une détérioration superficielle des spécimens s'est produite autour de certains types d'inclusion du métal, le reste de la surface n'étant pas affecté. Une relation a été établie entre la résistivité des inclusions et leur efficacité pour amorcer un arc.

Handelsübliche und im Laboratorium hergestellte Proben aus rostfreiem Stahl und aus Kupfer wurden metallographisch vorbereitet und danach als negative Elektrode einer kleinen Funkenstrecke in Wasserstoff unter niedrigem Druck verwendet, um die etwaige Eignung dieser Metalle für Bestandteile thermonuklearer Ausrüstungen zu untersuchen. Die mikroskopische Untersuchung nach dem Abfunken zeigte, dass die Oberflächenschädigung der Proben in der Umgebung gewisser Arten von Einschlüssen eingetreten war; der Rest der Oberfläche war unbeeinflusst geblieben. Eine Beziehung zwischen dem elektrischen Widerstand der Einschlüsse und ihrer Wirksamkeit als Zündstellen für Gasentladungen wurde aufgestellt.

1. Introduction

Attention has recently been focussed, in work associated with controlled thermonuclear reactions, upon the problem of electrical arcing between the plasma and any metal exposed to it with the consequent contamination, by metal atoms, of the plasma [1]). Plasma contamination may prevent suitable temperatures and reacting conditions being obtained owing to increased radiation losses.

While it has been recognised for some time that the nature of the cathode surface affects spark gap discharges [2, 3]), so far as we are aware detailed attention has not previously been given to the effects of the non-metallic inclusions of slags, refractories, oxides, nitrides, carbides and sulphides which are found in commercial metals and alloys.

2. Experimental Details

In the present work approximately 1 cm² of the surface of various specimens of commercial and laboratory-made austenitic stainless steels and copper were polished metallographically using fine diamond dust for finishing, and then made the cathode of a small spark gap. The anode was a molybdenum wire held 1–3 mm above the cathode. In another series of experiments the polarity was reversed but no interesting effects were found by microscopical examination of the anode. The apparatus was filled to a pressure of 20–100 μ of mercury with

Fig. 1. Nb-Stabilised Stainless Steel. Before Arcing. "A", "B", "C" are slag or refractory conclusions. The light grey particles (e.g. "x") are niobium carbide. 500 ×.

Fig. 2. As (fig. 1 but after arcing) can be seen arc damage has occurred around "A", "B" and "C" but not around the high conductivity niobium carbide. (repolished before arcing). 500 ×.

ordinary "tank" hydrogen from which the oxygen was removed with a catalytic purifier, and any solid matter in the gas stream taken out by gentle bubbling through low vapour pressure oil.

The majority of experiments were carried out by discharging a capacitor previously charged to 100–500 volts from a D.C. stabilised power supply. The discharge was initiated by ionising some of the hydrogen in the experimental tube with the output from a Tesla coil placed about 8 cm from the specimen. Under glow discharge conditions the current density at the cathode was approximately 10^{-4} amp/cm^2. The Tesla coil output was of itself not enough to cause observable damage on the cathode surface, but in another series of experiments qualitatively similar results were obtained in which the Tesla coil output alone produced sparks. The specimens were examined microscopically both before and after the experiments.

3. Results and Discussion

3.1. Nature off effect

Figs. 1 and 2 illustrate results typical of the experiments in which arcing damage is observed to be centred around certain inclusions while the rest of the material remains unaffected. All inclusions of the same chemical nature over an area large compared with the separation between inclusions (but dependent, to a certain extent, upon the gas pressure and the electrode spacing) were found to be affected irrespective of inclusion size in the range 10^{-5}–10^{-3} cm apparent diameter. However, variations in gas pressure from 20 to 100 μ of mercury and of electrode spacing from 0.5 to 3.0 mm did not affect the general results. Duplicate specimens

under the same conditions behaved identically and the specimens could be re-polished and re-tested to give reproducible results. However, such reproducibility was only obtained if the surface was free from grease, oil, dust and embedded polishing abrasive. Touching a degreased specimen at a place 1 cm away from the surface to be tested caused a difference in behaviour.

3.2. High resistivity inclusions

Typical commercial stainless steels contain slag and refractory inclusions, generally silicates, sulphides (mainly MnS), and also iron-chromium oxide or titanium or niobium oxides in the case of stabilised steels, and such inclusions were found to initiate arcs. Steels were also made in the laboratory in which inclusion materials were melted together with high purity austenitic steel, and arcing tests gave similar results. It is of interest that all the arc initiators possess low electrical conductivity, as does cuprous oxide which has been found to initiate arcs in copper. Poorly conducting inclusions in metals, therefore, promote arcing on to the metal surface at or near to the metal/inclusion interface.

In some instances small particles, which respond to polarised light, are found within titanium nitride inclusions, which are good conductors. They have the appearance of titanium dioxide and appear to have nucleated the nitride crystals on cooling. Arcing damage occurs on those nitride inclusions which contain these fine particles, indicating that if an insulator is present, arcing can occur on to titanium nitride just as well as on to the parent metal.

A sample of laboratory-made, inclusion-free steel, which was made by melting the alloy under an argon/hydrogen atmosphere in an arc furnace, did not arc when tested in these experiments even with the maximum available potential difference of 500 volts.

Copper of various grades of purity has also been tested and results obtained are consistent with those on steels. Very pure copper (vacuum melted O.F.H.C. containing 0.024 wt % oxygen in solution but no second phase) did not arc with a potential difference of 500 volts. Copper containing inclusions of Cu_2O (total oxygen content 0.57 wt %) arced when the potential difference was only 150 volts. The high purity copper, being very soft, was susceptible to accidental embedding of polishing abrasives and when this occurred arcing damage was found around the embedded particles with only 150 volts potential difference. Quantitative examination of the effects of dust particles on the arcing behaviour of inclusion-free cathodes is not yet complete; however, it has been found that alumina powder causes arcing whereas niobium carbide powder (of high electrical conductivity) does not.

Substances can be tested for their proneness to cause arcing by testing the effect of particles 10^{-4} to 10^{-5} cm radius on clean pure cathode surfaces.

The initiation of arcing around insulating inclusions in cathodes has also been found in experiments in which polished specimens were inserted in the Materials Testing Torus in the Metallurgy Division of AERE.

3.3. Films on inclusions

There exists an interesting complication with respect to the carbides of titanium and chromium which, though themselves good conductors, nevertheless cause arc initiation. The suggested explanation is that insulating oxide films are formed on them relatively rapidly on exposure to the atmosphere. Both titanium and chromium oxides are anisotropic and their formation during microscopical examination causes a response to polarized light to develop, but arcs may be initiated even though the films are too thin to give any response to polarized light from a mercury-vapour-lamp source. Preliminary exposure of such specimens to a glow discharge with insufficient potential difference across the electrodes to initiate arcs, caused a delay between the subsequent raising of the potential and the onset of the spark. This time delay increased with further treatment until it became indefinitely long, indicating that the oxide films had been affected or removed by

the ion bombardment. The original arcing behaviour was restored by momentary exposure to atmospheric gas, and the cycle could be repeated. The effects of hydrogen-ion bombardment on the electrical properties of poor conductors appear important, and further experiments are intended.

On the other hand, titanium nitride and niobium carbide, also good conductors, do not oxidise in air at room temperature to an extent sufficient to show any response to polarized light even after fourteen days, and have not been found to give rise to arc initiation.

3.4. Practical implications

The difference between the behaviour of niobium carbide and titanium carbide suggests that, in this respect, niobium-stabilised steels offer an advantage over titanium-stabilised steels in minimising the tendency for arcs to form. However, commercial niobium-stabilised stainless steels generally contain a certain amount (of the order of 0.01 wt %) of carbon in solution which is precipitated as chromium carbide by heat treatment at a relatively low temperature, 425–800° C [4]). On reheating to 1000° C this carbon is taken back into solution or re-precipitated as niobium carbide, or partly re-dissolved and partly reprecipitated. A laboratory-made niobium-stabilised steel has been converted from "non-arcing" to "arcing" and back again by heat treatments at 700° C and 1000° C which precipitate and re-dissolve chromium carbide respectively.

Incidentally the generally accepted identification of these inclusions in stainless steels [4, 5]) has been confirmed by our experiments in which small quantities of the inclusions themselves were melted up with inclusion free steel. It should also be understood that the term "titanium nitride" used here includes materials with a similar structure and appearance in which some of the nitrogen is replaced by carbon, and likewise for the other phases in which carbon may replace nitrogen or vice-versa.

In the case of the oxides, vanadium oxide (V_2O_3) seems to be the only one, of those likely to be found in stainless steel, which possesses relatively good electrical conductivity (order of 10^{-1} ohm cm) and therefore may not give rise to arcing damage. Inclusion-free stainless steel to which vanadium and oxygen were added did not arc. However, when subsequently tested under more severe conditions in the Materials Testing Torus, arcing was found to be initiated by the V_2O_3 inclusions [6]). The essential difference between the conditions in the Torus and in the experimental spark-gap is that the ion currents to the specimen is higher by a factor of about 10^4 in the former. The addition of vanadium to oxygen-containing stainless steel therefore does not appear to give a low arcing material under severe conditions as was originally hoped.

3.5. General discussion

The work reported here is consistent with previous indications that the cathode surface affects the initiation of electrical discharges. Since some of the positive ions bombarding the cathode will strike any insulating particles present, their surfaces acquire a positive potential with respect to the remainder of the cathode. If the conductivity of the inclusion is relatively large then electrons will be able to neutralise many of the charges brought by incoming ions, and this may explain why V_2O_3 (of comparatively high conductivity) only initiates arcing if the current to the cathode is large. In this connection it should be pointed out that the conductivity of many materials, particularly the surface conductivity, is greatly affected by environment, and that this should be taken into account in the interpretation of experimental work on arcing behaviour. The mechanism by which local charges and potential differences lead to arc initiation is uncertain, and further work is required.

The present work suggests that metals free from poorly conducting inclusions should have superior arcing properties to typical currently available commercial metals, a factor of importance in the choice of metallic materials to be in contact with energetic plasmas. However,

the work to date indicates that a considerable effort would be required to produce low-arcing stainless steel on the ton scale.

4. Conclusions

Experimental work has shown that certain types of inclusion cause arc initiation in stainless steels and in copper; there seems to be no reason why other metals should not be similarly affected. The offending inclusions are those which have a comparatively high electrical resistivity.

Acknowledgements

Thanks are due to Mr. D. Arkell, Mr. S. D. Ford and to Mr. C. H. Thomas for assistance with the experiments, and to Dr. A. E. Robson, Dr. R. Hancox and Mr. J. Hedger for valuable discussions. We also wish to thank the British Iron and Steel Research Association for supplying high purity, de-oxidised iron, Messrs. Murex Limited for samples of nitrides and carbides, the Brown-Firth Research Laboratories and Imperial Chemical Industries Limited for analysing stainless steel and copper samples.

References

1) J. L. Craston, R. Hancox, A. E. Robson, S. Kaufmann, A. T. Miles, A. A. Ware and J. A. Wesson, Second Geneva Conference (1958), P/34
2) F. Llewelyn Jones, The Physics of Electrical Contacts (Oxford University Press, 1957)
3) F. Llewelyn Jones, Electrical Discharges in Gases (London, Methuen, 1956)
4) T. V. Simpkinson, Metallurgia **47** (1953) 18
5) T. V. Simpkinson, Trans. Amer. Soc. Metals **49** (1957) 721
6) J. Maskery, Private Communication

JOURNAL OF NUCLEAR MATERIALS - 3 (1959) 249–258 - NORTH-HOLLAND PUBLISHING CO., AMSTERDAM

LEAD-LITHIUM SHIELDING ALLOY – METALLURGICAL STUDIES

D. H. JANSEN and E. E. HOFFMAN

Metallurgy Division

and

D. M. SHEPHERD

Engineering and Mechanical Division, Oak Ridge National Laboratory, Tenn., USA †

Received 16 June 1959

Alloying and casting studies conducted on a lead-0.69 wt % lithium alloy, a proposed shielding material, are presented. The information obtained during this investigation was used in connection with the making of an experimental, laminated slab, 90 cm square and 10 cm thick, of the lead-lithium alloy. This slab was used to determine the neutron and gamma-ray shielding characteristics of the material. Shielding tests have demonstrated the effectiveness of the alloy in suppressing secondary gamma-ray production.

Mechanical property tests were conducted on the lead-lithium alloy and the results compared to those for a lead-0.06 wt % copper alloy, also being considered for shielding applications. It was found that the lead-lithium alloy has superior strength at room temperature, but the lead-copper alloy has superior creep strength at 110° C.

Tests at 110° C in air indicate that the lead-0.69 wt% lithium alloy oxidizes more rapidly than pure lead. The lead-lithium alloy is attacked by water with an accompanying volume increase and cracking. Corrosion was much more severe in boiling water than in room-temperature water.

The lead-lithium alloy has good rolling characteristics. No cracks or surface defects were observed on a piece which was rolled to 92.5 % reduction.

Des études sur l'élaboration et la coulée d'un alliage de plomb avec 0.69 % en poids de lithium, matérial proposé comme alliage de protection, sont présentées. D'intéressants renseignements ont été obtenus en relation avec la fabrication par laminage d'une plaque carrée de 91 mm de côté et 10 cm d'épaisseur. Cette plaque fut utilisée pour déterminer les caractéristiques de protection de cet alliage vis-à-vis des neutrons et des rayons gamma. Des essais de protection ont démontré l'efficacité de l'alliage en ce qui concerne la suppression de la production de rayons secondaires.

Des essais de propriétés mécaniques furent effectués sur l'alliage plomb-lithium et les résultats comparés à ceux obtenus sur un alliage de plomb contenant 0.06 % en poids de cuivre qui fut examiné aussi pour ses applications comme écran de protection. L'alliage plomb-lithium se révéla posséder une résistance supérieure à la température ambiante, mais l'alliage Pb-Cu a une résistance au fluage supérieure à 110° C.

Des essais dans l'air à 110° C indiquent que l'alliage Pb-0.69 % Li s'oxyde plus rapidement que le plomb pur.

L'alliage Pb-Li est attaqué par l'eau avec un accroissement de volume simultané et fissuration. La corrosion était beaucoup plus sévère dans l'eau bouillante que dans l'eau à température ambiante.

L'alliage Pb-Li a de bonnes caractéristiques de laminage. Aucune crique ou défaut de surface ne fut observé sur une pièce qui fut laminée à un taux de réduction de 92.5 %.

Untersuchungen über das Verhalten einer als Abschirmungsmaterial vorgeschlagenen Legierung (Blei mit 0.69 Gew. % Lithium) bei ihrer Herstellung und beim Guss wurden durchgeführt. Die hierbei gewonnenen Ergebnisse wurden im Zusammenhang mit der Herstellung einer Versuchsweise aus einzelnen Schichten aufgebauten Platte ($90 \times 90 \times 10$ cm^3) aus der Blei-Lithium-Legierung verwendet. Diese Platte wurde benutzt um die Abschirmeigenschaften dieses Materials bezüglich Gammastrahlen und Neutronen zu bestimmen. Die Untersuchungen zeigten, dass die Legierung praktisch alle sekundären Gammastrahlen absorbiert.

Mechanische Eigenschaften der Blei-Lithium- Legierung wurden untersucht und die Ergebnisse mit den-

† Operated for the United States Atomic Energy Commission by the Union Carbide Corporation.

jenigen einer anderen Legierung verglichen, die aus Blei und 0.06 Gew. % Kupfer besteht und ebenfalls als Abschirmungsmaterial in Betracht gezogen wird. Hierbei ergab sich, dass die Blei-Lithium-Legierung grössere Festigkeit bei Raumtemperatur besitzt, dass aber die Blei-Kupfer-Legierung die höhere Kriechfestigkeit bei 110° C hat.

Versuche bei 110° C in Luft zeigen, dass die Blei-Lithium-Legierung schneller als reines Blei oxydiert. Die Blei-Lithium-Legierung wird von Wasser angegriffen. Hierbei treten Risse im Material sowie eine Volumenzunahme auf. Die Korrosion war in siedendem Wasser sehr viel stärker als im Wasser mit Raumtemperatur.

Die Blei-Lithium-Legierung besitzt gute Walzeigenschaften. An einer Probe, die um 92.5 % herabgewalzt worden war, wurden weder Risse noch Oberflächendefekte beobachtet.

1. Introduction

At the suggestion of the Neutron Physics Division of the Oak Ridge National Laboratory, the Metallurgy Division initiated a research program to determine the potential application of a lead-lithium alloy as a combination neutron and gamma-ray shielding material for both instruments and reactors. Lithium was chosen as the alloying element primarily because of its thermal neutron absorption properties. The reactions of thermal neutrons with lead are as follows:

$$n + {}_{82}Pb^{206,\,207,\,208} \rightarrow {}_{82}Pb^{207,\,208,\,209} + \gamma.$$

The capture gamma rays produced are emitted instantaneously, unlike those liberated by decay.

Lithium has an absorption cross section for thermal neutrons of 71 barns. The lithium-6 isotope, comprising 7.5 % of naturally occurring lithium, has an absorption cross section for thermal neutrons of 945 barns, with the reaction:

$$n + {}_3Li^6 \rightarrow {}_1H^3 + {}_2He^4.$$

The alpha particles resulting from this reaction have an extremely short range (several microns in lead) as compared with the range (several inches in lead) of the gamma rays produced in the neutron-lead reaction.

Lead-lithium alloys have been produced industrially for cable sheaths (0.002 to 0.01 wt% lithium) and bearing alloys (up to 0.1 wt % lithium) [1, 2, 3]. A phase diagram [4]) of the lead-rich end of the lead-lithium system is shown in fig. 1.

The information gathered in this metallurgical study was used in connection with the manufacture of an experimental lead-0.69 wt % lithium (eutectic composition) slab, 90 cm square and 10 cm thick. This slab was used to study the shielding characteristics of the alloy. Homogeneous distribution of the lithium in the lead was required in this experimental piece.

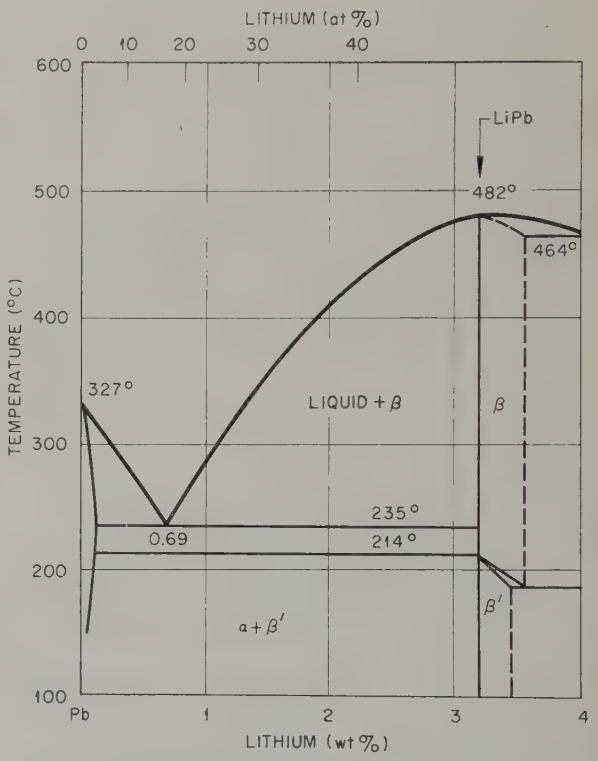

Fig. 1. Lead-rich end of lead-lithium phase diagram.

2. Preliminary Studies

2.1. Alloying and casting

Both lead-boron and lead-lithium were considered as possible shielding alloys. The first work done during this investigation was to determine the alloying characteristics of lead and boron. No information could be found in

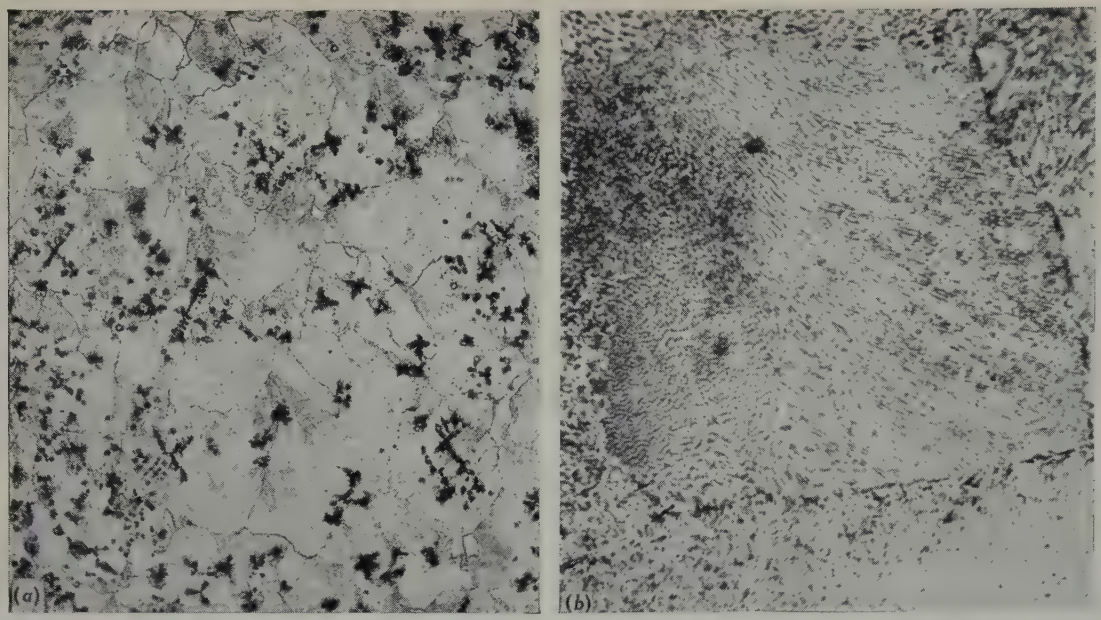

Fig. 2. A slightly hypereutectic (lead-0.75 wt % lithium) alloy at (a) 150 × showing primary beta dendrites (3.2 % Li) which have been heavily attacked by the etchant and (b) at 1000 × showing the lamellar type structure of the eutectic composition. Etchant: glycerine, nitric acid, and acetic acid.

the literature relative to the solubility of boron in lead. Attempts to prepare lead-boron alloys were unsuccessful due to the apparent low solubility of boron in lead (less than 0.07 wt % at 400° C) and no further studies were performed with this material.

Initial lead-lithium alloy castings were made with 0.1 and 1.0 wt % lithium, to study the segregation properties of these alloys. Homogeneous alloy castings of other than the eutectic composition could be made, provided the sections were thin enough to produce a chilled casting. Alloying operations were carried out in an inert-atmosphere chamber under purified argon. Solid lithium was added to molten lead at about 350 to 400° C. The alloying reaction proceeded rapidly, accompanied by the evolution of a large quantity of heat. Immediate temperature rises of 100 to 150° C in the interior of the melts were recorded when the small quantities of lithium were added to molten lead. The temperature rise at the surface was considerably higher. Heats of formation (ΔH) for Pb_xLi_y compounds are quite large; ΔH values for PbLi and $PbLi_4$ are –7300 and –8400 cal/mol, respectively [5]). The lead alloys containing 0.1 and 1.0 wt % lithium were chill cast from 400° C into a stainless steel mold and chemical analysis of various sections of the castings indicated a homogeneous distribution of lithium in the lead.

The eutectic composition was used in order to minimize segregation difficulties associated with the slow cooling rates encountered in large, relatively thick castings. As may be seen in fig. 1, the eutectic alloy contains 0.69 wt % lithium (17 at %) and melts at 235° C †. All additional studies were concentrated on this composition. The metallographic appearance of an alloy near the eutectic composition is illustrated in fig. 2.

During initial castings of the 0.69 wt % lithium alloy, it was found that from 0.03 to 0.07 wt % lithium was lost during the alloying reaction. This loss was attributed to: (1) reaction of oxides of lead with the lithium, (2) reactions between lithium and residual oxygen or nitrogen

† The relatively low melting point of the eutectic alloy (0.69 wt % Li) suggests that this material warrants consideration as a potential reactor coolant.

in the inert-gas atmosphere, and (3) vaporization of lithium. Oxygen in the lead was not considered to be a major contributor to this loss of lithium since less than 30 ppm oxygen was found in the lead.

In order to obtain castings of eutectic composition, an excess of lithium was added to the molten lead to make up for the lithium loss during the alloying reaction. Additions of 0.74 wt % lithium produced alloys close to the 0.69 wt % lithium composition.

2.2. Mechanical property experiments

Although the primary interest in the lead-lithium alloy was its possible use as a shielding material, during initial studies it became evident that small additions of lithium had a pronounced hardening effect on the pure lead. This hardness increase was found to be a function of the amount of lithium in the lead. Illustrated in fig. 3 are observed hardness values vs lithium content of some as-cast alloys.

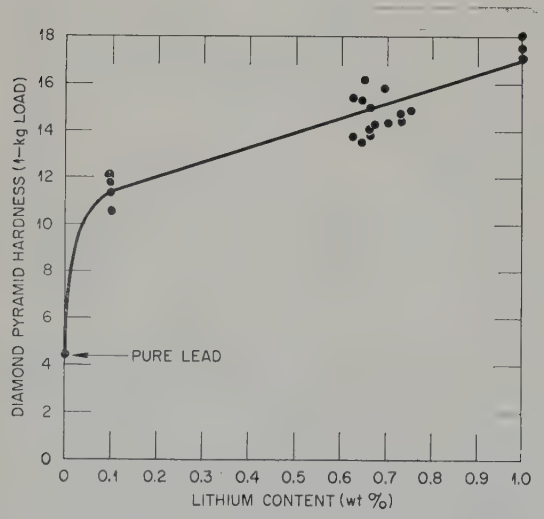

Fig. 3. Hardness vs lithium content of lead-lithium alloys.

As a result of the observed increases in hardness, it was decided that additional mechanical data on the 0.69 % alloy should be obtained. Therefore, creep tests and tensile tests at both room and elevated temperatures were conducted on the alloy.

2.3. Tensile tests

Tensile tests were conducted in room temperature air and at 110° C in oil. Room temperature tests were used to determine relative strength of the lead-0.69 wt % lithium alloy compared to lead-0.06 wt% copper and pure lead. Lead-copper is another alloy being considered for shield applications. The 110° C temperature was chosen as a typical shield temperature associated with reactors operating at relatively high power levels.

The results of tensile tests at room temperature are listed in table 1 and those at 110° C are listed in table 2. Any large differences in the

Table 1

Results of tensile tests on lead-lithium alloy in air at room temperature

Lithium content (wt %)	Strain rate (cm/cm/min)	Tensile strength (psi)	Elongation (% in 7.5 cm)
0.65	0.05	5485	39
0.67	0.05	6308	22
0.65	0.25	7654	22
0.67	0.25	6490	16
0.68	0.25	6879	14
0.70	0.25	6860	11
0.71	0.25	7892	29
0.72	0.25	7230	23
† Pure lead	0.25	1433	33
† Pb-0.06 wt % Cu	0.25	1746	53

† Included for comparison.

Table 2

Results of tensile tests on lead-lithium alloy at 110° C in oil

Lithium content (wt %)	Strain rate (cm/cm/min)	Tensile Strength (psi)	Elongation (% in 7.5 cm)
0.63	0.17	3502	55
0.64	0.17	3019	56
0.67	0.17	3553	55
† Pure lead (99.99+%)	0.17	1088	63
† Pb-0.06 wt % Cu	0.17	1365	38

† Included for comparison.

elongation results in table 1 can be attributed to casting flaws in the gagelength portion of the test specimens. The superior strength of the lead-lithium alloy is evident when compared with the lead-copper alloy and pure lead.

2.4. Creep tests

The results of creep tests at relatively high stress levels (1000 to 3000 psi) conducted at room temperature are listed in table 3 and plotted in fig. 4. For a comparison of these creep values with that of pure lead, stress rupture life of common, desilverized lead is

Table 3

Results of creep tests on lead-lithium alloy in air at room temperature

Lithium content (wt %)	Stress (psi)	Elongation (% in 7.5 cm)	Stress-rupture life (h)
0.67	1000	1.8	†
0.63	1500	52.0	1008
0.68	2000	10.0	297
0.71	2500	30.3	198
0.66	3000	26.6	41.8

† Test terminated after 1000 h.

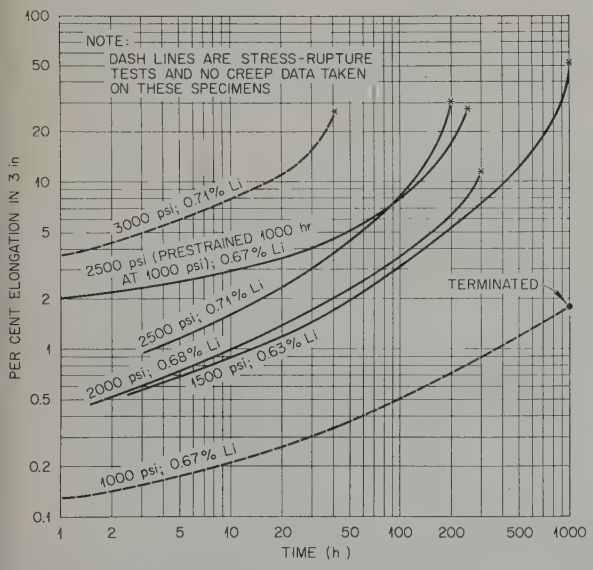

Fig. 4. Creep curves for lead-lithium specimens in air at room temperature. Note: The 1000 psi test was terminated after 1000 h and the prestrained specimen used for a creep test at 2500 psi.

Table 4

Results of creep tests on lead-0.69 % lithium alloy in air at 110° C

Stress (psi)	Rupture life (h)	Elongation (% in 7.5 cm)
100	12 382 (in test)	9.6
200	6 354	39.0
300	2 276	36.4
400	1 400	28.0
500	598	19.3
600	198	39.9
100 (Pb-0.06 wt % Cu alloy)	20 885 (in test)	9.6

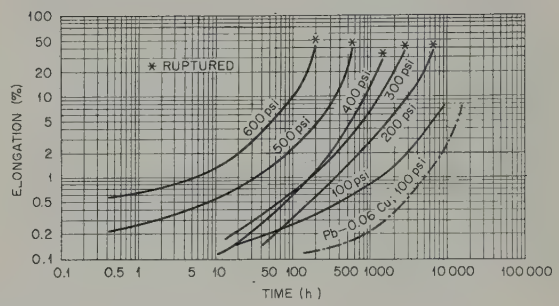

Fig. 5. Creep curves for lead-lithium alloy in air at 110° C. Lead-copper included for comparison purposes.

approximately 10 h at 1000 psi [6]) while the lead-0.69 wt % Li alloy showed a stress rupture life of 1008 h at 1500 psi (fig. 4). Creep tests at lower stress levels (100 to 600 psi) in 110° C air were conducted also and the results are listed in table 4 and plotted in fig. 5. By comparing curves in fig. 5 it can be seen that the lead-copper alloy has better creep resistance at 110° C than the lead-lithium alloy. The effect of oil and air on the creep strength of the lead-lithium alloy has not been determined. Interaction between specimen and environment may be a contributing factor to the creep behavior of this alloy at elevated temperatures.

2.5. Corrosion experiments

Aqueous corrosion tests were conducted on samples of the alloy since the experimental 90 cm-square by 10 cm thick slab was to be

TABLE 5

Results of aqueous corrosion tests on lead-0.65 wt % lithium alloy in distilled water (Surface-to-volume ratio = 0.08 cm^{-1})

Water temperature (° C)	Test duration (h)	Specimen wt gain (g/cm^2)	Lithium dissolved (mg of Li per cm^2 of alloy surface)	Diameter increase (%)
100	50	0.010	10.4	5.7
100	100	0.018	11.6	5.7
20	50	0.006	1.1	2.8
20	100	0.013	2.6	5.7

immersed in water during subsequent shielding experiments.

The corrosion specimens, 9 mm dia rods, were subjected to distilled water at room temperature and at 100° C for various times, and the water then analyzed for lithium content. Table 5 lists results of individual tests including specimen weight gains. Weight gains on corrosion specimens were approximately linear for the times and temperatures used. The loss of lithium to the water per unit area of alloy surface increased with time of exposure and test temperature.

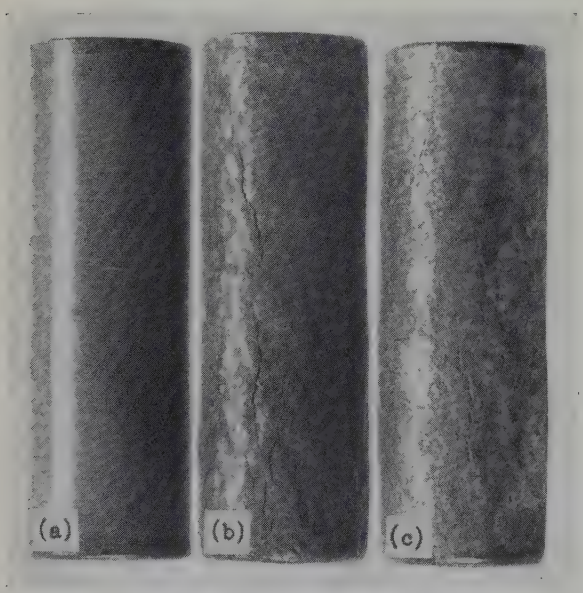

Fig. 6. Lead-0.65 wt % lithium alloy specimens. (a) As-machined, (b) tested in distilled water at room temperature for 100 h, (c) tested in boiling distilled water for 100 h. Note cracks and dimensional increases that have occurred in the tested specimens.

The volume increase and tendency for the alloy to crack when exposed to water are illustrated in fig. 6.

2.6. Oxidation tests

Due to the reactivity of lithium, it was desired to determine whether the small quantity of lithium present in the alloy would cause it to oxidize more readily than does pure lead. Oxidation tests were performed on the material in air at 110° C for various periods. Pure lead samples were included as control pieces. Machined cylindrical pieces were used for test specimens. Volume increases of the order of 0.1 to 0.2 % were observed on all oxidation samples. Small weight changes (table 6) also accompanied each test.

TABLE 6

Results of oxidation tests on lead-lithium and pure lead specimens in 110° C air

Time (h)	Weight change (mg/cm^2)	
	Pure lead	Alloy
100	− 0.13	+ 0.20
500	Nil	+ 0.62
1000	Nil	+ 0.53

Metallographic examination of the oxidized lead-lithium alloy specimens showed a white band approximately 2 mils deep on the edges (fig. 7). This shallow case had become depleted in lithium during the oxidation process. Chemical analysis showed a 0.4 wt % lithium

content in 2 mils of turnings machined off the surface of the test specimen following the 500-h oxidation test whereas this layer contained 0.7 wt % lithium before test.

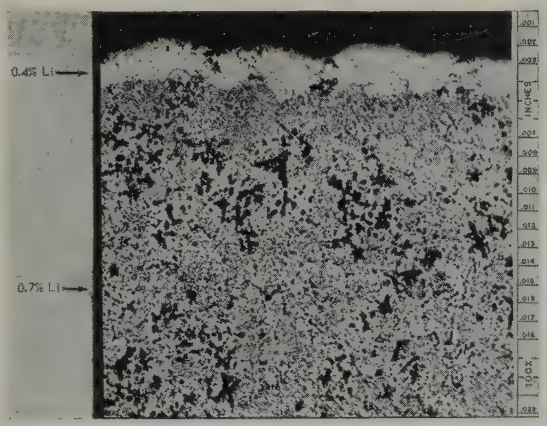

Fig. 7. Lead-lithium alloy oxidized in air for 500 h at 110° C. The white band at the edge contains approximately 0.4 wt % lithium. Attack can be seen at the edge of the specimen to a depth of about 2 mils (0.05 mm). Original lithium content was 0.7 wt %. Etchant: glycerine, HNO_3, and acetic acid.

3. Alloying, Casting and Rolling of Lead-Lithium Billets

To determine the shielding characteristics of the lead-0.69 wt % lithium alloy, the Bulk Shielding Facility (Swimming Pool Reactor) required a 90 cm square by 10 cm thick slab of the material to immerse in the pool, adjacent to the reactor. Since this slab would weigh approximately 1000 kg, it was not possible with the available equipment to melt a charge of this size under an inert atmosphere and cast it in one piece. Therefore 8 billets, 54 cm square and 4.4 cm thick (weight approximately 150 kg each) were cast and rolled to 1.2 cm thickness and sheared to 90 cm square to make a 10 cm thick laminated slab composed of 8 plates.

Rolling characteristics of the lead-0.69 wt % lithium alloy were studied. A 2.5 cm dia disc 1.5 cm thick was rolled to 92.5 % reduction with no cracking or rolling defects observed. Hardness of the alloy did not increase during rolling.

The method for preparing the billets is shown

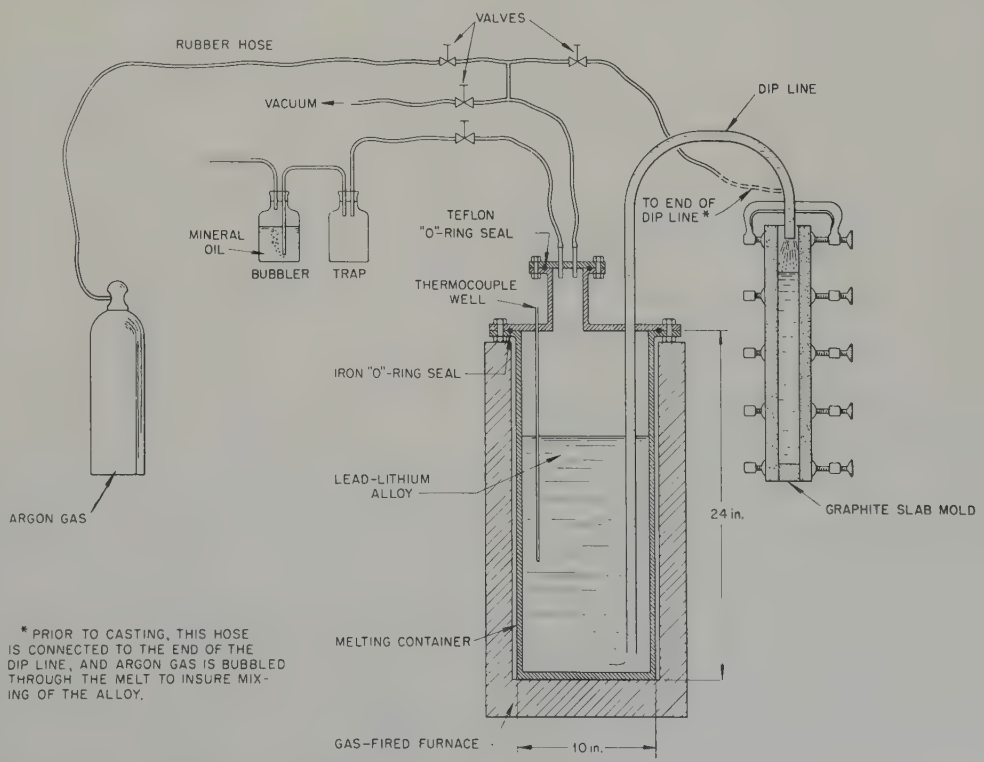

Fig. 8. Schematic diagram of apparatus used to cast lead-lithium slabs.

schematically in fig. 8. An iron pot 25 cm in dia and 60 cm high, fitted with a dip line and vacuum-tight loading port, was used as the melting and alloying container. Suitable fittings were attached to provide either vacuum or argon gas in the container. The charge consisted of 140 kg of chemical lead (99.90 %) and 1 kg of low-sodium-grade lithium (0.72 wt % of the total charge).

The alloying pot containing the charge was evacuated prior to heating. The charge was then heated utilizing a protective argon atmosphere. Rapid alloying as evidenced by a temperature rise in the melt pot was found to begin at a temperature of approximately 300° C. The charge was heated to a temperature of 360° C. Purified argon was then bubbled through the melt for about five minutes to assure adequate mixing of the alloy. The melt pot was evacuated for five minutes to degas the alloy prior to casting. Argon gas pressure was then applied to the surface of the melt and the alloy blown through the dip line into a graphite mold preheated to about 300° C. The alloy was prevented from sticking to the graphite mold by coating the mold with a paste of zirconium flour. Sound castings were made by preheating the molds and controlling the rate and direction of cooling.

To minimize oxidation of the alloy during solidification, the dross which was formed on the surface was not skimmed off. After solidification and cooling, the dross (approximately 2.5 to 5 cm) was sawed off the top of the casting and discarded. This dross was rich in metallic lithium, as evidenced by a rapid reaction and the evolution of hydrogen when placed in water. Large amounts of lithium oxide and lithium nitride were also present. The upper portion of the casting may also have become lithium-rich due to segregation of the lighter PbLi intermetallic phase if the alloy was of hypereutectic composition (greater than 0.69 wt % lithium) at the time of casting.

Samples for lithium analysis were taken from the bottom, middle, and top at the edge of each casting after removing dross and from the corners of each rolled plate after shearing off excess material. The location and lithium content of these samples are shown in tables 7 and 8.

The areas which were found to be exceptionally high in lithium content (greater than 0.9 % lithium) may have occurred as a result of entrapment of dross in these areas. Due to size limitations, it was not possible to saw off more than two inches from the top of each billet. Partial lithium enrichment of the upper areas may have been due to segregation of the less dense PbLi compound but this is not thought to be the major factor, since all billets would have been consistently high in lithium near the top if this were the principal segregation mechanism. No difficulty was encountered during rolling or shearing the billets. Shielding tests made on the finished plates have demonstrated that the lead-lithium alloy minimizes secondary gamma-ray production.

TABLE 7

Location and analysis of samples from the eight cast lead-lithium alloy billets

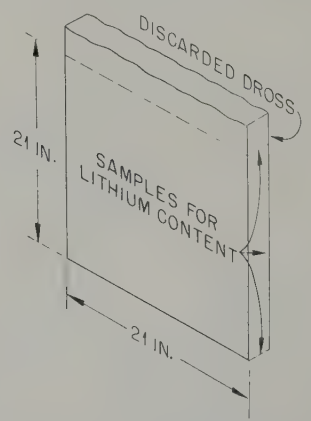

Lithium content (wt %)

Top	Middle	Bottom
1.21	0.82	0.78
0.82	0.74	0.74
0.86	0.70	0.71
0.76	0.68	0.66
0.82	0.68	0.78
0.64	0.78	0.75
0.64	0.74	0.73
0.92	0.83	0.76

Table 8

Location and analysis of samples from the eight rolled lead-lithium alloy plates

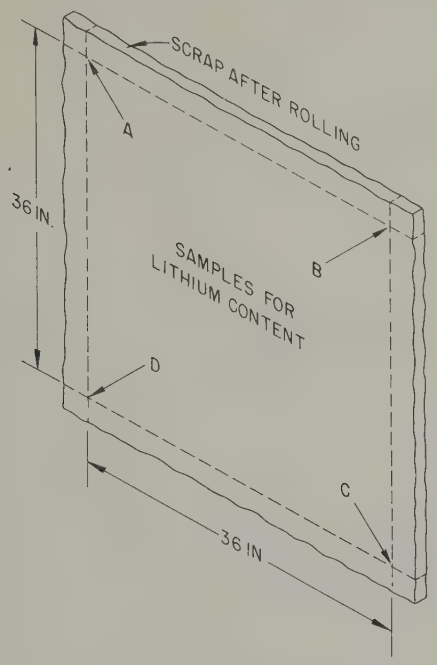

Lithium content (wt %)

A	B	C	D
0.84	0.78	0.72	0.61
1.37	1.19	0.78	0.68
1.25	1.11	0.61	0.76
0.87	0.97	0.71	0.80
0.99	0.66	0.62	0.57
0.68	0.72	0.62	0.69
0.67	0.82	0.62	0.74
0.68	0.64	0.59	0.61

4. Miscellaneous

4.1. Joining lead-lithium alloy

The feasibility of joining lead-lithium alloys by conventional "burning" (melting the edges of two pieces of lead with a gas torch and allowing the pieces to fuse), inert-gas welding, and soldering (the joining of two pieces by fusing their edges and filler rod of the same material with a hot iron) was determined. Soldering requires no flame and the best penetration was obtained by this method (fig. 9). The reactivity of lithium is responsible for the limited usefulness of the high temperature joining methods.

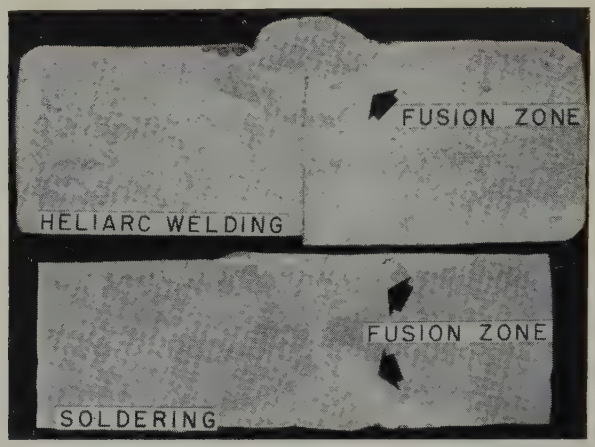

Fig. 9. Cross section of lead-0.69 wt % lithium alloy joined by heliarc welding and soldering. (2 ×)

4.2. Density measurements

Density measurements were made on the cast lead-lithium alloy by means of a Jolly balance. A value of 10.5 g/cc, determined with this instrument, was used in making up all pot charges of the alloy.

4.3. Chemical compositions of lead

The analyses of the *Doe Run* † lead used to fabricate all mechanical and corrosion test

Table 9

Compositions of types of lead used in metallurgical studies

Element	Percentage by weight		
	Doe Run lead (Max.)	Chemical lead (Max.)	Chemical lead (Min.)
Arsenic, antimony, tin	0.0001	0.002	
Copper	0.0001	0.080	0.040
Iron	0.0001	0.002	
Zinc	0.0001	0.001	
Silver	0.0003	0.020	0.002
Bismuth	0.0019	0.005	
Cadmium	0.0004		
Nickel, cobalt	0.0001		
Minimum lead (by difference)	99.9969		99.9

† „Doe Run" is a copyrighted trade name of the St. Joe Lead Company.

specimens, and that of chemical lead used in making the experimental neutron-gamma-ray shield, are given in table 9.

Acknowledgements

Chemical analyses included in this report were made by the Special Analysis Laboratory under the direction of W. R. Laing. Mechanical tests were conducted by C. W. Dollins and other members of the Mechanical Properties Testing Group of the Metallurgy Division under the direction of D. A. Douglas. Metallographic work was done by the Metallographic Group under the direction of R. J. Gray.

Special thanks are extended to the Neutron Physics Division of the Oak Ridge National Laboratory for initiating this study.

References

1) E. Koch, Lead Cable Sheaths Containing Lithium, U.S. Patent 926,545
2) G. Welter, Lithium Containing Bearing Metals, U.S. Patent 1,652,077
3) G. Welter, Lead-Alkali Metal Containing Bearing Metal Alloys, U.S. Patent 1,652,078
4) W. Hofmann, Blei und Bleilegierungen
5) O. Kubaschewski and J. A. Catterall, Thermochemical Data of Alloys, (Pergamon Press, London and New York, 1956) p. 13
6) C. W. Dollins and Cecil E. Betzer, Creep, Fracture and Bending of Lead and Lead Alloy Cable Sheathing, University of Illinois Engr. Expt. Station, Bulletin No. 440, p. 24

JOURNAL OF NUCLEAR MATERIALS - 3 (1959) 259–270 - NORTH-HOLLAND PUBLISHING CO., AMSTERDAM

FRITTAGE DE L'OXYDE D'URANIUM DANS L'HYDROGENE A 1350° C

A. BEL, R. DELMAS et B. FRANÇOIS

Centre d'études nucléaires de Saclay, Gif-sur-Yvette (S & O) France

Reçu 1 Mai 1959

Le frittage dans l'argon d'oxydes de grande surface spécifique conduit à des produits de plus gros grains (5–10 μ) mais de même densité que ceux obtenus de façon identique dans l'hydrogène. L'écart à la composition stoechiométrique des poudres ne paraît pas avoir d'influence sur la densité apparente du fritté.

Plusieurs oxydes de grande surface spécifique obtenus à partir d'uranate d'ammonium et de peroxyde d'uranium ont fait l'objet d'une étude systématique de frittage en atmosphère d'hydrogène. Pour une surface spécifique donnée, les densités obtenues varient en fonction de la température du palier de frittage suivant des courbes à maximum; la température correspondant à ce maximum est d'autant plus faible que la surface spécifique est plus grande.

Un procédé de préparation de poudre d'oxyde d'uranium à partir d'uranate d'ammonium et de frittage de cette matière première dans l'hydrogène à 1350° C est proposé: il permet d'obtenir des frittés à grain fin de densité 10,6.

Sintering in argon of oxides of large specific surface area produces a more coarse-grained product (5–10 μ) than does hydrogen sintering; the density is the same in each case. Departure from stoichiometric composition of the powders does not appear to influence the density of the sintered compact.

The sintering, in hydrogen, of various oxides of large specific surface area, obtained from ammonium uranate and uranium peroxide, was studied in a systematic way. With a given specific surface area, the final density varied as a function of the sintering temperature, with a maximum density for a particular temperature. This temperature is lowest when the specific surface area of the powder is the greatest.

A process is described for the preparation of uranium oxide powder from ammonium uranate and its sintering in hydrogen at 1350° C; in this way a fine-grained product of density 10.6 can be obtained.

Wenn man Oxyde mit grosser spezifischer Oberfläche unter Argon sintert, so erhält man ein grobkörnigeres Material (5–10 μ), als wenn man Wasserstoff benutzt; die Dichte ist in beiden Fällen gleich. Abweichungen von der stöchiometrischen Zusammensetzung scheinen die Dichte des gesinterten Materials nicht zu beeinflussen.

Der Sinterprozess verschiedener Oxyde mit grosser spezifischen Oberfläche, die aus Ammoniumuranat und Uranperoxyd gewonnen worden waren, wurde in Wasserstoff systematisch untersucht. Bei gegebener spezifischer Oberfläche ist die Dichte des gesinterten Materials Funktion der Sintertemperatur, mit einer Maximaldichte bei einer bestimmten Temperatur. Diese Temperatur ist umso niedriger, je grösser die spezifische Oberfläche des Oxydpulvers ist.

Es wird ein Verfahren zur Herstellung von Uranoxyd-Pulver aus Ammoniumuranat und seine Sinterung in Wasserstoff bei 1350° C vorgeschlagen; auf diese Weise lässt sich ein feinkörniges Produkt der Dichte 10.6 erzeugen.

Introduction

Le problème du frittage de l'oxyde d'uranium à une densité suffisante pour son utilisation en pile a donné lieu à des travaux très importants.

Depuis les expériences d'irradiation américaines [1]) et canadiennes [2]), on admet que la libération, hors du réseau cristallin de l'oxyde, des gaz de fission produits sous flux de neutrons, s'effectue suivant une loi de diffusion simple.

On conçoit que la fraction de gaz de fission libérée soit étroitement liée à la valeur de la porosité.

On constate en effet que la densité apparente du produit fritté influe d'une façon très importante sur ce phénomène d'évolution des gaz formés au cours de l'irradiation.

Une densité de l'ordre de 95 % de la densité théorique, soit 10,4 à 10,5, est considérée comme satisfaisante.

Les efforts déployés dans différents pays pour atteindre cet objectif dans des conditions aussi économiques que possible [3, 4, 5]), ont permis une meilleure compréhension des phénomènes et conduit à la mise en œuvre de procédés de production à une échelle parfois importante.

La matière première s'obtient généralement par calcination puis réduction dans l'hydrogène, d'uranate ou de diuranate d'ammonium. L'oxyde en poudre obtenu dans la plupart des cas a une surface spécifique faible: de l'ordre de 1 à 3 m^2/g et une composition globale $UO_{2,03}$ à $UO_{2,10}$. Son frittage s'effectue dans l'hydrogène ou l'ammoniac craqué sec à des températures de l'ordre de 1600 à 1750° C; l'introduction de vapeur d'eau semble permettre d'atteindre une densité du même ordre à une température sensiblement plus basse.

En France, une première série d'expériences [6]) effectuées sur des oxydes issus de peroxyde d'uranium a montré qu'une voie économique et techniquement très satisfaisante consistait à utiliser des poudres d'oxyde de finesse accrue. Plusieurs faits expérimentaux exposés dans cette étude paraissaient en contradiction avec les idées généralement admises [7, 8]).

Certains oxydes, de surface spécifique élevée, conduisent à des frittés de densité apparente plus importante à 1400° qu'à 1600° C.

Les différences de densités obtenues par frittage de ces oxydes dans l'hydrogène ou dans l'argon ne paraissent pas significatives.

Le frittage dans l'hydrogène sec de ces poudres d'oxyde, à basse température (1200° à 1400° C) est susceptible de conduire à des frittés de haute densité.

Au cours du présent travail, nous nous sommes efforcés de préciser ces phénomènes, d'étendre l'étude aux oxydes dérivant d'uranate d'ammonium produit par l'Usine du Bouchet [9]) et de déterminer, à une échelle supérieure à celle du laboratoire, les conditions d'application d'un procédé de frittage à basse température.

A. INFLUENCE DE L'ECART A LA STOECHIOMETRIE ET DE L'ATMOSPHERE DE FRITTAGE

1. Préparation des matières premières

La préparation des petites quantités d'oxydes nécessaires à ces essais a été effectuée suivant un procédé décrit précédemment [6]), qui permet d'obtenir, avec une précision acceptable, des poudres de surface spécifique fixée à l'avance.

Un lot de peroxyde d'uranium calciné pendant 5 heures à 450° C a conduit à un UO_3 de 13 m^2/g de surface spécifique. La réduction de cet oxyde s'opérait dans l'hydrogène suivant un programme de température comportant deux paliers successifs de deux heures chacun, l'un à 400° C, l'autre à une température appelée ici "température de réduction" dont la valeur détermine la surface spécifique du produit final; les températures de réduction étudiées ont été de 600, 800 et 1000° C.

Une partie de chacun des oxydes produits a été réoxydée d'une façon ménagée, l'autre conservée et manipulée sous argon pur.

Les compositions et les surfaces spécifiques des oxydes ainsi obtenus sont indiquées dans le tableau 1.

Tableau 1

Echantillon	Température réduction (° C)	Surface (m^2/g)	Composition UO_x x =
G 01 a	600	14	2,03
b			2,21
J 01 a	800	8	2,04
b			2,13
L 01 a	1000	4,5	2,00
b			2,06

2. Mise en forme et frittage

Les oxydes ont été comprimés (avec 3 % de camphre et 0,5 % de stéarine) à 4 t/cm^2 en pastilles de 10 mm de diamètre et de 5 à 6 mm de hauteur; la densité en cru variait de 5 à 6,2.

Les frittages ont eu lieu à 3 températures:

Tableau 2

Poudre	O/U	Frittage à 800° C sous		Frittage à 1000° C sous		Frittage à 1200° C sous	
		hydrogène	argon	hydrogène	argon	hydrogène	argon
G 01 a	2,03	5,64	5,28	9,64	9,69	10,62	10,35
b	2,21	6,23	6,12	9,32	9,30	10,63	10,39
J 01 a	2,04	6,14	6,04	9,17	9,32	10,37	10,29
b	2,13	6,00	6,18	9,55	9,00	10,56	10,43
L 01 a	2,00	6,26	6,36	7,85	8,68	10,06	10,14
b	2,06	6,20	6,20	7,39	7,84	9,81	9,96

800, 1000 et 1200° C sous hydrogène et sous argon avec une vitesse de chauffe de 150°/heure et une durée de maintien en palier de 3 heures. La descente en température était inférieure à 300°/heure. La détermination de la densité apparente et de la porosité des pastilles s'effectuait par pesée hydrostatique dans l'eau; certains échantillons ont été polis et attaqués pour en révéler les grains.

3. Résultats

Les densités obtenues sont rassemblées dans le tableau 2 et leurs variations en fonction de la température de palier de frittage portées sur les courbes de la figure 1.

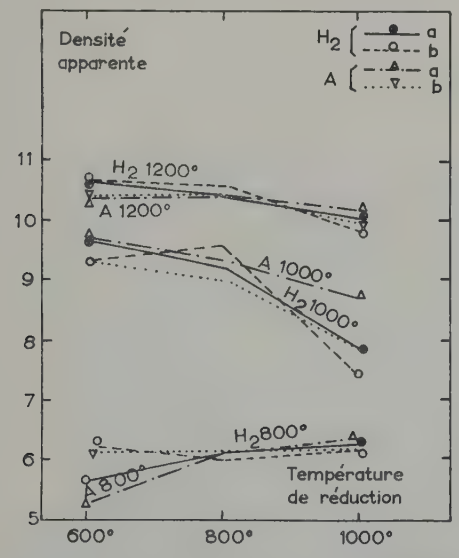

Fig. 1. Densité en fonction de la température de réduction des oxydes à température de frittage constante.

Le début du frittage se produit généralement entre 800 et 1000° C sous hydrogène comme sous argon. A 1200° C, il n'y a pas de différence notable entre les densités des pastilles frittées sous argon et sous hydrogène. Dans les deux cas les porosités ouvertes sont nulles ou presque nulles.

Les examens micrographiques révèlent par contre une différence essentielle. Dans l'hydrogène à 1200° C le frittage conduit à des oxydes à grains fins (1 μ) et à porosité dispersée aux joints de grains (fig. 2). Dans l'argon les grains sont beaucoup plus gros (5 à 10 μ) et enferment une partie importante des pores (fig. 3).

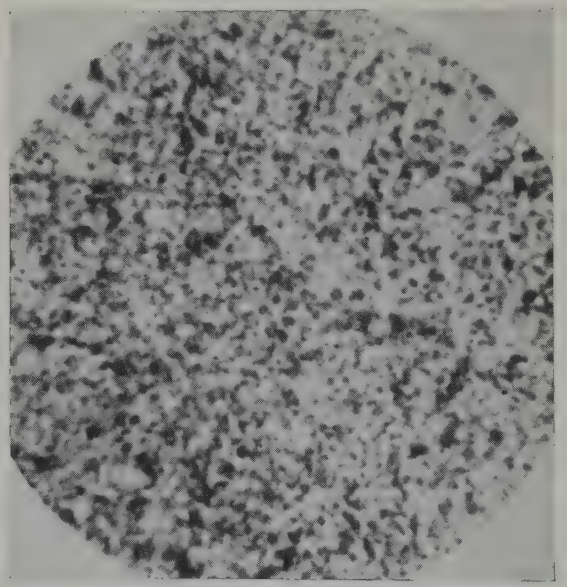

Fig. 2. Attaque oxydante. Frittage à 1200° C dans l'hydrogène. G 01 a × 1000.

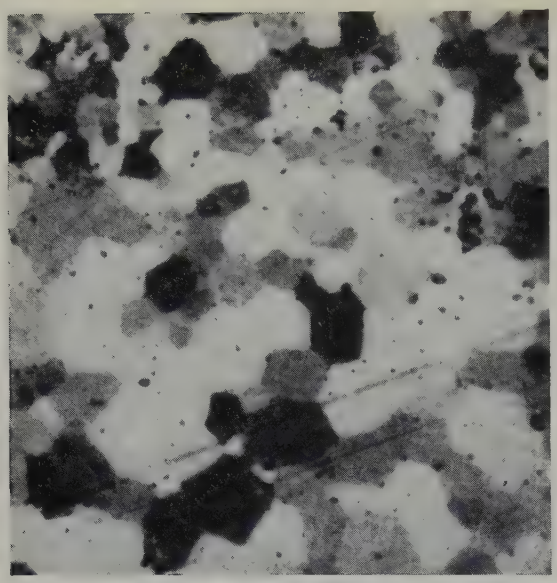

Fig. 3. Attaque oxydante. Frittage à 1200° C dans l'argon. G 01 a × 1000.

Cette cristallisation plus rapide en atmosphère neutre qu'en atmosphère réductrice est à rapprocher du comportement déjà signalé [6]) des poudres qui ont subi des traitements analogues.

Par ailleurs on ne constate pas de différences significatives de densité, dans l'une ou l'autre atmosphère, selon l'écart à la composition stoechiométrique.

B. ETUDE DU FRITTAGE DANS L'HYDROGENE SEC D'OXYDES DE GRANDE SURFACE SPECIFIQUE

1. Etude systématique des oxydes issus de peroxyde d'uranium

1.1. Mode operatoire

Une quantité homogène de trioxyde, de 13 m^2/g de surface spécifique, préparée par calcination de peroxyde à 450° C, a servi de matière première aux expériences décrites ci-dessous.

Cet UO_3 a été réduit par l'hydrogène lors de cycles de températures comportant un palier de 2 heures à 400° C puis un palier de 2 heures à une température variable de 500 à 1100° C. Les poudres d'UO_2 ont été protégées de la réoxydation par une atmosphère d'argon à la sortie du four.

Les oxydes ont été comprimés sous 4 t/cm^2 (après incorporation de 3 % de camphre et 0,5 % de stéarine) en cylindres de diamètre 10 mm, hauteur 5 à 6 mm.

La densité du comprimé cru variait de 5 à 6,2.

Le frittage a été conduit sous hydrogène sec à des températures comprises entre 900 et 1500° C, la vitesse de chauffe étant de 150° C/heure et la durée du palier de température constante de 3 heures.

La densité apparente et la porosité des échantillons frittés ont été mesurées par pesée hydrostatique dans l'eau.

1.2. Resultats

Le tableau 3 rassemble les valeurs obtenues:

La figure 4 représente, pour chaque poudre, la variation des densités apparentes en fonction des températures de palier.

A chaque température de réduction inférieure à 1000° C correspond une température optimum de frittage, comprise entre 1250 et 1400° C.

Cette température optimum parait d'autant plus faible que la température de réduction est plus basse.

De plus il semble exister une température

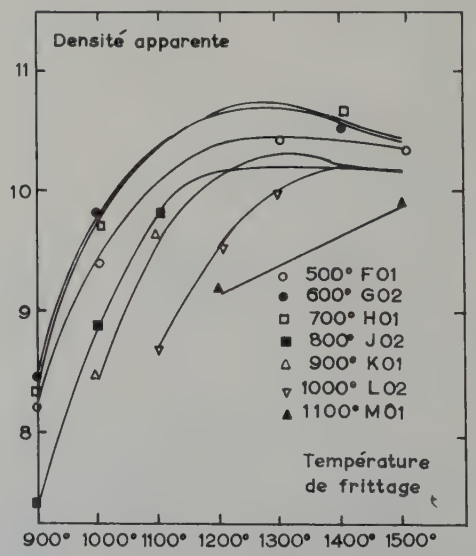

Fig. 4. Densité en fonction de la température de frittage, à température de réduction constante.

Tableau 3

Poudre	Température de réduction (° C)	Température de frittage (° C)						
		900	1000	1100	1200	1300	1400	1500
F 01	500	8,24	9,42	10,15	10,33	10,44	10,36	10,41
G 02	600	8,49	9,81	10,35	10,65	10,71	10,56	10,45
H 01	700	8,33	9,71	10,35	10,65	10,73	10,62	10,45
J 02	800	7,43	8,92	9,85	10,19	9,98	10,35	10,32
K 01	900		8,46	9,61	10,05	10,33	10,15	10,19
L 02	1000			8,72	9,56	10,06	10,29	10,17
M 01	1100				9,25	9,26	9,68	9,85

optimale de réduction de l'oxyde supérieur examiné, comprise entre 600 et 700° C.

Enfin l'allure du frittage traduite par la courbe relative à l'oxyde réduit à 1100° C, de faible surface spécifique, est cohérente avec les indications habituelles de la littérature; cet oxyde parait représentatif de celui qui est généralement préparé en vue de son frittage.

L'emploi de poudres de grande finesse permet donc l'obtention de densités très élevées par frittage à basse température.

2. Extension aux oxydes dérivés d'uranate d'ammonium

2.1. Mode operatoire

Cette étude, parallèle à la précédente, a été menée avec le souci d'une application industrielle proche; les oxydes obtenus ont donc été réoxydés d'une façon ménagée, après leur réduction, dans un mélange d'azote et de 2 % d'oxygène. Dans ces conditions, il a paru nécessaire de reprendre l'examen comparatif d'oxydes provenant de peroxyde et d'uranate.

Leur origine et leurs surfaces spécifiques sont notées dans le tableau 4.

Après incorporation de 3 % de camphre et 0,75 % de stéarine et granulation à travers un tamis 30 ASTM ces poudres étaient comprimées en cylindres de diamètre 10 mm, hauteur 10 à 12 mm sous 5 t/cm², au moyen d'une presse hydraulique à commande manuelle (voir tableau 5).

Tableau 5

	Densité apparente du granulé	Densité apparente des comprimés ($p = 5$ t/cm²)	Rapport de compression †
Poudre B	1,35	5,25	3,9
„ C	1,4	5,6	4
„ D	1,6	6,1	3,8
Poudre H	1	5,5	5,5
„ J	1,45	6,3	4,3

† Rapport entre la hauteur de poudre admise dans la matrice et la hauteur du comprimé.

Il convient de signaler un défaut de mise en forme qui se produit lors de l'éjection, sur la face supérieure des pièces. Il se manifeste par l'abattement de l'angle vif. Ce phénomène disparait si le démoulage a lieu en maintenant

Tableau 4

Matière première	Oxyde intermédiaire	Référence UO_2	Surface spécifique (m²/g)	Composition
Peroxyde d'uranium	UO_3 13 m²/g	B	17	$UO_{2,30}$
		C	10	$UO_{2,18}$
		D	5,5	$UO_{2,09}$
Uranate d'ammonium	UO_3 17m²/g	H	16	—
		J	4,5	—

le poinçon supérieur au contact du comprimé.

Pour éviter l'oxydation des résistances de molybdène des fours de frittage, les liants organiques ont été éliminés par chauffage de deux heures sous un vide d'un millimètre de mercure à 180° C.

Les frittages sous ammoniac craqué sec ont suivi le cycle thermique suivant: chauffage 75° C/heure, palier de 5 heures à température maximum, refroidissement à 100° C/heure.

Les températures de palier examinées ont couvert le domaine 1200–1650° C.

Les densités apparentes ont été déterminées par pesée hydrostatique dans le toluène.

2.2. Densification

Les figures 5 et 6 établies d'une manière analogue à la figure 4 rendent compte de la variation de densité apparente en fonction de la température du palier, pour des oxydes en provenance respectivement de peroxyde et d'uranate d'ammonium.

Les variations définies par ces séries de courbes confirment qualitativement les résultats exposés plus haut.

Cependant les densités obtenues lors de ces essais sont généralement inférieures à celles signalées au cours de l'étude systématique (*B.* 1). A cet égard il faut signaler que les modes opératoires sont différents sur les points suivants:

Le mode de pressage: la commande de la presse est automatique pour la première série d'essais, manuelle en ce qui concerne la seconde.

La différence de hauteur des cylindres comprimés.

La différence de composition chimique entre les oxydes engagés au frittage: quasi-stoechiométriques dans la première série, ils sont largement réoxydés dans la seconde.

La comparaison entre les oxydes issus de peroxyde ou d'uranate est favorable à ces derniers: la vitesse de densification semble plus grande et les densités obtenues un peu plus élevées.

2.3. Recristallisation

Les examens micrographiques ont été effectués après sectionnement des échantillons par un plan passant par leur axe et attaque d'une surface polie mécaniquement.

Le tableau 6 donne en regard de résultats suédois [10]) l'ordre de grandeur des dimensions de grains. Il indique nettement une croissance

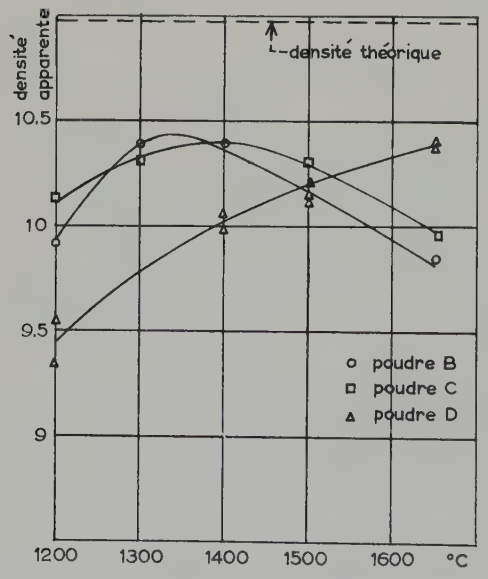

Fig. 5. Densité en fonction de la température de frittage, surface spécifique de poudre constante (au départ de peroxyde d'uranium).

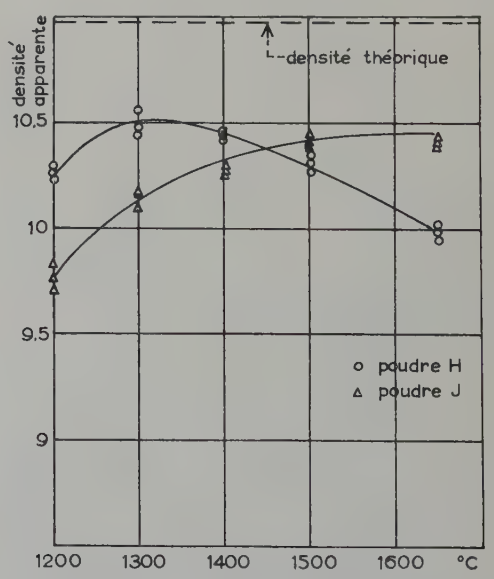

Fig. 6. Densité en fonction de la température de frittage, surface spécifique de poudre constante (au départ d'uranate d'ammonium).

Tableau 6

Température de frittage (° C)	Poudre B		Poudre D		Poudre H		Poudre J		UO_2 suédois
	Diamètre moyen (μ)	densité apparente	Diamètre moyen (μ)	densité apparente	Diamètre moyen (μ)	densité apparente	Diamètre moyen (μ)	densité apparente	Diamètre moyen (μ)
1200	< 1	9,9	< 1	9,5	< 1	10,3	< 1	9,8	
1300	1	10,4	1	9,8	3	10,5	1	10,1	
1400	3	10,4	2	10,0	3	10,45	3	10,3	0,7
1500	15	10,2	5	10,2	10	10,3	5	10,4	
1600									2,4
1650	10	9,8	8	10,4	15	10,0	7	10,4	
1800									11

des cristaux plus rapide dans le cas des frittés provenant des poudres les plus fines.

Il faut remarquer par ailleurs que la porosité est placée généralement aux joints de grain.

Les figures 7, 8, 9 et 10 montrent des surfaces polies d'UO_2 provenant de poudre H frittés respectivement à 1300, 1400, 1500 et 1650° C.

Par comparaison avec la figure 10 la figure 11 représente un oxyde issu de poudre J fritté à la même température (1650° C).

2.4. Interpretation

Les plus faibles valeurs de densité obtenues, dans le cas de poudres de grande surface spécifique, et pour les températures de frittage les plus élevées sont à rapprocher de la vitesse de grossissement des grains lors de ces frittages (figs. 4, 5 et 6). Nous proposons d'interpréter ce comportement par une compétition entre deux phénomènes: la croissance des cristaux et l'élimination des pores, le premier étant prépondérant à haute température.

J. E. Burke [11]) a fait des remarques analogues dans le cas du frittage de l'alumine: l'introduction d'inhibiteurs de cristallisation favorisait le phénomène global de densification. Ici l'inhibition de la cristallisation se réduit à un effet de température.

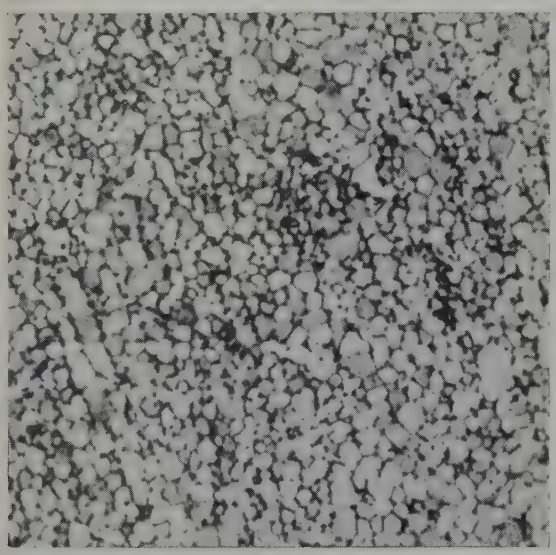

Fig. 7. Attaque acétonitrique. Frittage à 1300 ° C dans l'hydrogène. H. × 1000.

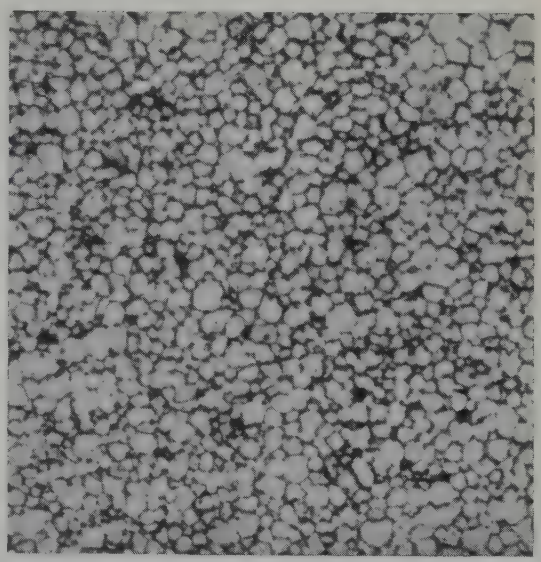

Fig. 8. Attaque acétonitrique. Frittage à 1400° C dans l'hydrogène. H. × 1000.

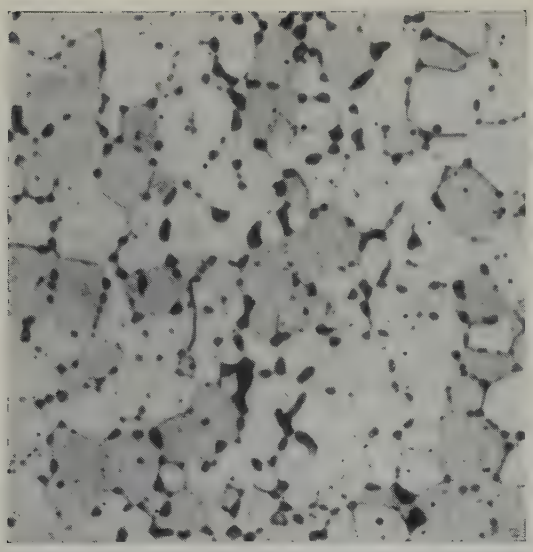

Fig. 9. Attaque acétonitrique. Frittage à 1500° C dans l'hydrogène. H. × 1000.

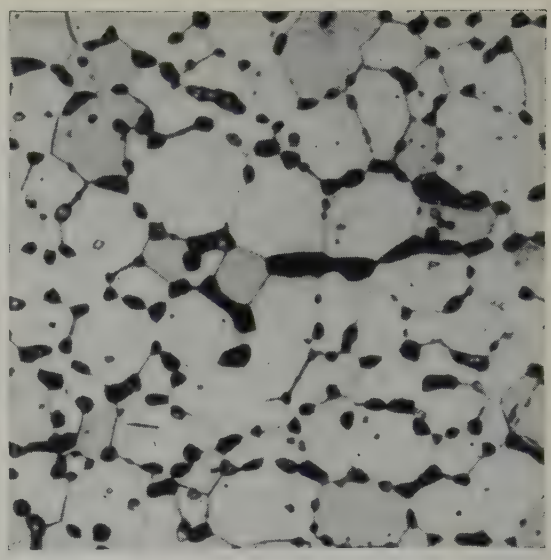

Fig. 10. Attaque acétonitrique. Frittage à 1650° C dans l'hydrogène. H. × 1000.

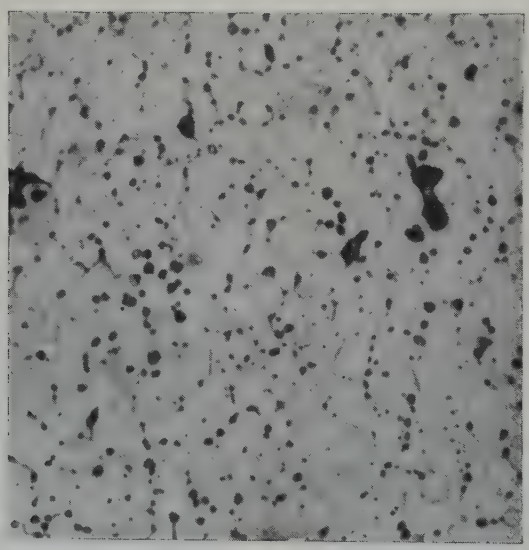

Fig. 11. Attaque acétonitrique. Frittage à 1650° C dans l'hydrogène. J. × 1000.

C. ESSAI DE DEFINITION D'UN PROCEDE

Les résultats décrits ci-dessus suggéraient d'étudier, à une échelle plus proche des conditions de la production, la préparation de poudres de caractéristiques repérées et leur frittage dans l'hydrogène à basse température.

1. Préparation des poudres

1.1. Calcination

On sait que l'évolution de la composition chimique et de la structure des précipités lors de leur calcination à l'air provoque une variation concomitante des surfaces spécifiques.

Les essais ont été conduits de la manière suivante:

α) Séchage du produit précipité à 120° C pendant 24 heures et broyage sommaire.

β) Maintien à une température de calcination constante pendant 5, 10 et 20 heures.

Les températures mises en œuvre ont été de 350, 400, 450 et 500° C.

Les textures des poudres ainsi obtenues ont été repérées par mesure de leur surface spécifique (technique BET).

Chaque essai portait sur 6 kg de produit précipité disposés dans deux capsules de porcelaine.

Le four de calcination était un four électrique à résistances de kanthal dont la régulation était assurée par un thermocouple voisin des résistances; le repérage de la température moyenne de la poudre traitée s'effectuait par un thermocouple plongé au cœur de la charge.

Les variations de surface spécifique en fonction du temps, à température constante, sont représentées sur les figures 12 en ce qui concerne le peroxyde d'uranium et 13 pour l'uranate d'ammonium.

Ces courbes mettent en évidence une différence nette de comportement entre les deux produits examinés: alors que la surface spécifique évolue considérablement à chaque température dans le cas du peroxyde, elle reste approximativement constante dans un large domaine de températures et de durée dans le cas de l'uranate d'ammonium.

Il est probable que ces résultats peuvent s'interpréter par la différence de structure entre les trioxydes obtenus au départ de chacun de ces deux composés [12]).

La calcination du peroxyde conduirait à un UO_3 amorphe dont l'évolution progressive vers une phase cristallisée se ferait avec une diminution de surface interne.

Au contraire, le trioxyde provenant d'uranate d'ammonium aurait la structure cristalline d'un oxyde hydraté de formule $UO_3 \,.\, nH_2O$ de texture vraisemblablement beaucoup moins dépendante des conditions de calcination.

1.2. Reduction

Les poudres obtenues étaient disposées en lits de 1 cm d'épaisseur sur sole de Mo, dans des fours électriques à résistances apparentes de Mo, fonctionnant sous atmosphère réductrice d'ammoniac craqué séché sur silicagel et perchlorate de magnésium.

La charge unitaire de chaque four avoisinait 1 kg.

Débit moyen: de l'ordre de 6 l/minute,

Régime de température: palier de 20 heures

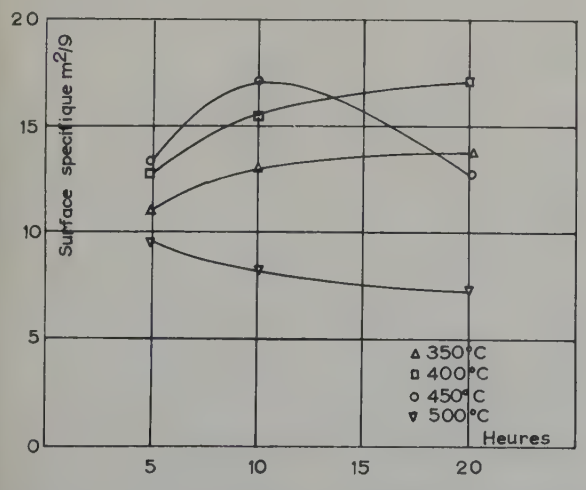

Fig. 12. Surface spécifique en fonction du temps de calcination du peroxyde d'uranium à température constante.

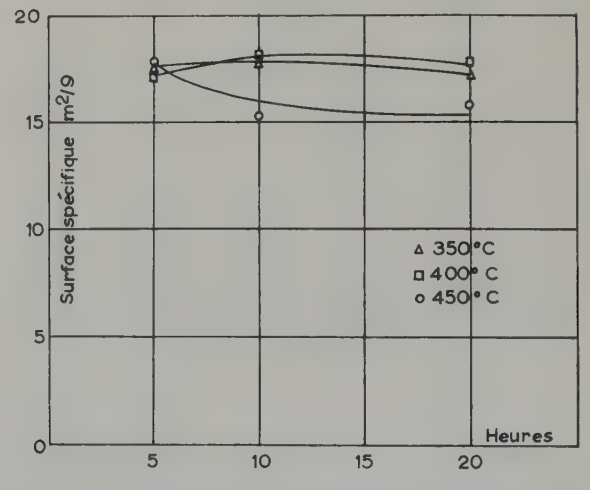

Fig. 13. Surface spécifique en fonction du temps de calcination de l'uranate d'ammonium à température constante.

Tableau 7

Matière première	Oxyde intermédiaire		Régime de réduction		Produit obtenu après réoxydation ménagée	
	Régime de calcination	Surface spécifique (m^2/g)			Surface spécifique	O/U
Peroxyde d'uranium	20 h—350° C	14	20 h—400° C	2 h— 650° C	17 †	2,30
				2 h—1000° C	5	2,08
	20 h—400° C	17	20 h—400° C	2 h— 650° C	20	2,25
	20 h—450° C	13	20 h—400° C	2 h— 650° C	10	2,18
				2 h—1000° C	5	
	20 h—500° C	7,5	20 h—400° C	2 h— 650° C	7	2,16
Uranate d'ammonium	20 h—350° C	17	20 h—400° C	2 h— 650° C	16	2,27
				2 h—1000° C	4,5	2,07
	20 h—400° C	18	20 h—400° C	2 h— 650° C	14	
				2 h—1000° C	5	non mesuré
	20 h—450° C	16	20 h—400° C	2 h— 650° C	13,5	
				2 h—1000° C	6	non mesuré

† L'augmentation de surface spécifique est significative. Elle peut s'interpréter par une évolution de la texture de l'oxyde entre 350 et 400° C avant que la réduction soit complète à coeur de grain.

à 400° C, puis palier de 2 heures soit à 650 soit à 1000° C, refroidissement complet dans l'hydrogène et réoxydation dans un mélange d'azote à 2 % d'oxygène.

Le palier à 400° C a pour objet d'obtenir la réduction quasi-complète de l'oxyde supérieur sans diminution de surface spécifique.

La durée de 20 heures a été adoptée comme standard, étant donné l'épaisseur des lits de poudres en traitement et les médiocres caractéristiques de contact solide-gaz imposées par le type de four utilisé.

Les résultats acquis précédemment ont déterminé le choix des températures de 650 et 1000° C.

Le tableau 7 rend compte de quelques résultats relatifs à des poudres de surface spécifique variable.

1.3. En resume

La calcination de l'uranate d'ammonium permet l'obtention de trioxyde d'uranium de surface spécifique 15 m^2/g environ si la température est comprise entre 350 et 450° C.

Ce comportement offre une grande sécurité pour la production industrielle de poudres de caractéristiques constantes, dans la mesure où la surface spécifique peut être considérée comme critère de l'aptitude au frittage.

Un procédé de préparation continue, dont l'étude va débuter, utilisera des fours rotatifs.

2. Mise en forme et frittage

a) Les essais ont été conduits sur une quantité de 1 kg d'oxyde en provenance d'uranate d'ammonium, de caractéristiques suivantes:

Surface spécifique: 13,5 m^2/g.

Composition: $UO_{2,23}$.

b) Le granulé obtenu dans les conditions habituelles (partie B. 2) à partir de cette poudre, avait une densité apparente de 1. Cette valeur conduit sous une pression de 5 t/cm^2 à un rapport de compression de l'ordre de 5, donc à des hauteurs de matrice de pressage trop élevées et à des dosages volumétriques imprécis.

Il est donc indispensable, en fabrication, d'effectuer une compression préliminaire et un concassage des comprimés obtenus.

Ce procédé permet d'obtenir un granulé de caractéristiques améliorées:

Sa densité apparente est de l'ordre de 2,5 donc son rapport de compression de 2 à 2,5.

Son écoulement est plus facile, donc son dosage volumétrique dans la matrice de mise en forme plus précis.

La densité apparente des comprimés crus est généralement augmentée.

Le granulé, mis en forme à la presse hydraulique automatique sous une pression de 4 t/cm² appliquée pendant 5 secondes, a permis d'obtenir des cylindres de diamètre 9,9 mm, de hauteur 12 mm et de densité apparente en cru 5,50.

c) Après élimination du camphre sous vide à 180° C pendant 2 heures ces comprimés ont été frittés à 1350° C dans l'ammoniac craqué sec pendant 2, 5 et 10 heures avec les régimes de chauffage et de refroidissement habituels.

Les densités apparentes des produits frittés ainsi obtenus sont respectivement de: 10,50, 10,60 et 10,63.

Les cylindres frittés ont une hauteur de 9,5 mm et un diamètre de 7,9 mm. La différence entre les diamètres de la section médiane et de la face supérieure de la pastille reste nettement inférieure à 1/10 de mm.

Un procédé de fabrication d'oxyde fritté de haute densité peut être défini ainsi:

Calcination d'uranate d'ammonium – 5 h à 400° C.

Réduction dans l'ammoniac craqué en deux paliers de température: 400° C puis 650° C.

Réoxydation ménagée à froid dans un courant d'azote à 2 % d'oxygène.

Incorporation de 3 % de camphre et 0,75 % d'acide stéarique en solution dans un solvant volatil.

Première compression sous vide dans une presse à compacter.

Concassage du pain comprimé et tamisage des granulés.

Mise en forme à la presse verticale sous une pression de l'ordre de 5 t/cm².

Elimination des liants sous vide à 180° C.

Frittage à 1350° C dans l'ammoniac craqué pendant 5 h dans un four à résistances de molybdène.

Conclusions

Les faits expérimentaux qui viennent d'être exposés confirment et permettent de développer une thèse qui s'oppose aux idées généralement exprimées à propos du frittage de poudres d'oxyde d'uranium de grande surface spécifique:

1. La densité apparente d'un oxyde fritté, obtenu à partir d'une poudre donnée, suivant un cycle de frittage déterminé, en atmosphère d'hydrogène sec, varie en fonction de la température-palier de ce frittage suivant une courbe à maximum.

2. La température correspondant au maximum de densité est d'autant plus basse que la surface spécifique de la poudre utilisée est plus grande.

3. Dans les cas envisagés, étant donné les techniques opératoires utilisées, l'emploi d'une atmosphère d'argon ne parait pas apporter d'amélioration au résultat global de l'opération; de plus les différences constatées selon les valeurs des rapports O/U dans l'une ou l'autre atmosphère, ne paraissent pas significatives.

L'évolution des oxydes obtenus aux dépens de peroxyde d'uranium ou d'uranate d'ammonium a été suivie en fonction des traitements de calcination et de réduction et le comportement de ces oxydes au cours de leur frittage dans l'hydrogène sec a été examiné.

La comparaison des résultats a conduit à proposer un procédé de frittage dans l'hydrogène à 1350° C, susceptible de fournir de l'oxyde d'uranium stoechiométrique de densité moyenne 10,6.

Bibliographie

[1] J. D. Eichenberg *et al.*, Westinghouse Atomic Power Division (USA) rapport WAPD 183 (1957)

[2] J. A. L. Robertson *et al.*, Deuxième Conférence de Genève (1958) 15/P/193

[3]) G. H. Chalder *et al.*, Deuxième Conférence de Genève (1958) 15/P/192
[4]) J. Belle, Conférence de Genève (1958) 15/P/2404
[5]) U. Runfors *et al.*, Conférence de Genève (1958) 15/P/142
[6]) A. Bel et Y. Carteret, Conférence de Genève (1958) 15/P/1165
[7]) P. Murray *et al.*, Uranium dioxide as a reactor fuel, Symposium technique des éléments combustibles (Paris, novembre 1957), USAEC Document TID 7546 p. 432
[8]) J. Williams *et al.*, AERE (Harwell) Report M/R 2653 (1958)
[9]) J. Decrop *et al.*, Deuxième Conférence de Genève (1958) 15/P/1252
[10]) R. Kiesling et U. Runfors, Sintering of uranium dioxide, Symposium technique des éléments combustibles (Paris, novembre 1957), USAEC Document TID 7546 p. 402
[11]) J. E. Burke, J. Am. Cer. Soc. **40** (1957) 80
[12]) Y. Carteret, communication personnelle

JOURNAL OF NUCLEAR MATERIALS - 3 (1959) 271-280 - NORTH-HOLLAND PUBLISHING CO., AMSTERDAM

HYDROGEN ABSORPTION BY NICKEL ENRICHED ZIRCALOY-2

W. YENISCAVICH, R. A. WOLFE and R. M. LIEBERMAN

Westinghouse Electric Corporation, Bettis Laboratory, Pittsburgh, Pa., USA

Received 17 July 1959

Specimens of Zircaloy-2 with varying nickel contents were exposed to autoclave corrosion, and also simultaneous corrosion and reactor irradiation in a hot water loop. Increasing the nickel content of Zircaloy-2 (0.05 weight per cent Ni) to 0.75 weight per cent nickel caused a gross increase in hydrogen absorbtivity, which resulted in embrittlement and severe loss of mechanical strength.

Des échantillons de Zircaloy-2 contenant différentes teneurs en nickel furent exposés à la corrosion dans un autoclave et aussi simultanément à la corrosion et à l'irradiation dans un réacteur dans une boucle à eau chaude. L'élévation de la teneur en nickel du Zircaloy-2 (0.05 % en poids de Ni) jusqu'à 0.75 % en poids de Ni augmentait beaucoup la tendance de l'alliage à absorber de l'hydrogène, ce qui provoquait de la fragilité et une diminution importante de résistance mécanique.

Proben aus Zircaloy-2 mit verschiedenen Nickelgehalten wurden in einem Autoclaven korrodiert und ausserdem in einer Heisswasser-Schleife gleichzeitig der Korrosion und der Reaktorstrahlung ausgesetzt. Wenn man den Nickelgehalt des Zirzaloy-2 von 0.05 Gew. % auf 0.75 Gew. % steigert, so erzielt man hierdurch eine sehr grosse Zunahme der Fähigkeit, Wasserstoff zu absorbieren; dies hat eine Versprödung und eine beträchtliche Abnahme der mechanischen Festigkeit zur Folge.

1. Introduction

The hydrogen absorption of zirconium is a subject of considerable interest, mainly because of the adverse effects on the physical properties of zirconium associated with the precipitation of zirconium hydride. Increasing the hydrogen content in zirconium or Zircaloy-2 above 10 ppm has been found to give considerable increase in the notched bar impact transition temperature [1]), and in fact, the ductility of zirconium is continuously reduced as the hydrogen content is increased even in slow tensile tests of unnotched specimens [2]).

Particularly high hydrogen absorptions by Zircaloy-2 clad, nickel-diffusion-bonded fuel elements were found to occur during reactor irradiation in a hot water loop. Absorptions as high as 4000 ppm were found and the Zircaloy suffered severe loss of mechanical strength. These fuel elements were made by a eutectic diffusion-bonding process in which the Zircaloy-2 components were bonded with a eutectic mixture of zirconium and nickel, and the nickel was subsequently diffused from the bonding surfaces into the zirconium matrix [3]).

It was postulated that the increased nickel content resulting from nickel diffusion bonding had increased the rate of hydrogen absorption. However, the much smaller increase of hydrogen absorption observed in autoclave testing of nickel diffusion-bonded specimens was not compatible with the gross amounts absorbed during irradiation. Also, other factors were present which confused the interpretation, such as: a) effects associated with recoil phenomena from the fuel surface, b) the possibility of interaction zones between the UO_2 fuel and the Zircaloy cladding, which when exposed to hot water corrode rapidly releasing hydrogen [3]), c) the redistribution of hydrogen in Zircaloy under thermal gradients [4]).

An experiment was therefore initiated to determine the quantity of hydrogen absorbed by Zircaloy-2 as a function of nickel content during

exposure to reactor irradiation in high temperature water. Some iron and copper-enriched Zircaloy specimens were included since these elements are also used for diffusion bonding.

2. Experimental Procedure

This investigation consisted of two separate irradiation experiments in the Materials Testing Reactor (MTR). In the first phase, specimens of normal Zircaloy-2 (0.102 cm thick with 0.047 weight percent Ni) and nickel enriched Zircaloy (0.102 cm thick with 0.60 wt % Ni) were exposed to two corrosion environments. These environments were, (1) simultaneous irradiation and corrosion in a hot water, dynamic loop, and (2) corrosion in a refreshed autoclave (i.e. one in which the hot water environment is slowly but continuously renewed). In the second phase, Zircaloy specimens with various concentrations of nickel, and also copper-enriched and iron-enriched specimens were exposed to three corrosion environments. Two of these environments were the same as those of the first phase; however, an additional set of specimens were exposed in an out-of-reactor section of the in-pile loop. These latter specimens thus were exposed to the same water as the irradiated samples, but not to the neutron irradiation. Since the quantity of hydrogen absorbed by the specimens was of primary interest, a molecular hydrogen concentration of 25 to 30 cc/kg at STP was maintained in all corrosion environments. Table 1 lists the water and neutron conditions for each exposure environment in both phases of this investigation.

The enriching of all specimens in either nickel, iron, or copper was done by diffusion bonding. Preparation for bonding consisted of plating the interior surface of one Zircaloy sheet with approximately 5 microns of the diffusion bonding material, followed by edge welding of the plated sheet to an unplated sheet of the same thicknesses. The sheets were diffusion bonded at approximately 1000° C in a furnace evacuated to 0.3 microns of Hg and then pressurized with four atmospheres of helium.

Table 1

Water and irradiation condition for the various exposure environments

Exposure environment	Time and temperature	Pressure atmosphere	Flow	Average integrated thermal neutron flux †
PHASE I				
Irradiation	37 days at 270° C	150	268 cm/sec	4.4×10^{20}
	11 days at 95° C	150	268	
Autoclave	42 days at 290° C	105	††	–0–
PHASE II				
Irradiation	31 days at 275° C	150	268 cm/sec	3.8×10^{20}
	30 days at 95° C	150	268	
In-loop control	31 days at 275° C	150	268 cm/sec	–0–
Autoclave	14 days at 315° C	135	††	–0–
	14 days at 290° C	135	††	
	*14 days at 290° C	—	††	

* The final 14 days period of this corrosion exposure was in steam. All other corrosion exposures were in the liquid phase with these additional parameters:

Hydrogen concentration:	25–30 cc/kg at STP
Oxygen concentration:	less than 0.14 ppm
*p*H:	9.5–10.5 with LiOH

† The nominal ratio of epithermal (> 0.625 eV) to thermal neutron flux: 0.6.

†† The water content of the autoclave was renewed at a rate equivalent to replacement every 6 hours.

TABLE 2

Concentrations of diffusion bonding materials in Zircaloy-2

Specimen designation	Specimen thickness (cm)	Diffusion bonding conditions: Temperature (° C)	Time at temperature (h)	Concentration of diffusion bonding material wt % †		
				Ni	Cu	Fe
PHASE I						
Normal Zr-2	0.127	Not diffusion bonded		0.047	< 0.003	0.106
Ni enriched	0.127	1010	2	0.60 ± 0.06 *	< 0.002	0.111
PHASE II						
Ni free	0.076	Not diffusion bonded		0.002		0.13
Normal Zr-2	0.102	Not diffusion bonded		0.049	< 0.002	0.105
Ni enriched	0.305	1035	4½	0.27 ± 0.02 *	< 0.002	0.105
Ni enriched	0.203	1035	2	0.40 ± 0.04 *	< 0.004	0.140
Ni enriched	0.102	1035	½	0.75 ± 0.06 *	< 0.002	0.118
Fe enriched	0.102	1035	½	0.046	< 0.002	0.70 ± 0.06 *
Cu enriched	0.102	1035	½	0.046	0.50 ± 0.06 *	0.118

* These concentrations were calculated using the measured thickness of diffusion bonding material that was plated on the Zircaloy. The other concentration values reported were obtained by chemical analyses.

† The Zircaloy materials used in this investigation all contained 1.38–1.46 wt % tin, 0.099–0.114 wt % chromium, and less than 0.07 wt % total amount of other impurities.

The samples were inserted in the hot furnace, held at temperature for a specified time, and then returned to the cold zone. The cooling rate from the diffusion bonding temperature was greater than 90° C per minute. In table 2 are listed the specimen thicknesses, the concentration of bonding material in the specimens, and their respective times at the diffusion bonding temperature. In addition, one sample of low nickel (0.002 wt %) Zircaloy-2 was included in the phase II test and is shown in table 2.

Concentration-distribution curves were obtained by chemical analyses of the 0.305 and 0.203 cm thick specimens after diffusion bonding to determine the distribution of diffusion bonding materials. A typical curve is given in fig. 1. and shows that the nickel is nearly uniformly distributed throughout the zirconium, but that the iron and copper show a concentration gradient from the center to the surface of the samples.

After diffusion bonding, flat tensile specimens were machined from the sheets. These specimens had a 2.54 cm gauge length and were 0.381 cm wide in the gauge section. Their thickness was that of the diffusion bonded Zircaloy sheets. Normal Zircaloy-2 specimens and the nickel free specimen were machined directly from solid sheets. The normal Zircaloy-2 specimens were given a heat treatment analogous to diffusion bonding in order to be in the same initial heat treated condition as the diffusion bonded specimens. Various heat treatments were given the specimens as listed in tables 3 and 4.

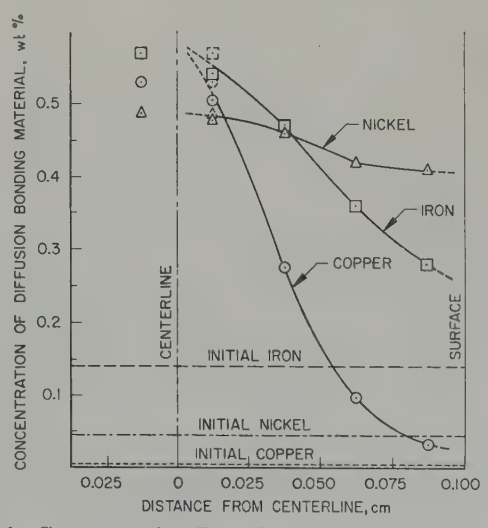

Fig. 1. Concentration-Distribution curves for 0.203 cm thick diffusion bonded specimens.

3. Results

The results of this investigation were obtained by tensile testing with a cross-head speed of 0.130 cm/min, by hydrogen analyses using the warm vacuum extraction technique, and by metallographic examination. Corrosion weight gains were obtained only on the non-irradiated specimens.

Phase I

In Phase I, only 0.102 cm thick specimens with two nickel concentrations were used, namely, normal Zircaloy-2 with 0.047 wt % nickel and the nickel enriched Zircaloy with 0.60 wt % nickel. A correlation of ultimate tensile strength as a function of hydrogen content is shown in fig. 2. A marked dependence of ultimate strength on hydrogen contents in excess of 500 ppm is evident.

The variation of percentage elongation with hydrogen content shows a great deal of scatter (fig. 3) but it is apparent that the elongation decreases with increased hydrogen content. Also, as indicated in fig. 3, irradiation decreases the elongation of normal Zircaloy-2 with low

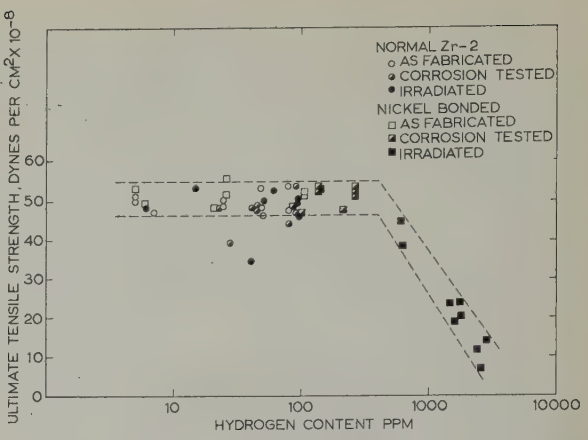

Fig. 2. Ultimate tensile strength as a function of hydrogen content for 0.102 cm thick specimens exposed to irradiation, autoclave corrosion; and in the as fabricated condition.

hydrogen content. However, this irradiation effect in nickel-enriched samples is overshadowed by embrittlement due to their higher hydrogen contents.

A tabulation of hydrogen absorption corresponding to the various specimen heat treatments is made in table 3. This table shows several interesting correlations.

Table 3

Hydrogen contents of normal and nickel enriched Zircaloy-2 specimens from Phase I

Group	Heat treatment *	Composition	Hydrogen content (ppm) †		
			As-Fabricated	Autoclave corrosion tested	Irradiated
1	Beta-quenched, from 1010° C	Normal Zr-2	54	80	95
		Nickel enriched	25	152	1620
2	Beta-quenched, 5 d in 400° C steam	Normal Zr-2	80	91	96
		Nickel enriched	105	148	618
3	Beta-quenched, Beta slow cool	Normal Zr-2	7	28	41
		Nickel enriched	6	102	2500
4	Beta-quenched, ½ h at 730° C	Normal Zr-2	25	46	38
		Nickel enriched	26	260	1950
5	Beta-quenched, 20 h at 800° C	Normal Zr-2	5	22	6
		Nickel enriched	5	160	2920
6	Beta-quenched, 20 h at 800° C, 5 d in 400° C steam	Normal Zr-2	42	41	52
		Nickel enriched	106	262	1810

* The post beta-quenching high temperature heat treatments in groups 4, 5, 6 were done in a vacuum atmosphere.

† The accuracy of these reported hydrogen contents is estimated to be ± 15 ppm.

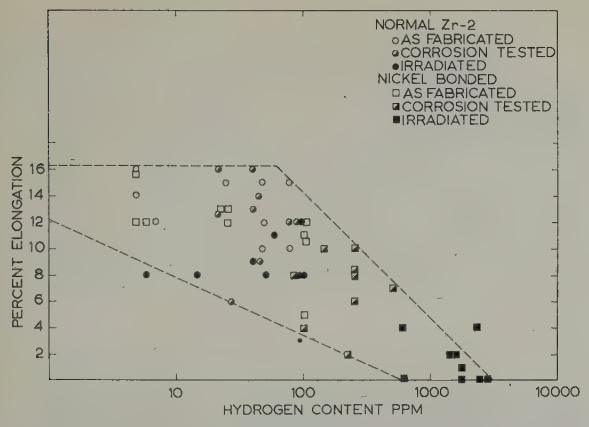

Fig. 3. Elongation as a function of hydrogen content for 0.102 cm thick specimens exposed to irradiation, autoclave corrosion; and in the as fabricated condition.

1. Gross amounts of hydrogen adsorption, 500–2900 ppm, were evidenced only by the irradiated, nickel enriched specimens.

2. Nickel-enriched specimens autoclave corrosion tested showed a much smaller hydrogen absorption than those exposed in-pile. However, the effect of nickel in increasing hydrogen uptake was evidenced even in out-of-pile tests.

3. Hydrogen absorption in the nickel-enriched specimens was increased by annealing after diffusion bonding. Nickel-enriched specimens in the annealed conditions (groups 3, 4, 5, 6) absorbed $1\frac{1}{2}$ to 2 times more hydrogen than the beta-quenched specimens (groups 1, 2).

4. The presence of an oxide film on the specimens prior to their in-pile exposure inhibits hydrogen absorption. This is seen by comparing groups 1 and 5 with groups 2 and 6 respectively. Groups 1 and 5 were heat treated identically to groups 2 and 6 except that the latter were corrosion tested in 400° C steam prior to irradiation to form an initial oxide film.

Metallographic examination after corrosion testing and again after irradiation showed no microstructural changes in any of the specimens, except those which were nickel bonded and irradiated. These specimens showed gross amounts of hydride precipitation as was to be expected from the hydrogen analyses and mechanical properties data. However, two different hydride distributions were observed. In the specimens in the beta-quenched condition (group 1 and 2), essentially all the hydride was concentrated in the boundaries of alpha platelets, (fig. 4*b*), while the specimens heat treated after beta quenching (group 4, 5, 6) had a more uniform hydride distribution, with the hydrides precipitated within the alpha platelets as well as at their boundaries (fig. 4*d*). Specimens which were slow cooled (group 3) showed intermediate structures with a high hydride concentration in the boundaries of the alpha platelets, and also some platelets which were completely hydrided.

The corrosion weight changes of the autoclave corrosion tested samples were measured and indicated no abnormal corrosion effects which could be held responsible for the high hydrogen absorption of the nickel-enriched samples; these weight gains were 0.08–0.22 mg/cm^2, which is a normal range for Zircaloy-2 at the temperatures in question. The theoretical yield of hydrogen from the corrosion reaction was calculated on the basis that the corrosion weight gain reaction yields two moles of hydrogen for each mole of water reacted. It was found that the nickel-enriched specimens autoclave corrosion tested absorbed from 148 to 430 percent of the theoretical hydrogen yield while the normal Zircaloy-2 samples absorbed from 0 to 112 percent of the theoretical hydrogen yield. This hydrogen absorption in excess of 100 percent theoretical is attributed to direct uptake of hydrogen from the water, which contained 25–30 cc hydrogen/kg at STP.

The hydrogen uptake in the nickel-enriched irradiated specimens was higher than that of the specimens corrosion tested out-of-pile by a factor of five to twenty (table 3). Evidence that these irradiation effects are to be associated with direct hydrogen absorption rather than increased corrosion in-pile was afforded by metallographic comparison of the thicknesses of the oxide films formed on the surface of the samples. The oxide film thickness of all specimens were found to be almost the same (approximately 2.5 microns). However, nickel enriched samples exposed in-pile and normal

Zircaloy-2 samples exposed to autoclave corrosion had hydrogen contents which differed by a factor of approximately 100.

A considerable variation in neutron flux was present during irradiation, from 1.7×10^{13} at one end of the fixture to 15.8×10^{13} nv at the center. However, the data show no correlation of mechanical properties or hydrogen absorption with increased neutron flux.

Phase II

Exposure of the specimens of the second phase of this investigation to simultaneous irradiation and corrosion in the hot water loop resulted in gross hydriding of the 0.102 cm thick nickel bonded specimens (0.75 wt % Ni). The hydriding was so severe that most of these specimens broke into pieces and were lost during their exposure. The remaining specimens were found

Fig. 4*a*

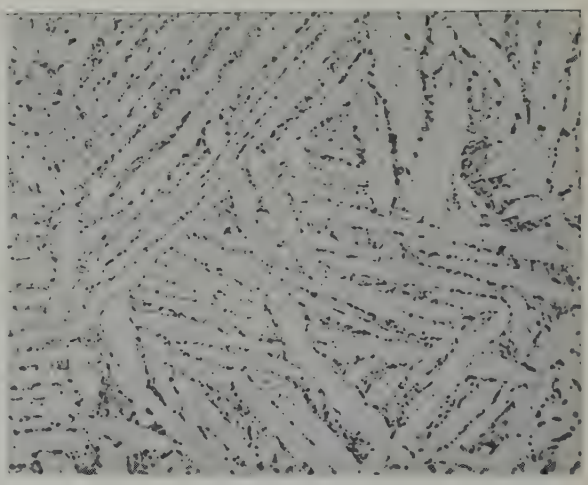

Fig. 4*c*

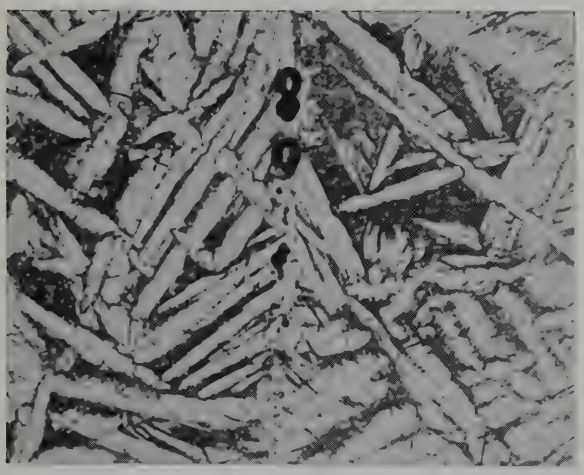

Fig. 4*b*

Fig. 4*d*

Fig. 4. Effect of heat treatment on hydride distribution in irradiated nickel-enriched Zircaloy-2 (0.60 wt % Ni). *a*. As fabricated (23 ppm H_2); *b*. As irradiated in high temperature water (1620 ppm H_2); *a* and *b*. Beta quenched from 1010° C. 250 ×. *c*. As fabricated (5 ppm H_2); *d*. As irradiated in high temperature water (2900 ppm H_2); *c* and *d*. Beta quenched from 1010° C and annealed 20 hrs at 800° C. 250 ×.

in general to show a 60 % reduction in elongation and a 10 % increase in yield and ultimate strengths. Exposure of the specimens in the irradiation loop in an out-of-reactor position also resulted in severe hydriding and loss of the 0.102 cm thick nickel bonded specimens. The remaining specimens in this set showed approximately a 30 % decrease in elongation, which is attributed to hydrogen absorption. The yield and tensile strengths during this exposure were essentially unaffected. The specimens exposed to autoclave corrosion had essentially the same physical properties as the as-fabricated specimens.

The hydrogen contents of Zircaloy specimens after the various corrosion exposures are given in table 4. Three heat treatments are reported, the beta-quench from the diffusion bonding temperature, beta-quenched plus reheat to beta and slow cool, and the beta-quench plus 20 hours at 800° C (annealed). All specimens were exposed to seven days corrosion in 400° C steam prior to the corrosion exposures listed in table 4.

The nickel free specimen listed in table 4 was not given the same pre-irradiation heat treatments and corrosion exposure as the other specimens. This specimen was annealed in the as-rolled condition for 24 hours at 750° C, and, instead of seven days corrosion, received only one day corrosion in 400° C steam.

The data in table 4 indicate the following general behavior:

1. Increasing the nickel content of Zircaloy-2 causes a gross increase in hydrogen absorption. Nickel contents of 0.75 wt % caused complete hydriding and loss of these specimens during their exposure in the hot water irradiation loop. Hydrogen absorption increased with increase in nickel content from 0.05 to 0.27 wt %; no

Table 4

Hydrogen contents of Zircaloy specimens from Phase II

Concentration of diffusion bonding material	Corrosion tested 7 days in 400° C steam			Autoclave corrosion			In-loop out-of-flux			Irradiated		
	Beta quenched	Beta slow cool	Annealed	Beta quenched	Beta slow cool	Annealed	Beta quenched	Beta slow cool	Annealed	Beta quenched	Beta slow cool	Annealed
0.002 wt % Ni			42			37			24			54
Normal Zr-2*	50	60	30	5	74	38	170	148	44	120	166	19
0.27 wt % Ni	50		30	65		59	167		153	168		140
0.40 wt % Ni	60		50	57		101	520		692	300		382
0.75 wt % Ni	125	110	80	46	240	222	very † high	1730	very † high	very † high	2680	very † high
0.50 wt % Cu	77	65	30	113	98	50	168	99	18	174	130	53
0.70 wt % Fe	98	51	32	72	41	109	70	79	34	130	112	70

* 0.049 wt % Ni, 0.105 wt % Fe, 0.002 wt % Cu.

† These specimens hydried so severely that they were lost during their exposures.

Notes:

1. The accuracy of these reported hydrogen contents is estimated to be ± 15 ppm.
2. All specimens were exposed to the 7 day corrosion test in 400° C steam prior to the other listed exposures.
3. Heat treatments
   a. Beta quenched—quenched in excess of 90° C per minute from the diffusion bounding temperature (approximately 1000° C).
   b. Beta slow cool—quenched as in "a", and then reheated to 1000° C and furnace cooled.
   c. Annealed—quenched as in "a", and then annealed 20 hours at 800° C.
4. The nickel free specimen (0.002 wt % Ni) was not beta quenched prior to annealing 24 hours at 750° C, and instead of 7 days corrosion, received only one day corrosion in 400° C steam.

effect of decreasing nickel content from 0.05 to 0.002 % was evidenced in this test.

2. Increasing the copper or iron content of Zircaloy-2 had no significant effect on hydrogen absorption during any of the corrosion or irradiation and corrosion exposures.

3. Hydrogen absorptions of specimens exposed in the hot water loop, both in the reactor flux and in out-of-flux positions were approximately equivalent. Hence there is no direct effect of irradiation of the metallic specimens on hydrogen absorption.

4. The general level of hydrogen absorption in the irradiated specimens of table 4 are less than those indicated in table 3 because of the prior corrosion film on the specimens of the second phase.

4. Discussion

The data described above show:

1. that increasing the nickel content of Zircaloy-2 causes an order of magnitude increased absorbtivity for hydrogen on exposure to high temperature water containing dissolved molecular hydrogen;

2. that irradiation in high temperature water further increases hydrogen absorptivity another order of magnitude;

3. that direct reactor irradiation exposure of the metallic specimens is not necessary to cause the increase of absorptivity;

4. that nickel additions have a specific effect which is not duplicated by iron or copper additions;

5. that an oxide corrosion film on the specimens prior to their irradiation exposure inhibits but does not prevent hydrogen uptake;

6. and that homogenization heat treatments increase hydrogen uptake during reactor irradiation and influence the final distribution of the hydride within the specimens.

Normal Zircaloy-2 exposed to high temperature water in the absence of irradiation absorbs only about 25 percent of the hydrogen liberated by the corrosion reaction [5]). This limited absorptivity has been attributed to several possible effects, the most likely of which are:

1. mechanical diffusion barrier afforded by the presence of a surface oxide corrosion film;

2. restricted solubility and hence restricted permeability of the ZrO_2 corrosion film to hydrogen because of its equilibrium defect structure.

Correspondingly it may be theorized that the addition of nickel to Zircaloy-2 enhances its hydrogen absorptivity by:

1. catalyzing reactions with hydrogen which enhance the solution rate or mobility of hydrogen in the ZrO_2 film;

2. altering the defect structure of the ZrO_2 film such as to enhance its solubility and hence permeability.

3. decreasing the mechanical adhesion or cohesion of the oxide film barrier.

The alteration of the defect structure and the decrease in mechanical adhesion are not considered as probable because of the approximately equivalent oxide film thicknesses and corrosion weight gains of the normal and nickel-enriched Zircaloy-2 specimens. Equivalent defect structures are indicated by the equivalent growth rates (weight gains), and equivalent adhesion is indicated by the equivalent film thicknesses.

Nickel additions have been made to aluminum to increase its corrosion resistance to high temperature water [6]). The effect of nickel in aluminum has been explained on the basis of the precipitated compounds with aluminum serving as cathodic sites for the recombination and release of atomic hydrogen formed during corrosion and thus preventing absorption and subsequent swelling of the aluminum base metal by precipitation of molecular hydrogen. In the case of nickel-enriched zirconium, however, nickel behaves in a diametrically opposite manner, in that it enhances the absorption by the base material. The effect of nickel in each case appears to be a catalytic one of accelerating attainment of hydrogen equilibrium between the environment and substrate.

Wanklyn and Hopkinson indicated that increased amounts of nickel content appreciably increased the hydrogen pickup in binary zir-

conium alloys during corrosion exposure [7]). Recent out-of-pile data by Kass and Kirk [8]) on the autoclave corrosion testing of normal and nickel free Zircaloy-2 have shown that the removal of nickel from this alloy appreciably decreased the hydrogen pickup. Their normal and nickel free materials contained 0.052 and 0.002 weight percent nickel, respectively. Testing was done in 315° C and 345° C water and also in 400° C steam. In all cases corrosion weight gains of both materials were equivalent but the quantity of hydrogen absorbed by the nickel-free material (11–21 % of that produced by the corrosion reaction) was considerably less than that absorbed by the normal Zircaloy-2 (32–60 %).

Based on the considerations described above, the effect of irradiation on these materials could be reconciled by assuming that irradiation:

1. induces formation of ions, radicals, or other species in the water environment which increases the hydrogen potential or activity of the environment relative to that of the nickel-enriched Zircaloy;

2. further decreases the adhesion of the oxide film;

3. creates lattice defects, which further enhance solubility and permeability for hydrogen.

Again the decrease in adhesion and the alteration of the lattice defect structure do not seem probable because of equivalent oxide film thickness between irradiated and non-irradiated nickel-enriched specimens. Also it appears that the irradiation-induced absorptivity must result from irradiation effects on the water environment since the out-of-flux in-loop samples were as heavily hydrided as the in-flux in-loop samples of Phase II of this study. With the flow rates used in the in-pile loop, approximately one minute elapsed between exposure of water to flux and its arrival at the out-of-flux specimen positions. This observation is difficult to reconcile with the experimental findings, since at the temperature of operation of the loop, recombination of irradiation-induced reactions in the water would be expected to be very rapid.

The hydrogen absorption which occurred in this particular hot water irradiation loop (WAPD 29 loop in the Materials Testing Reactor) used for this investigation is not a characteristic of the loop alone. From the fact that nickel-bonded fuel elements exposed in other hot water irradiation loops were also found to absorb large quantities of hydrogen it may be inferred that loop characteristics alone are not responsible for the accelerated pickup observed in-pile.

Another observation for which an explanation can be offered is the effect of heat treatment on the nickel enriched specimens of Phase I. The hydrogen absorption of the annealed specimens during irradiation was approximately twice that of the beta quenched specimens. Also the beta-quenched specimens hydrided selectively, whereas the annealed specimens hydrided uniformly. A possible explanation for these effects is the decreased solubility of hydrogen in oxygen-enriched zirconium [9]). When specimens are beta-quenched, oxygen partitioning occurs, and the primary alpha grains are enriched in oxygen compared with the grain boundaries. Absorbed hydrogen will thus tend to segregate in the grain boundary regions where its solubility is greatest. Annealing subsequent to beta quenching or slow cooling from the beta region diffuses the oxygen

Fig. 5. Cross section of oxygen enriched Zircaloy-2 clad which hydrided severely. Oxygen enriched areas are white, hydrided areas are gray. 250 ×.

more uniformly and thus permits the entire microstructure to absorb hydrogen. This is further substantiated by metallographic evidence shown in fig. 5. Fig. 5 is a cross section of a piece of cladding which was in contact with UO_2 fuel during diffusion bonding. This resulted in interaction and oxygen enrichment of the Zircaloy cladding. Diffusion from the interaction interface gave an inner layer of oxygen enriched Zircaloy and also resulted in certain grains, which extended to the external surface of the clad, becoming enriched with oxygen. This fuel element had been fabricated by nickel diffusion bonding and hydrided severely during its corrosion exposure; however, the oxygen enriched areas are free of hydride precipitation.

5. Conclusions

It has been found that nickel content is an important variable in determining the hydrogen absorptivity of Zircaloy-2. For example, increasing the nickel content of normal Zircaloy-2 to 0.75 weight percent resulted in an order of magnitude increased in hydrogen absorption during autoclave corrosion, and two orders of magnitude increase in hydrogen absorption during simultaneous corrosion and reactor irradiation. Furthermore, it was not necessary to expose the Zircaloy specimens directly to irradiation to obtain this additional order of magnitude increased absorptivity; it was sufficient to expose only the corrosion water. This increased hydrogen absorptivity appears to be a unique effect of nickel, because Zircaloy-2 specimens with increased iron and copper contents were also exposed to simultaneous corrosion and reactor irradiation, and these elements were found to have no significant effect on hydrogen absorptivity.

Acknowledgments

The authors wish to acknowledge the assistance of Messrs. B. Lustman, L. J. Jones and M. L. Bleiberg in preparing this paper, and F. S. Susko for performing the hydrogen analysis on the irradiated specimens.

The authors are indebted to the U.S. Navy, the Atomic Energy Commission, and the Westinghouse Electric Corporation for permission to publish this work, which was performed under contract no. AT-11-1-GEN-14.

References

1) B. Lustman and F. Kerze Jr., The Metallurgy of Zirconium (McGraw-Hill, New York, 1955)

2) F. Forscher, Strain Induced Porosity and Hydrogen Embrittlement in Zirconium. Transactions AIME **206** (1956) 536

3) J. Glatter, E. F. Losco, N. J. Hurford, J. S. Theilacker, R. L. Fischer, N. T. Saunders and R. A. Wolfe, The Manufacture of PWR Blanket Fuel Elements Containing High Density Uranium Dioxide, Proceedings of the Second International Conference on Peaceful Uses of Atomic Energy (1958)

4) J. M. Markowitz, Hydrogen Redistribution in Zircaloy-2 Under Thermal and Mechanical Stress Gradients, WAPD (Report) TM-171, (1959). (Available from the office of Technical Services, Department of Commerce, Washington 25, D.C.)

5) R. F. Boyle and T. J. Kisiel, Hydrogen Permeation of Zircaloy-2 Corrosion Films, Bettis Technical Review, WAPD (Report) BT-10, (1958) (Available from the Office of Technical Services, Department of Commerce, Washington 25, D.C.)

6) J. E. Draley and W. E. Ruther, Aqueous Corrosion of Aluminum Alloys at Elevated Temperatures, Proceedings of the first International Conference on Peaceful Uses of Atomic Energy, 2 (1955) 391

7) J. N. Wanklyn and B. E. Hopkinson, The Role of Hydrogen in the High-Temperature Corrosion of Zirconium and Its Alloys, I. The Effect of Cathodic Polarization on Corrosion in Water at 325° C, Journal of Applied Chemistry **8** (1958) 496

8) S. Kass and W. W. Kirk, Corrosion and Hydrogen Pickup Evaluation of Nickel-Free Zircaloy-2. Zirconium Highlights, WAPD (Report) ZH-15 (1959) (Available from Technical Information Service Extension, P.O. Box 62, Oak Ridge, Tennessee)

9) M. N. A. Hall, S. L. H. Martin and A. L. C. Rees, Solubility of Hydrogen in Zirconium and Zirconium-Oxygen Solid Solutions, Transactions of the Faraday Society **41** (1945) 306

JOURNAL OF NUCLEAR MATERIALS - 3 (1959) 281–288 - NORTH-HOLLAND PUBLISHING CO., AMSTERDAM

THE LATTICE SPACING OF THORIUM, WITH REFERENCE TO CONTAMINATION

D. S. EVANS and G. V. RAYNOR

Department of Physical Metallurgy, The University of Birmingham, Edgbaston, Birmingham, 15, UK

Received 17 July 1959

In view of the wide range of values reported in metallurgical literature for the lattice spacing of thorium, the effects of contamination, and methods for minimising such contamination, have been investigated. Serious contamination, chiefly by nitrogen, has been found to occur if the filings are prepared in air. Other stages at which contamination occurs are on exposure to air of filings prepared out of contact with air, on annealing in vacuo at pressures as low as 5×10^{-6} mm Hg, and on initial heating up to the annealing temperature by gas evolved from the walls of the boats in which the filings are contained. Unless stringent precautions are taken, results varying from 5.0740 *kX* to 5.089 *kX* may be obtained. The necessary precautions are discussed, and it is shown that by preparing filings out of contact with air, and avoiding all contact with air prior to heat-treatment, stress-relief anneals may be successfully carried out in closed or sealed boats of tantalum foil without introducing impurity in sufficient quantity to affect the lattice spacings by amounts exceeding normal experimental error. The lattice spacing of iodide thorium was determined as 5.0741 ± 0.0002 *kX*; values in the range 5.078 to 5.082 *kX* correspond with material highly contaminated or saturated with introduced nitrogen.

En raison de la grande dispersion des valeurs signalées dans la littérature métallurgique pour le paramètre réticulaire du thorium, les effets de la contamination et les moyens de minimiser celle-ci ont été étudiés. On a constaté qu'une sérieuse contamination, principalement par l'azote, se produisait si les échantillons filiformes étaient préparés à l'air. La contamination peut se produire à d'autres stades: au cours du contact à l'air des échantillons après leur préparation à l'abri de l'air, au cours du recuit sous vide à des pressions aussi basses que 5×10^{-6} mm Hg et au cours du chauffage initial jusqu'à la température de recuit en raison des gaz dégagés par les parois des nacelles dans lesquelles sont contenus les échantillons filiformes. A moins que des précautions sévères soient prises, les résultats peuvent varier de 5.0740 *kX* à 5.089 *kX*. Les précautions nécessaires sont discutées: il est montré qu'en préparant les échantillons filiformes hors du contact de l'air et en évitant tout contact avec l'air avant le traitement thermique, les recuits nécessaires pour éliminer les tensions peuvent être réalisés avec succès dans des nacelles fermées ou scellées de feuille de tantale sans qu'il y ait introduction d'impurités en quantité suffisante pour affecter les mesures de paramètre d'une valeur excédant l'erreur expérimentale normale. Le paramètre réticulaire du thorium à l'iodure fut ainsi déterminé être égal à 5.0741 ± 0.0002 *kX*. Les valeurs comprises entre 5.078 et 5.082 *kX* correspondent à un métal fortement contaminé ou saturé d'azote.

Wegen den sehr verschiedenen Werten der Gitterkonstante des Thorium die in der Literatur angegeben wurden, sollte der Einfluss der Verunreinigungen und die Mittel diese zu vermeiden, untersucht werden. Wenn das Metall an der Luft gefeilt wird, so findet man erhebliche Verunreinigung, hauptsächlich durch Stickstoff. Wenn Späne ohne Kontakt mit der Luft hergestellt werden, so kann immerhin bei späterem Liegen an der Luft eine Verunreinigung zustande kommen; dies kann ebenfalls während des Glühens bei nur 5×10^{-6} Torr Luftdruck geschehen, oder auch während des Aufheizens durch Gase die vom Behälter abgegeben werden. Wenn die nötigen strenge Massnahmen vernachlässigt werden erhält man Werte zwischen 5.0740 *kX* und 5.089 *kX*. Diese Massnahmen werden besprochen und es wird gezeigt dass, wenn man Späne ohne Kontakt mit der Luft herstellt und allen solchen Kontakt vor dem Glühen vermeidet, so kann man innere Spannungen erfolgreich durch Glühen in geschlossenen oder versiegelten Tantalbehältern beseitigen, ohne dass die Gitterkonstante durch die zugefügte Verunreinigung mehr als gemäss den experimentalen Fehlerbetrag verändert wird. Die Gitterkonstante des Iod-Thorium wurde zu 5.0741 ± 0.0002 *kX* bestimmt; Werte im Gebiet 5.078–5.082 *kX* findet man mit Metall das schwer oder bis zur Löslichkeitsgrenze mit Stickstoff beladen ist.

1. Introduction

The values quoted for the lattice spacing of thorium in the metallurgical literature and in reference books vary considerably. A selection of such values is given in table 1. For a reactive metal which is difficult to obtain in a pure state this variability is not unexpected, but even in relatively recent work, in which metal of high purity has been available, the differences in the values obtained are considerable. This could be accounted for by the varying initial purity of the metal, and by impurities introduced into annealed filings by the use of different techniques.

In the course of systematic work in the authors' laboratory on the lattice spacings of heavy metal alloys, the spacing of thorium was investigated, and, with the techniques initially adopted, again proved to be variable. It was therefore of interest to attempt to discover the main cause of the lack of reproducibility, and to develop a technique by which reproducible results could be obtained. The present paper summarizes the work carried out, and the conclusions which may be drawn.

TABLE 1

Nature of specimen	Lattice spacing, kX	Year	Ref.
Not stated	5.12	1920	[1]
Not stated	5.04	1921	[2]
Not stated	5.074 $\pm$ 0.002	1930	[3]
345 ppm of carbon 195 ppm of nitrogen	5.091 $\pm$ 0.004	1933	[4]
—	5.077 $\pm$ 0.003	1936	[5]
Iodide thorium	5.075 $\pm$ 0.003	1949	[6]
—	5.075	1950	[7]
—	5.0768 $\pm$ 0.0002	1951	[8]
Not stated	5.0771 $\pm$ 0.0005	1953	[9]
99.8 % thorium	5.079 $\pm$ 0.001	1954	[10]
Iodide thorium	5.0741 $\pm$ 0.0001	1956	[11]

2. Materials and Methods

Three grades of thorium have been used in the present work †:

† Samples were kindly presented by AERE, Harwell.

(i) Iodide thorium, containing less than 0.1 % of metallic impurities, and 0.02 % of carbon, 0.01 % of nitrogen and 0.1 % of oxygen.

(ii) Electrolytic thorium, stated to be 99.5 % pure, with oxygen as the main impurity, together with 0.015 % of nitrogen and 0.02 % of calcium.

(iii) Sintered bar thorium, stated to be of approximately the same purity as the electrolytic material.

In the initial experiments filings were prepared using a dead-smooth file; no special precautions were taken to exclude air, and an attempt was made to anneal such filings within the silica capillaries in which they were subsequently to be exposed to X-rays. In spite of preliminary outgassing of the capillaries, and evacuation to $<10^{-5}$ mm Hg before sealing, marked increases in lattice spacing, and in the intensities of lines on the diffraction pattern corresponding to thorium oxide and nitride, were observed. This technique was thus abandoned, and annealing of filings for the relief of stress was carried out in a continuously evacuated system. The filings were contained in boats made from tantalum sheet, which was chosen because it would begin to absorb, from the furnace atmosphere, oxygen and nitrogen at temperatures exceeding 200° and 600° C respectively [12]), while removal of these gases from the metal is negligible at temperatures below 2000° C. In the course of the work, four types of boat were used:

i) An open tray, measuring approximately 12×5 mm, and 3 mm deep.

(ii) A similar tray, covered with a close-fitting lid, and referred to below as a "closed boat".

(iii) A closed boat contained in a further closely-fitting tray, referred to as a "doubly-closed boat".

(iv) A "sealed boat", made from three turns of tantalum sheet on a cylindrical $\frac{1}{8}''$ diameter former, with the ends tightly folded after loading with filings.

In all cases the boats were degreased, cleaned and degassed at 950° to 1000° C before use,

and a separate boat was used for each sample of filings.

For the annealing of filings, use was made of a vacuum annealing furnace, in which a pressure less than 5×10^{-6} mm Hg, as measured by a cold-cathode ionization gauge, could be maintained within a silica furnace tube heated at temperatures up to 1100° C. The vacuum system consisted of a rotary backing pump and a 1″ diameter diffusion pump using silicone oil as the working fluid. A liquid nitrogen trap was interposed between the diffusion pump and the furnace tube, and a system of taps allowed the use of auxiliary pump for rough evacuation of the furnace tube after loading, which could be achieved without disturbing the main pumping system.

In a typical experiment, the silica furnace tube containing an empty boat was outgassed at 950° to 1000° C until the pressure had fallen to 2×10^{-6} mm Hg. The tube was then cooled, isolated from the pump, and filled with purified argon at atmospheric pressure. The boat was then loaded, placed at the cool end of the furnace tube which projected from the furnace windings, and the system again evacuated and outgassed. The loaded boat was pushed magnetically to the hot end of the furnace tube, and the heat-treatment temperature was approached at such a rate that the pressure at no stage exceeded 5×10^{-5} mm Hg. At the temperature of heat-treatment the vacuum improved to 5×10^{-6} mm Hg after $\frac{1}{2}$ hour, or 2×10^{-6} mm Hg after 1 hour, thereafter remaining constant in long heat-treatments. After heat-treatment, filings were rapidly cooled by removal of the furnace. When cold, the furnace tube was filled with argon; the filings were extracted and immediately enclosed in silica capillaries for X-ray examination.

Following experiments on filings prepared in air, it became clear that precautions were necessary to exclude air at all stages prior to heat-treatment. Specimens were therefore filed under carbon tetrachloride, and loaded into the degassed boats while still wet with this liquid. After transfer to the cold end of the silica furnace tube, as described above, the carbon tetrachloride was removed by means of the auxiliary pump; the main pumps were then connected to the system, and the experiment proceeded as already outlined.

Some experiments were made with filings in highly evacuated glass bulbs, sealed at the heat-treatment temperature under a pressure of less than 3×10^{-6} mm Hg. Filings of iodide thorium treated in this way for 14 hours correspond to lattice spacings almost identical with those of samples treated in the continuously evacuated system for much shorter periods, and, though restricted to heat-treatment temperatures of approximately 600° C, the technique proved useful for abnormally long experiments, as, for instance, in the slow cooling of certain samples to room temperature.

Specimens were exposed to copper Kα radiation in silica capillaries sealed under a pressure of 10^{-1} mm Hg, using a Philips 11.483 cm diameter Debye–Scherrer camera. Spacings were calculated assuming the following wavelengths:

$$\mathrm{CuK}\alpha_1 = 1.537\ 395\ kX$$
$$\mathrm{CuK}\alpha_2 = 1.541\ 232\ kX$$

and the Nelson–Riley function [13]) was used to correct for systematic errors. The results were also corrected for refraction effects [14]), and it is estimated that the spacings quoted are accurate to within $\pm$ 0.0001 to 0.0002 kX, except where otherwise stated.

3. Experimental Results

3.1. Preliminary work

The first series of experiments was made on filings of electrolytic thorium, prepared in air and heat-treated in open boats at temperatures up to 1050° C for times varying from 20 minutes to 5 hours. The results are plotted in fig. 1, in which the numerals attached to points denote the length of annealing in hours. Considerable variation in spacing is shown, but there is no clear correlation with either vacuum conditions or duration of heat-treatment. There is, how-

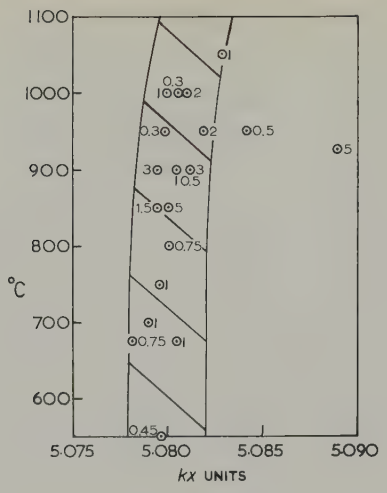

Fig. 1. Lattice spacings of electrolytic thorium, as a function of time and temperature of annealing. The filings were prepared in air and annealed in open boats.

ever, a tendency for both the value of the spacing, and the spread of the results to increase with rising temperature. Iodide thorium filings behaved similarly; thus filings of material of original lattice spacing equal to 5.0740 kX, after annealing in open boats for 1 hour and 3 hours at 970° C concurrently, corresponded to spacings of 5.0803 and 5.0780 $\pm$ 0.0002 kX respectively.

3.2. Spacing of uncontamined thorium

Since the above results indicated that serious contamination was probable, a reference value for the spacing of material which had no similar opportunity for contamination was established by the examination, without heat-treatment, of a small polycrystalline fragment detached from a bar of iodide thorium. The lattice spacing obtained, 5.0740 $\pm$ 0.0002 kX, is in excellent agreement with that obtained by James and Straumanis [11]) using similar methods †. The same fragment, after handling in air prior to heat-treatment in a closed boat at 600° C for 2 hours corresponded to a spacing of 5.0746 kX, while a similar fragment, detached and handled under carbon tetrachloride before undergoing the same heat-treatment, had a lattice spacing of 5.0741 $\pm$ 0.0002 kX. Though solid material may therefore be heat-treated without excessive contamination, filings may be expected to be more sensitive, and this was confirmed by heat-treating a solid fragment and filings together for 1 hour at 970° C in the same sealed boat. The spacings measured were 5.0745 kX (fragment) and 5.0762 kX (filings), showing that contamination of the filings had occurred to the greater extent.

† It is of interest to note that James and Straumanis were unable to carry out stress-relief annealing treatments without excessive contamination.

3.3. Contamination effects

The general indication of the preliminary results was that gaseous contamination was responsible for lack of reproducibility of the spacings determined for heat-treated filings, and experiments were carried out to determine at which stage in the process this occurred. Thus, filings prepared in air were annealed in both open and closed boats for various times at 970° C. As shown in fig. 2, filings annealed in

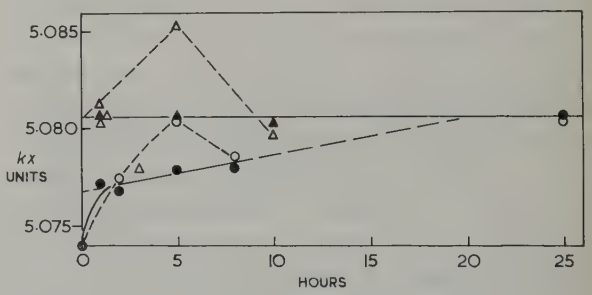

Fig. 2. Lattice spacings of iodide thorium, as a function of time of annealing at 970° C.

△ Filings prepared in air and annealed in open boats.
▲ Filings prepared in air and annealed in closed boats.
○ Filings prepared under carbon tetrachloride and annealed in open boats.
● Filings prepared under carbon tetrachloride and annealed in closed boats.
□ Filings prepared under carbon tetrachloride and annealed in sealed boats.
n Specimen annealed in an atmosphere of nitrogen at low pressure.
× Specimen in form of a polycrystalline fragment.

open boats gave rise to variable results, but for specimens annealed in closed boats the spacings were substantially constant at 5.0807 $\pm$ 0.0003 kX, suggesting that such closed boats allow little

progressive contamination during heat-treatment. The contamination responsible for the high spacings must therefore have been present before heat-treatment of the filings prepared in air, and to test this conclusion, similar experiments were made, using filings prepared under carbon tetrachloride as previously described, and protected from the air at all stages prior to annealing. Filings prepared in this way and annealed at 600° C corresponded with lattice spacings of 5.0739 ± 0.0002 kX, in excellent agreement with that of the standard solid fragment. If, however, filings made under carbon tetrachloride and dried were allowed to stand in air for 5 minutes, the spacing increased after annealing at 600° C to 5.0748 ± 0.0002 kX, indicating that adsorption of gas by mere exposure to air was responsible for some contamination. For comparison with the results for filings prepared in air, the lattice spacings of filings prepared out of contact with air and annealed for various times at 970° C are given in fig. 2. The results for heat-treatment in open boats are again variable, while those corresponding to closed boats are consistent in showing a steady increase with time of annealing, eventually reaching a value of 5.0806 ± 0.0003 kX. This value is almost identical with that for filings made in air and similarly heat-treated. The use of closed boats therefore does not entirely prevent contamination, from the low-pressure furnace atmosphere, of filings which were not initially heavily contaminated by exposure to air. This conclusion was confirmed by the additional observation that when filings (prepared in air) were annealed in double closed boats, lattice spacings lower by 0.0005 kX than the corresponding values for closed boats could be obtained.

Fig. 3 summarizes the results presented, together with those of other experiments. It is particularly interesting to observe that filings prepared under carbon tetrachloride and annealed at 950° C in a closed boat suffer a marked increase in lattice spacing, which is reduced by the use of a sealed boat. A specimen in the form of a crystallite, however, may be heat-treated in a sealed boat at 970° C with only a slight degree of contamination, leading to a slightly increased spacing. A further point illustrated by fig. 3 is that filings deliberately contaminated

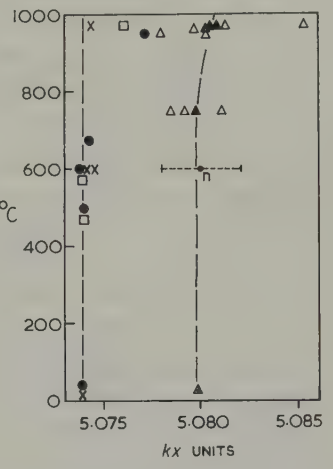

Fig. 3. Lattice spacings of iodide thorium, as a function of temperature and annealing conditions.

△ Filings prepared in air and annealed in open boats.
▲ Filings prepared in air and annealed in closed boats.
○ Filings prepared under carbon tetrachloride and annealed in open boats.
● Filings prepared under carbon tetrachloride and annealed in closed boats.
□ Filings prepared under carbon tetrachloride and annealed in sealed boats.
n Specimen annealed in an atmosphere of nitrogen at low pressure.
× Specimen in form of a polycrystalline fragment.

by heat-treatment in an atmosphere of nitrogen at 5×10^{-3} mm Hg corresponded to a lattice spacing of 5.080 ± 0.002 kX, which falls within the range of values obtained for filings prepared in air and annealed in open or closed boats. The diffraction pattern of the deliberately contaminated filings contained also lines due to a face-centred cubic lattice of spacing 5.17 ± 0.002 kX, which is in reasonable agreement with the values of Rundle [15]) and Chiotti [16]) for ThN.

4. Discussion

The results summarized in figs. 1, 2 and 3 illustrate the complex nature of contamination effects on the lattice spacing of thorium. The

results as a whole are consistent with contamination at various stages, which may be considered in turn.

4.1. Contamination during filing in air

As shown in fig. 3, the lattice spacings of thorium filings prepared in air are approximately 0.006 kX greater than those prepared out of contact with air, after comparable heat-treatments, suggesting that major contamination occurs during the filing operation in air. If the filings are annealed in closed boats, the spacings are almost independent of time of annealing; since it is improbable that these results represent a constant amount of contamination, they strongly suggest that the spacings observed correspond to the solubility limit of the contaminant in thorium. The effects obtained by annealing in open boats are referred to in § 4.4. below. Direct evidence on the nature of the contaminant is difficult to obtain, but choice is limited by the marked expansion of the lattice which occurs. This consideration eliminates contamination by iron from the file used, and directs attention to oxygen, hydrogen, carbon and nitrogen. Oxygen may be eliminated since the thorium as received was saturated with this element; thoria lines were faintly observable in the diffraction patterns of filings having the lowest spacings. Work quoted by Rough and Bauer [17]), which failed to increase the oxygen content of the iodide thorium matrix by annealing in oxygen at 1415° C for 3 hours is consistent with this suggestion. Hydrogen may also be discounted, since the work of Mallet and Campbell [18]) indicates that it is completely removed at the temperatures and under the vacuum conditions used in the present work. The lattice spacing shown in fig. 3 for filings deliberately contaminated with nitrogen, and the observation of thorium nitride lines in diffraction patterns of filings heat-treated in a closed boat for 10 hours at 970° C, together with the fact that such lines were not observed in diffraction patterns of uncontaminated thorium, make it very probable that nitrogen is the contaminant responsible for the increased spacings. As shown in § 4.3. below, saturation by contamination from the furnace atmosphere of originally uncontaminated material requires 20 hours at 970° C, while a further 5 hours would be necessary to produce nitride lines of intensity equal to those in the specimen annealed for 10 hours at 970° C. Further, as shown in fig. 2 the value of the lattice spacing corresponding to saturation is attained after only one hour at 970° C in a closed boat. It is therefore concluded that the filings prepared in air were already heavily contaminated with nitrogen in solid solution, introduced during the filing operation, before heat-treatment.

4.2. Contamination by adsorbed gas

Referring to the experiments described in § 3.2., it is possible to obtain a lattice spacing difference of 0.0005 kX, after identical heat-treatments, between solid crystallites of which one was exposed to air before annealing. This suggested that exposure to air had resulted in surface-adsorbed gas which, if not removed in the vacuum furnace at low temperatures, would be adsorbed by the specimen. To test this, filings which had been prepared in air were heated to the annealing temperature of 600° C at a lower rate than normal (i.e. at 1° C/min) and held for 2 hours at this temperature. By such slow heating the pressure was maintained below 5×10^{-6} mm Hg, and the spacings obtained in two independent experiments were respectively 0.0011 and 0.0012 kX lower than for filings which had received a normal heat-treatment in which the pressure rose to 5×10^{-5} mm Hg. Adsorption of surface gas thus produces contamination on heat-treatment, but the effect on the lattice spacings (approximately 0.001 kX) is small.

4.3. Contamination of filings in closed boats by the furnace atmosphere

According to the results summarized in fig. 2, the annealing in closed boats of filings prepared in air, and therefore heavily contaminated with nitrogen, leads to very little variation of spacing. The lattice spacings of filings prepared under

carbon tetrachloride, however, increase with time of annealing in closed boats. Progressive contamination from the furnace atmosphere thus takes place. After very long periods at 970° C (exceeding 20 hours) the spacings approximate to those of filings made in air and annealed in closed boats, which strongly suggests that it is again reaction with traces of nitrogen which is responsible for the increased spacings. An extrapolation of the smooth curve of spacing against time of annealing at 970° C to zero annealing time corresponds to a spacing value of 5.0768 kX. This is greater than that of uncontaminated filings, suggesting that a relatively constant amount of contamination, probably by gas liberated from the walls of the boat, occurs during the initial heating to the annealing temperature. Some confirmation of this is given by the observation that on slow heating to the annealing temperature (see § 4.2. above), the spacing of filings prepared out of contact with air was 5.0761 $\pm$ 0.0002 kX, while an unexposed solid fragment in the same boat corresponded to 5.0744 $\pm$ 0.0002 kX. Initial contamination by gas evolved from the walls of the boat during the early stages of annealing is therefore very probable. The presence of faint thorium nitride lines in the diffraction patterns of filings annealed for 25 hours at 970° C again suggests that nitrogen is responsible for the contamination, and is able to reach the specimens in spite of the use of closed tantalum boats.

4.4. Contamination of filings in open boats by the furnace atmosphere

The lattice spacings obtained after annealing in open boats (fig. 2) cover a wide range, and may be both smaller and larger than those of thorium saturated with nitrogen. The smaller values may be explained in terms of the observation referred to above that slow heating, corresponding to very good vacuum conditions throughout the heat-treatment, leads to decreased lattice spacings. Thus filings insufficiently contaminated with nitrogen for saturation may lose some of the adsorbed proportion of this contaminant during the early stages of heat-treatment under good vacuum conditions and the spacing will correspondingly fall. By contrast, the use of closed boats will tend to prevent such loss, maintaining saturation or near-saturation conditions. The larger values observed may be due to the action of an additional contaminant in the furnace atmosphere, access of which to the specimen is completely prevented by the use of a closed boat. In view of the unsatisfactory nature of the open boat technique, the problem was not further investigated.

5. Conclusions

From the work described, it is clear that the annealing of filings of thorium for the relief of stress demands the most stringent attention to vacuum conditions, and that the use of open boats of tantalum foil is prohibited as it leads to inconsistent results. The use of closed, doubly closed, or sealed boats is essential. Even under good conditions, contamination may result from:

(i) Filing in air, which results in the solid solution of nitrogen. This source of contamination may be eliminated by filing under carbon tetrachloride.

(ii) Surface adsorption of gas by exposure to air prior to heat-treatment, which must be avoided.

(iii) Extended heat-treatment at high temperatures. A closed container of tantalum foil is satisfactory for the prevention of this stage of contamination, except for that caused by reaction with nitrogen, which can, however, be minimised by the use of thoroughly outgassed and highly evacuated glass or silica capsules.

(iv) The initial heating of the filings to the annealing temperature, which may be minimised by reducing the rate of heating, and saturating the walls of the boats, after outgassing, with argon.

Using the precautions referred to, it is estimated that the error introduced into the lattice spacing by the annealing of thorium filings should not exceed 0.0002 kX. It will be noted that the wide range of lattice spacings

observed in the present work (5.0740 to 5.0890 kX), characteristic of the preparation and heat-treatment of filings under a variety of conditions, some of which allowed controlled contamination, corresponds with the range of values quoted in table 1. This suggests that the values already in the literature are seriously affected by uncontrolled contamination, and the evidence of the present work is that the lowest values (5.0740 to 5.0741 kX) are to be preferred for iodide thorium.

Appendix

The lattice spacings of arc-melted iodide thorium, electrolytic thorium, and sintered-bar thorium

Because of the possibility of introducing contaminants during arc-melting of iodide thorium or in the preparation of alloys by arc-melting, the lattice spacings of filings of arc-melted material were determined, after preparation under carbon tetrachloride and annealing with all the precautions necessary to avoid contamination at this stage. The value obtained was 5.0740 ± 0.0002 kX, which confirmed that the lattice spacing was unaffected by the melting operation.

The lattice spacings of uncontaminated electrolytic and sintered-bar thorium were also determined; the values obtained were respectively 5.0778 ± 0.0002 kX and 5.0777 ± 0.0002 kX.

References

1) H. Bohlin, Ann. Phys. Lpz. **61** (1920) 421
2) A. W. Hull, Phys. Rev. **18** (1921) 88
3) W. G. Burgers and J. A. M. van Liempt, Z. Anorg. Chem. **193** (1930) 512
4) J. G. Thompson, Metals and Alloys **4** (1933) 114
5) M. C. Neuberger, Z. Krist. **93** (1936) 1
6) R. W. M. D'Eye, AERE (Harwell) Report C/R 425 (1949)
7) N. C. Baenziger, quoted by H. A. Wilhelm and P. Chiotti, Trans. Amer. Soc. Metals. **42** (1950) 1295
8) B. S. Borie, quoted by H. A. Wilhelm and P. Chiotti, loc. cit.
9) H. A. Wilhelm, O. N. Carlsen and H. E. Lunt, USAEC Report AECD 3603 (1953)
10) P. Chiotti, J. Electrochem. Soc. **101** (1954) 567
11) W. J. James and M. E. Straumanis, Acta Cryst. **9** (1956) 376
12) E. A. Gulbransen and K. F. Andrew, Trans. AIME **188** (1957) 566
13) J. P. Nelson and D. P. Riley, Proc. Phys. Soc. (London) **57** (1945) 160
14) A. J. C. Wilson, Proc. Camb. Phil. Soc. **36** (1940) 485
15) R. E. Rundle, Acta Cryst. **1** (1948) 180
16) P. Chiotti, J. Amer. Ceram. Soc. **35** (1952) 123
17) F. A. Rough and A. A. Bauer, USAEC Report BMI-1300 (1958)
18) M. W. Mallet and I. Campbell, J. Amer. Chem. Soc. **73** (1951) 4850

JOURNAL OF NUCLEAR MATERIALS - 3 (1959) 289–299 - NORTH-HOLLAND PUBLISHING CO., AMSTERDAM

THE ALLOY SYSTEM URANIUM-TITANIUM-ZIRCONIUM

B. W. HOWLETT

Research Laboratory, Associated Electrical Industries Limited, Aldermaston Court, Aldermaston, Berks., UK †

Received 19 May 1959

The uranium-titanium-zirconium system in the composition range to 40 atomic per cent titanium, 70 atomic per cent zirconium is reported in nine isothermal sections between 575° and 1000° C. The principal features of the alloys are discussed.

Le système uranium-titane-zirconium dans le domaine de composition allant jusqu'à 40 at % de titane et 70 at % de zirconium est représenté dans neuf sections isothermes entre 575° C et 1000° C. Les principales caractéristiques des alliages sont discutées.

Das System Uran-Titan-Zirkon im Bereich 0 bis 40 At % und 0 bis 70 At % Zirkon wird in neun isothermen Querschnitten zwischen 575° C und 1000° C dargestellt. Die hauptsächlichen Merkmale der Legierungen werden diskutiert.

1. Introduction

The only previous work reported on this ternary system was carried out by Saller, Rough, Bauer and Doig [1]) who examined a vertical section between the compounds of the binary systems. Probably due to insufficient annealing their results differ considerably in detail from the present work although there is agreement on broad outlines. They found complete solid solubility at 900° C between the γ phase of the uranium-titanium and uranium-zirconium systems, a maximum solubility of 1.4 at % zirconium in U_2Ti at 575° C and a maximum solubility of 0.7 at % titanium in the ε phase of the uranium-zirconium system at 550° C. The γ phase finally disappeared by eutectoidal decomposition to U_2Ti and the ε phase at 575° C.

The present investigation has been limited to the uranium rich corner of the ternary diagram extending up to 70 at % zirconium and 40 at % titanium.

2. Materials Used and Experimental Methods

The uranium used in the investigation was provided by A. E. R. E. Harwell. Most of the work was carried out on uranium bar material which after arc melting had a total impurity content of 400–450 ppm of which 200–250 ppm was carbon. Some of the work at the high uranium end was carried out with material of higher purity containing considerably less carbon. Titanium produced in this Laboratory by the iodide process was used throughout the investigation; typical material had a hardness of 60–70 V.P.N. and a purity of 99.5 at %. The zirconium was produced by the Metropolitan-Vickers Electrical Company using the iodide process. This material contained about 3 at % hafnium. A small quantity of "hafnium-free" zirconium became available from the same source during the course of the investigation. This material had a hardness of 83 V.P.N. and was used for alloys close to the $\gamma_1+\gamma_2$ miscibility gap.

The alloys were prepared by arc-melting on a water cooled copper hearth under a gettered argon atmosphere. To produce homogeneous alloys, the beads were turned over and remelted several times and were kept to less than 20 g in weight. Weight losses on alloying were usually

† Present address: Department of Metallurgy, Massachusetts Institute of Technology, Cambridge 39, Massachusetts, USA.

quite small (<0.25 %) and in the bulk of the work synthesised compositions have been used. Any alloys showing a higher weight loss were rejected.

For annealing, specimens were loosely wrapped in molybdenum or tantalum foil and sealed in silica capsules under a vacuum of better than 10^{-4} mm. Tantalum was used for temperatures greater than 800° C and molybdenum at lower temperatures. There was no evidence of any molybdenum or tantalum pickup. Annealing was carried out in horizontal tubular furnaces which contained metal blocks for reducing temperature gradients. At 850° C and below, furnaces were controlled by Sunvic RT2 proportional controllers through platinum resistance thermometers which gave a control of ± 1° C. Above 850° C, Electroflo controllers were used which gave a control of ± 5° C. Quenching was effected by breaking the silica capsules under water immediately on removal from the furnace.

Specimens for metallographic examination were prepared in the usual manner by grinding on successively finer grades of silicon carbide under water and were polished on 4 micron and 1 micron diamond dust.

The principal etching reagent used in the work consisted of:

20 ccs	30 % hydrogen peroxide
10 ccs	0.880 S.G. ammonium hydroxide
1 g	ammonium persulphate

The ammonium persulphate must be dissolved in the hydrogen peroxide before the ammonium hydroxide is added. Alloys were etched for 20–40 seconds. This stained U_2Ti bright blue, α and decomposed β uranium light brown, decomposed γ uranium light yellow and retained γ uranium and ε were unattacked.

In addition electrolytic etching of mechanically polished specimens was carried out in 20 % potassium hydroxide at 30 volts. This produced coloured epitaxial films and was of considerable value in differentiating between γ uranium and ε.

Quantitative metallography using a "Swift Automatic Point Counter" was carried out on several series of alloys to check that the compositions of phases existing in two and three phase fields were in agreement with the positions of the boundaries as determined by ordinary metallography. Good agreement was obtained in all cases.

Whenever possible, confirmation of the metallographic work was obtained by X-ray diffraction using powder techniques and also glancing-angle techniques on metallographic specimens. Powder specimens were heat treated in a similar manner to the block specimens. The wavelength assumed for $CuK\alpha_1$ was 1.540 51 Å and all lattice parameters are therefore quoted n absolute Ångstroms.

3. The Binary Systems

3.1. The binary system uranium-titanium

This binary system has been studied in detail by many investigators [2, 3, 4]. In the present work the diagram due to Knapton [2] shown in fig. 1 has been used. In this the liquidus and

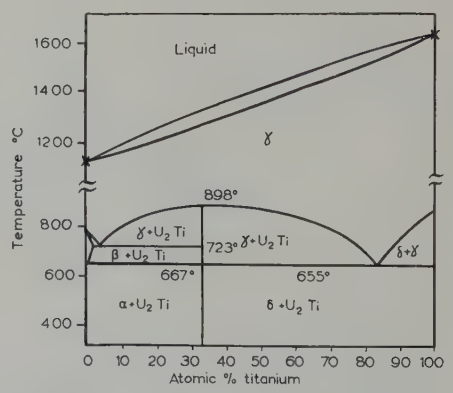

Fig. 1. Uranium-titanium system.

solidus show a smooth increase from the melting point of uranium to that of titanium. A continuous series of solid solutions is formed between the γ modification of uranium and the β modification of titanium. The addition of titanium lowers the $\beta \rightarrow \gamma$ transformation from 771° C in pure uranium to a eutectoid with the intermediate phase U_2Ti at 723° C and 4 at % titanium. β uranium dissolves about 1.5 at % titanium at the eutectoid temperature.

A hexagonal phase, U_2Ti having the C32 structure separates at 898° C from the γ solid solution. It extends over a small homogeneity range of about 0.5 at %.

A eutectoid is formed between U_2Ti and α-titanium at 655° C and 83 at % titanium. The solubility of uranium in α-titanium at the eutectoid temperature is about 0.8 at %.

3.2. The binary system uranium-zirconium

Previous work by Summers–Smith [5]) in this Laboratory led to the publication of a phase diagram. After the completion of this work, American investigators reported phase diagrams which differed in several respects from that of Summers–Smith. The chief discrepancy was the presence of an ε, UZr_2 phase separating at about 70 at % zirconium and 600° C from the γ solid solution. A further feature of difference is the presence in Summers–Smith's diagram of an extensive $(\beta+\gamma_2)$ field compared with the restricted field with peritectoid α-uranium formation favoured by American [6]) and French [7]) workers. These discrepancies led to a re-investigation of this portion of the diagram by Knapton [8]) of this Laboratory and the diagram which is used in the present work is that due to Summers–Smith with the modifications introduced by Knapton and is reproduced in fig. 2.

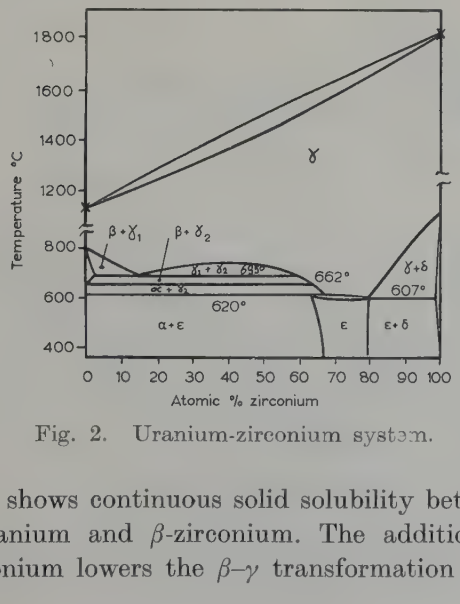

Fig. 2. Uranium-zirconium system.

It shows continuous solid solubility between γ-uranium and β-zirconium. The addition of zirconium lowers the β–γ transformation from 771° C in pure uranium to a monotectoid at 693° C and 14.5 at % zirconium. β-uranium dissolves about 1.5 at % zirconium at the monotectoid temperature. At this temperature a $\gamma_1+\gamma_2$ miscibility gap extends from 14.5 at % to 57 at % zirconium. The maximum in the gap occurs at 740° C and between 34 at % and 40 at % zirconium. The compound ε forms peritectoidally at 620° C and 63 at % zirconium. It forms a eutectoid with α-zirconium at 607° C and 79 at % zirconium. At this temperature the solubility of uranium in α-zirconium is about 1.0 at %.

3.3. The binary system titanium-zirconium

The metals titanium and zirconium were found by Fast [9]) to be completely soluble in both the α and β modifications and the constitution diagram is, therefore, a very simple one. There is a minimum in the solidus and liquidus and in the transformation range between the α and β forms. In the former it occurs at 33 at % zirconium and 1560° C and in the latter at 50 at % zirconium and 540° C.

3.4. Experimental results

Nine isothermal sections through the solid ternary equilibrium diagram have been determined and are shown in figs. 3–11. These sections are based on many more specimens than are represented in the isothermal diagrams which contain only critical alloy compositions. Long annealing times were necessary on multiphase alloys before precipitate particles were coarse enough to be identified metallographically. The minimum annealing times used were:

Temperature (° C)	850	800	750	700	662	650	625	575
Annealing time (weeks)	1	2	3	4	6	8	12	12

3.5. The 1000° C isothermal section

After homogenisation for four weeks at 1000° C all alloys were examined metallographically and found to be consistent with being quenched from a single phase field. This confirmed complete solid solubility over the composition range examined.

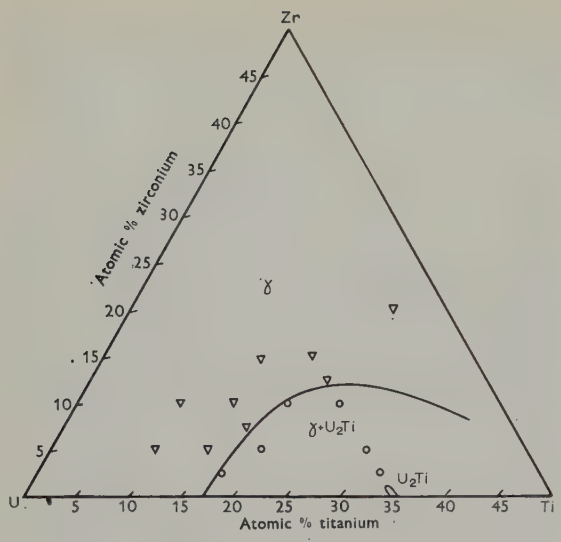

Fig. 3. Uranium-titanium-zirconium 850° C isothermal section.

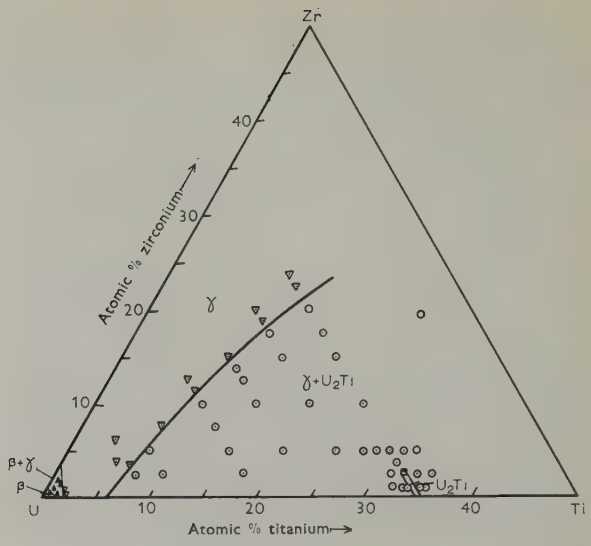

Fig. 5. Uranium-titanium-zirconium 750° C isothermal section.

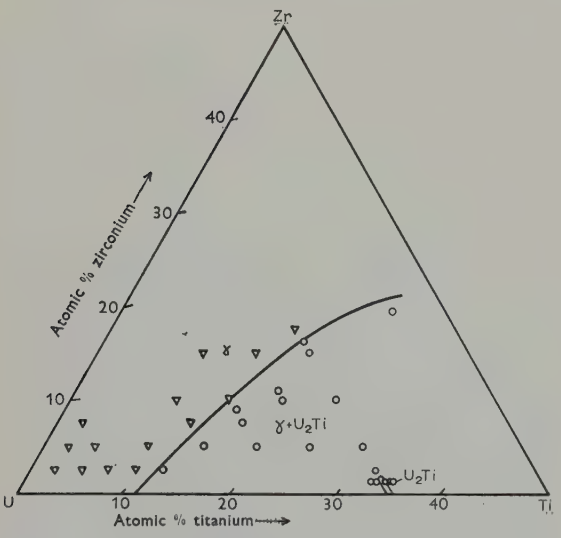

Fig. 4. Uranium-titanium-zirconium 800° C isothermal section.

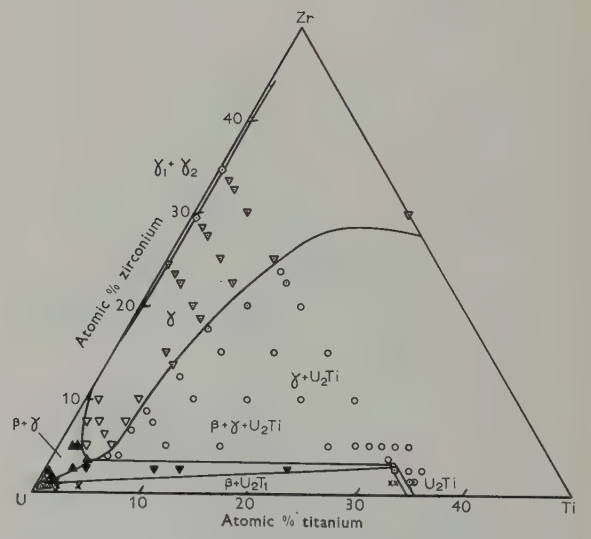

Fig. 6. Uranium-titanium-zirconium 700° C isothermal section.

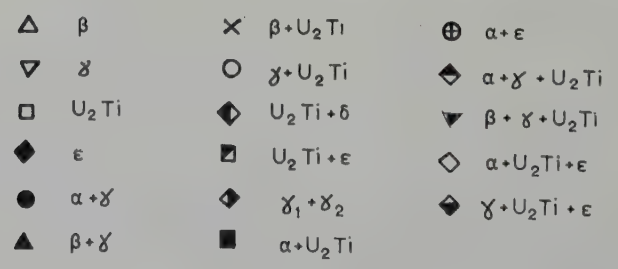

Key to figures 3–11.

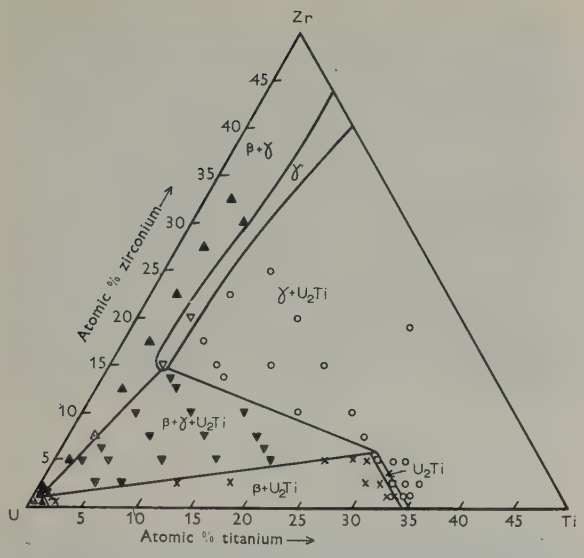

Fig. 7. Uranium-titanium-zirconium 662° C isothermal section.

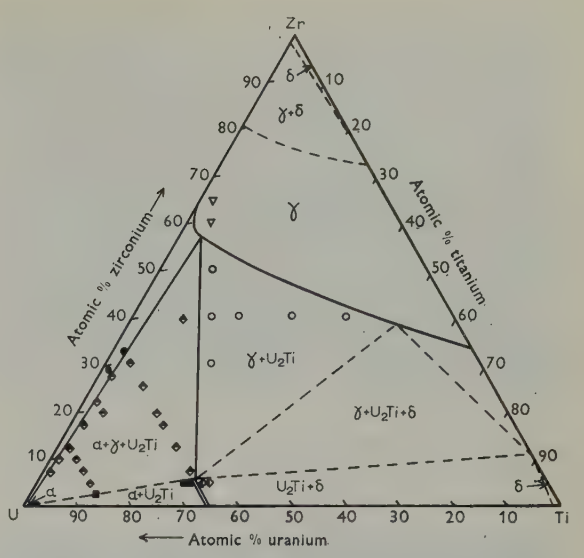

Fig. 9. Uranium-titanium-zirconium 625° C isothermal section.

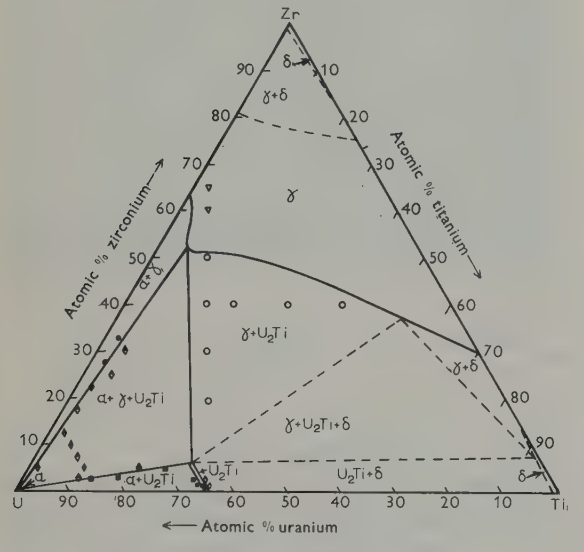

Fig. 8. 650° C isothermal section.

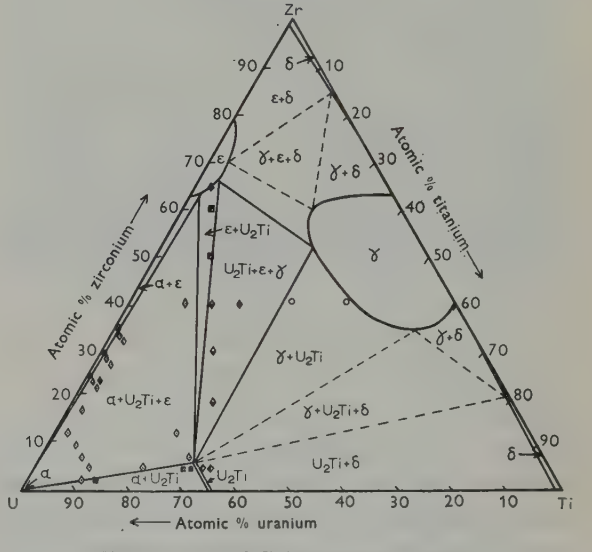

Fig. 10. 575° C isothermal section.

3.6. The 850° C isothermal section (fig. 3)

At 850° C the hexagonal U_2Ti phase is present in the uranium-titanium binary wall and has dissolved approximately 1 % zirconium by direct replacement of titanium. This is accompanied by a $(\gamma + U_2Ti)$ phase field extending to a maximum of 15 at % zirconium.

3.7. The 800° C isothermal section (fig. 4)

At 800° C the U_2Ti compound has dissolved about 2 at % zirconium and is accompanied by a corresponding extension of the $(\gamma + U_2Ti)$ phase field.

3.8. The 750° C isothermal section (fig. 5)

In pure uranium the β–γ transition occurs at 769° C so that at 750° C in both the uranium-titanium and uranium-zirconium binary systems there are small β and $(\beta+\gamma)$ phase fields. In the ternary section the $\beta/(\beta+\gamma)$ and $(\beta+\gamma)/\gamma$ boundaries can be represented as straight lines joining the respective binary limits. At this

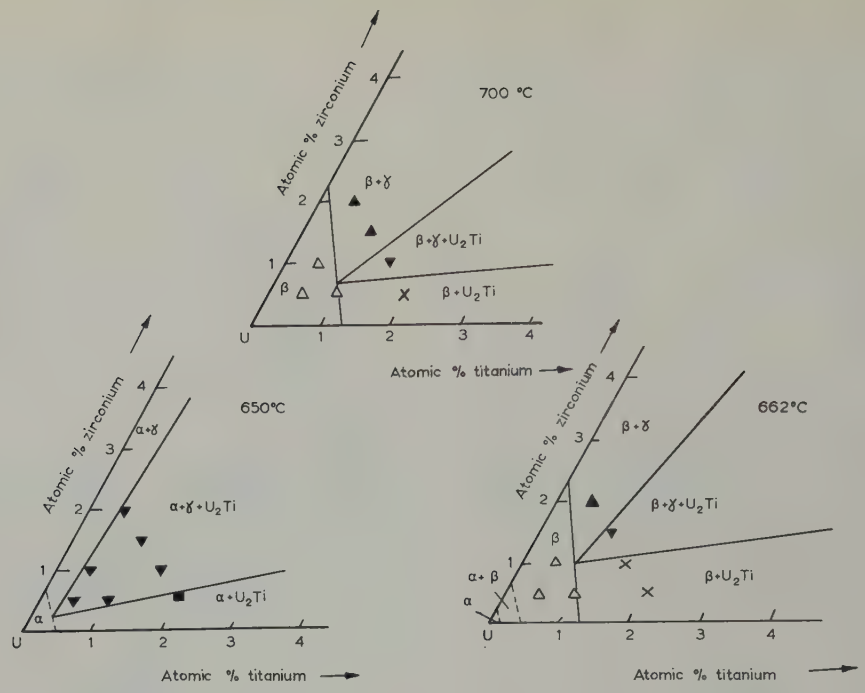

Fig. 11. Uranium-titanium-zirconium isothermal sections.

temperature U_2Ti dissolves a maximum of 3 at % zirconium and the associated ($\gamma + U_2Ti$) field projects to a maximum of about 25 at % zirconium.

3.9. The 700° C isothermal section (fig. 6)

At 723° C and 4 at % titanium in the uranium-titanium binary system, γ decomposes eutectoidally into ($\beta + U_2Ti$), whereas in the uranium-zirconium system γ decomposes by a monotectoid reaction at 693° C. In the ternary system at 700° C the γ phase field has consequently broken away from the uranium-titanium binary wall resulting in the formation of a narrow ($\beta + \gamma + U_2Ti$) three phase field. At this temperature a miscibility gap extends from 18.5 to 55.5 at % zirconium in the uranium-zirconium system in which two body-centred-cubic phases, γ_1 and γ_2, with different compositions and lattice parameters coexist. The addition of only a small percentage (0.6) of titanium stabilises the single γ phase.

In order to check that the hafnium present in the zirconium was not having any effect on the quantity of titanium necessary to stabilise the single γ phase, several alloys were made up in the field using hafnium-free zirconium and high purity uranium. No significant differences were observed.

The microstructures of alloys quenched from the γ phase at this temperature varied considerably. Banded structures were observed on quenching alloys from 750° C and 700° C in the composition range 5–10 at % titanium, 0–15 at % zirconium, 85–90 at % uranium. Fig. 12 shows a typical banded microstructure. In the particular alloys shown, the banded structure was only visible round the edges of the specimen. The centre of the alloy showed the type of decomposition structure illustrated in fig. 13. This is similar to structures observed in the uranium-niobium system [10]). For uranium contents greater than 90 at % the martensitic type of decomposition structure was observed as shown in figs. 14 and 15. In alloys containing between 75 % and 50 % uranium, no decomposition structures were visible under the microscope although X-ray glancing angle photo-

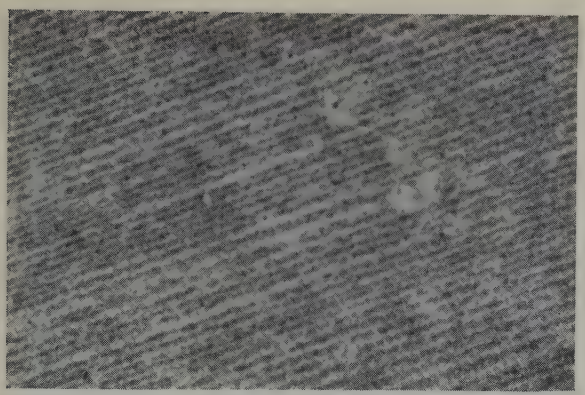

Fig. 12. 80 at % U, 5 at % Ti, 15 at % Zr. Annealed 700° C. Water quenched. Etched in hydrogen peroxide. Banded structure in transformed γ. × 825.

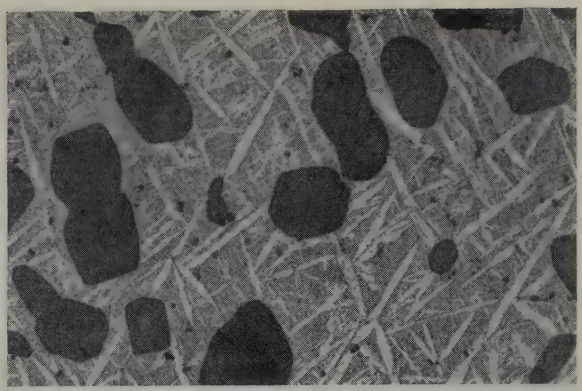

Fig. 14. 95 at % U, 2.5 at % Ti, 2.5 at % Zr. Annealed 700° C. Water quenched. Electroetched in potassium hydroxide. β (dark grey) + transformed γ. × 200.

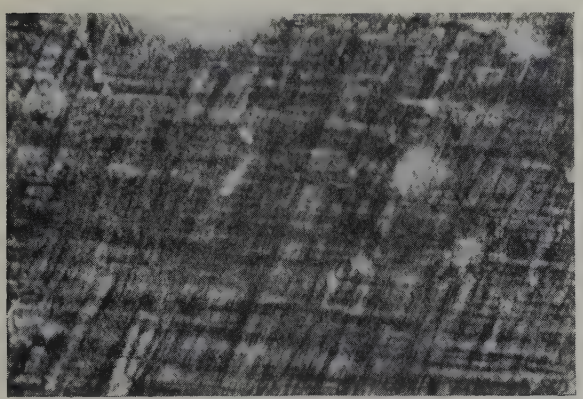

Fig. 13. 80 at % U, 5 at % Ti, 15 at % Zr. Annealed 700° C. Water quenched. Electropolished chromic acid/nitric acid. Transformed γ. × 300.

Fig. 15. 91 at % U, 5 at % Ti, 4 at % Zr. Annealed 750° C. Water quenched. Etched in hydrogen peroxide. Martensitic transformed γ. × 200.

graphs gave patterns characteristic of the distorted α-uranium structure produced by decomposition of γ-uranium during quenching. On quenching compositions containing less than 50 at % uranium, it was possible to stabilise γ to room temperature.

3.10. The 662° C isothermal section (fig. 7)

In alloys made from high purity uranium in the high uranium corner of the section at 662° C, the β phase is still present and the β solubilities are only slightly less than at 700° C. This corner of the diagram is shown on an enlarged scale in fig. 11 together with results on the same alloys at 700° C and 650° C. As the α–β allotropic change in pure uranium takes place at 667° C, it implies that the β phase is decomposing eutectoidally into ($\alpha + U_2Ti$) on the titanium rich side of the section and into $\alpha+\gamma$ on the zirconium rich side of the section. This confirms the eutectoidal decomposition of α-uranium found by Knapton and Summers-Smith in the uranium-titanium and uranium-zirconium binary systems.

There is a marked change in the solubility of zirconium in U_2Ti between 700° C and 662° C. It increases from 3 at % at 700° C to 6 at % at 662° C. Solution always occurs by direct replacement of titanium atoms by zirconium atoms such that the uranium content of the U_2Ti phase remains constant.

At 662° C the γ phase has disappeared from

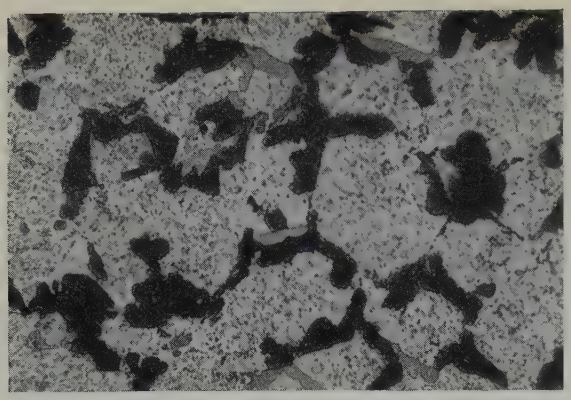

Fig. 16. 80 at % U, 10 at % Ti, 10 at % Zr. Annealed 662° C. Water quenched. Etched in hydrogen peroxide. β (black) + U_2Ti (dark grey) + γ (light grey). × 400.

the high uranium alloys in the binary systems, but it is still present in the ternary as a narrow tongue approximately parallel to the uranium-zirconium binary wall. The accompanying ($\beta+\gamma+U_2Ti$) field, of which a typical microstructure is shown in fig. 16, has enlarged considerably. The ($\gamma_1+\gamma_2$) phase field has been eliminated.

3.11. The 650° C isothermal section (fig. 8)

Between 662° C and 650° C a marked change in appearance occurs in the isothermal sections. At 650° C the β phase has completely disappeared, and the tongue of γ has retreated to the titanium-zirconium side of the diagram. Quantitative metallography has confirmed the composition of the γ phase existing in the ($\alpha+\gamma+U_2Ti$) three phase field.

3.12. The 625° C isothermal section (fig. 9)

There is little difference in appearance between the 650° C and 625° C isothermal sections. The γ field has become slightly more restricted and the vestigial remnant of the γ tongue is less obvious, but there is no change in the phases existing in equilibrium.

3.13. The 575° C isothermal section (fig. 10)

The γ phase in the uranium-zirconium system disappears at 620–600° C with the formation of the ε phase, whose composition limits are 63–80 at % zirconium. This phase enters into simple equilibrium with U_2Ti. There is a consequent formation of large ($\alpha+U_2Ti+\varepsilon$) and ($U_2Ti+\varepsilon+\gamma$) three phase fields. The ε phase has only a small solubility for titanium, about 4 at % at 575° C, whilst the solubility of zirconium in U_2Ti remains substantially constant at 6 at % between 662° C and 575° C.

4. Lattice Parameters of U_2Ti

The variation of the lattice parameters of U_2Ti with composition was investigated using annealed and quenched powder or filings in order to confirm the metallographic evidence for the high solubility of zirconium in the phase U_2Ti. The crushed powder obtained from annealed metallographic specimens was placed in open ended alumina quills, sealed in evacuated silica capsules, and annealed at the requisite temperatures for 24 hours. The results obtained are reproduced in table 1 and fig. 17

Table 1

Composition in atomic per cent (all contain 65 at % uranium)	Temperature (° C)	a parameter (Å)	c parameter (Å)	c/a
2.5 % Zr	700	4.8327 ± 0.0003	2.8494 ± 0.0005	0.5896
2.5 % Zr	662	4.8328 ± 0.0003	2.8492 ± 0.0005	0.5896
3.75 % Zr	750	4.8337 ± 0.0003	2.8498 ± 0.0005	0.5896
3.75 % Zr	700	4.8346 ± 0.0003	2.8505 ± 0.0005	0.5896
5.0 % Zr	700	4.8351 ± 0.0003	2.8506 ± 0.0005	0.5896
5.0 % Zr	662	4.8369 ± 0.0003	2.8516 ± 0.0005	0.5896
7.5 % Zr	800	4.8313 ± 0.0003	2.8485 ± 0.0005	0.5896
7.5 % Zr	750	4.8333 ± 0.0003	2.8497 ± 0.0005	0.5896
7.5 % Zr	662	4.8386 ± 0.0003	2.8526 ± 0.0005	0.5896

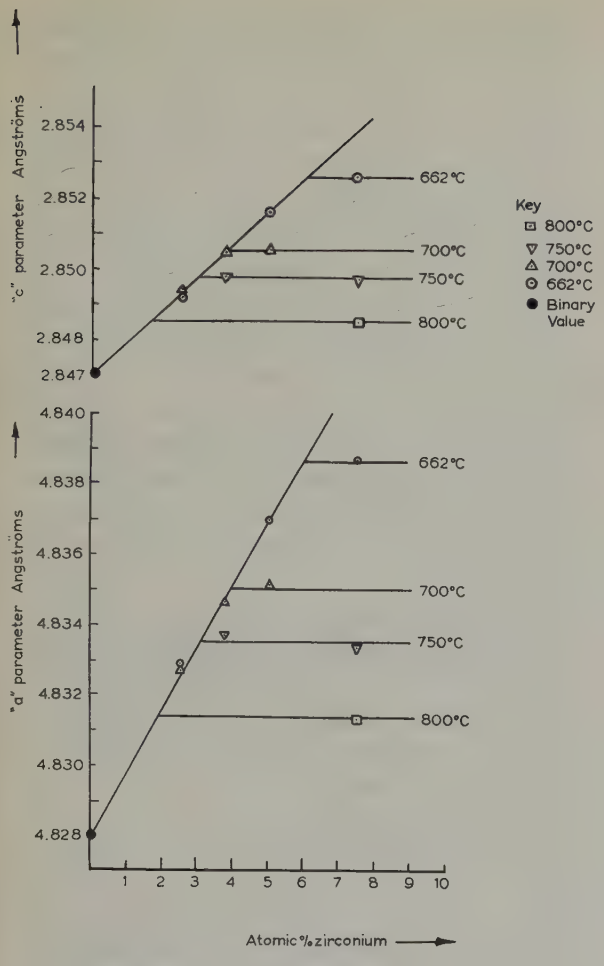

Fig. 17. Lattice parameters of U_2Ti.

and show that the introduction of zirconium atoms in place of titanium atoms causes a general dilation of the structure that maintains c/a constant. The solubilities of zirconium in the U_2Ti structures at various temperatures as given by the X-ray results are, 800° C, 2.0 at % zirconium; 750° C, 3.0 at % zirconium; 700° C, 4.0 at % zirconium; 662° C, 6 at % zirconium. These values are in good agreement with the metallographically determined solubilities.

5. Conclusions

The main features of the constitution of uranium-titanium-zirconium alloys are:

1. The addition of <1 at % of titanium causes the disappearance of the $(\gamma_1+\gamma_2)$ miscibility gap and the stabilisation of a single γ phase.

2. Although the U_2Ti compound has a narrow homogeneity range in the binary system, it dissolves up to 6 at % zirconium by direct replacement of titanium.

3. The ε compound of the uranium-zirconium system will only dissolve about 4 at % titanium at 575° C although it has a wide homogeneity range in the binary. At the temperatures at which the ε phase is present, it is in direct equilibrium with the compound U_2Ti and an extensive $(\varepsilon+U_2Ti)$ field is formed.

4. No ternary compounds are present in the system.

6. Discussion

The relatively high solubility (6 at %) of zirconium in the U_2Ti compound is interesting in view of the low homogeneity range (≈ 0.5 at %) of this phase in the uranium-titanium binary system. The zirconium dissolves by direct replacement of titanium atoms, maintaining the uranium content constant. The C32 structure of U_2Ti is of the layer type with alternate planes of titanium and uranium atoms normal to the c axis [11]). Each titanium atom is surrounded by twelve uranium atoms six in the layer above and six below at a distance of 3.14 Å and by two titanium atoms at 2.847 Å. Each uranium atom is surrounded in the uranium plane by an equilateral triangle of uranium atoms at 2.787 Å, and by two uranium atoms, one in the plane above and one below at 2.847 Å. When the axial ratio is <0.87, this structure possesses the geometric property that if the uranium and titanium atoms behave as solid spheres, then the uranium and titanium atoms are not in contact with one another [12]). With the c/a ratio characteristic of U_2Ti ($c/a=0.5896$), the uranium atoms form hexagonal networks in the (001) plane of the type shown in fig. 18 and the titanium atoms form interpenetrating chains parallel to the c axis. A section through the structure on the (210) plane is shown in fig. 19. Here it can be seen that apparently the uranium and titanium atoms do not touch one another but that it is the distance between the titanium atoms which

determines the c parameter and the spacing of the uranium network which determines the a parameter. Hence on replacing some of the titanium atoms by zirconium atoms it would be expected that the c parameter would be increased due to the greater size of the zirconium atom (11.6 % larger than the titanium atom) and the a parameter to be relatively little affected. However, the addition of 6 at % of zirconium to the structure causes the a parameter to expand from 4.828 Å to 4.838 Å, the c parameter to expand from 2.847 Å to 2.852 Å and maintains the c/a ratio constant at 0.5896 Å. Therefore it appears that the factor which stabilises the structure is the lattice of uranium atoms and the introduction of some zirconium atoms in place of titanium causes a uniform dilation of the structure and maintains the c/a ratio constant. The relatively high solubility of zirconium in the structure must be attributed to the similar electronic nature of titanium and zirconium which allows the electronic structure of the U_2Ti phase to be preserved.

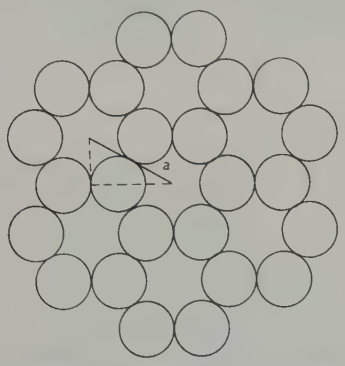

Fig. 18. Uranium network on (001) plane in U_2Ti.

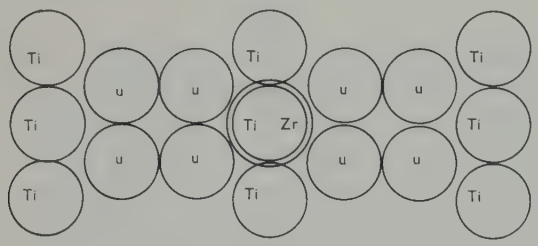

Fig. 19. Section through (210) plane of U_2Ti.

In the uranium-zirconium system, the $(\gamma_1+\gamma_2)$ miscibility gap extends from 14 to 57 at % zirconium over a temperature range of 693 to 735° C. It disappears rapidly on the addition of titanium so that at 700° C the gap only projects into the ternary to the extent of between 0.5 and 1.0 % titanium. The existence of miscibility gaps can be attributed to a high strain energy in the γ solid solution and this aspect of their formation will be considered in detail in a later publication. In the ternary system the smaller titanium atom (2.94 Å) reduces the strain energy produced in the γ solid solution by alloying zirconium (3.20 Å) with uranium (3.10 Å) and hence causes the disappearance of the gap.

The work on the ternary system has confirmed certain features of the binary uranium-titanium and uranium-zirconium diagrams which are still controversial.

Thus in the uranium-titanium system, the eutectoidal decomposition of β uranium and the narrow homogeneity range of the phase U_2Ti has been found in agreement with the work of Knapton [2]) whereas Udy and Boulger [3]) found peritectoidal decomposition of β uranium and a wide homogeneity range for U_2Ti.

In the uranium-zirconium system β uranium is again found to decompose eutectoidally as against the peritectoidal formation favoured by the American [6]) and French [7]) workers. This is in agreement with the wide $\beta+\gamma_2$ field found by Summers–Smith [5]) and confirmed by Knapton [8]).

As in the study of the uranium-titanium system previously carried out in this Laboratory [2]), alloys at the high uranium corner of the ternary system have been made with the two different grades of uranium described on page 289. These showed that titanium and zirconium differ in their ability to reduce UC, and account for the failure by Summers–Smith [5]) to detect any significant effect of carbon during his study of the uranium-zirconium binary system.

Although there is some doubt about the values of the heats of formation of the various carbides, figures given by Quill [13]) are:

	$\triangle H_{298}$ (kcals/g mol)
UC	— 40.0
TiC	— 57.3
ZrC	— 35.5

which are in agreement with the experimental observations.

Acknowledgements

The author wishes to express his thanks to the Director of the Atomic Energy Research Establishment, Harwell, and to Dr. T. E. Allibone, F.R.S., Director of the Associated Electrical Industries Research Laboratory, for premission to publish this paper and to Dr. G. A. Geach and Dr. A. G. Knapton for their helpful encouragement.

Grateful acknowledgment is also made to Mr. P. S. Desbrow for his assistance with the experimental work.

References

[1]) H. A. Saller, F. A. Rough, A. A. Bauer and J. R. Doig, Battelle Memorial Institute (USA) Report, BMI-990 (1955)

[2]) A. G. Knapton, J. Inst. Metals **83** (1955) 497

[3]) M. C. Udy and F. W. Boulger, Trans. AIME **200** (1954) 207

[4]) D. J. Murphy, Trans. Amer. Soc. Metals **50** (1958) 884

[5]) D. Summers–Smith, J. Inst. Metals **83** (1954–5) 277

[6]) F. A. Rough, A. E. Austin, A. A. Bauer and J. R. Doig, Battelle Memorial Institute (USA) Report, BMI-1092 (1956)

[7]) J. Philibert, Y. Adda, G. Cabane, J. Bellot, P. Dosiere and J. M. Henry, Société Française de Metallurgie, Journées d'Automne (1957)

[8]) A. G. Knapton, Unpublished work (1957)

[9]) J. D. Fast, Rec. Trav. Chim. Pays-Bas **58** (1939) 973

[10]) P. C. L. Pfeil, J. D. Brown and G. K. Williamson, AERE Harwell (UK) Report M/R 2498 (1958)

[11]) A. G. Knapton, Acta Cryst. **7** (1954) 457

[12]) F. Laves, Theory of Alloy Phases, (Cleveland, American Society for Metals, 1956) p. 124

[13]) L. L. Quill, Chemistry and Metallurgy of Miscellaneous Materials (Thermodynamics), (New York, McGraw–Hill, 1950)

JOURNAL OF NUCLEAR MATERIALS - 3 (1959) 300–301 - NORTH-HOLLAND PUBLISHING CO., AMSTERDAM

LETTRE A L'EDITEUR

ETUDE DE L'AUTODIFFUSION DE L'URANIUM EN PHASE β

Y. ADDA, A. KIRIANENKO et C. MAIRY

Centre d'Etudes Nucléaires de Saclay, Gif-sur-Yvette (S & O), France.
Département de métallurgie et chimie appliquée

Reçu le 20 septembre 1959

L'autodiffusion de l'uranium en phase β a été étudiée en partant de couples constitués d'uranium naturel et d'uranium enrichi en U^{234}, en utilisant une technique déjà décrite dans un précédent travail concernant l'autodiffusion de l'uranium en phase γ [1]).

Rappelons que, dans cette technique, deux cylindres de 10 mm de diamètre et 10 mm de hauteur, l'un d'uranium naturel, l'autre d'uranium enrichi, sont polis électrolytiquement puis soudés bout à bout en les portant à 600° C pendant 1 heure sous vide, dans une presse à vis, suivant un procédé décrit antérieurement [2]). Les échantillons sont ensuite traités à la température de l'essai de diffusion, sous un vide inférieur à 5×10^{-6} mm de Hg et sans aucune pression extérieure.

L'application rigoureuse de cette technique s'est révélée difficile car les deux échantillons qui constituaient les couples se séparaient au cours du traitement de diffusion. Bien que nous n'ayons pu établir clairement la cause de ces ruptures, on a constaté que celles-ci étaient complètement supprimées si les couples étaient maintenus sous une légère compression au cours du traitement.

Ceci est réalisé en effectuant simultanément la soudure et le traitement de diffusion dans une presse à vis. Les pressions mises en jeu sont alors probablement suffisamment faibles pour ne pas influencer sensiblement l'autodiffusion de l'uranium. La température des traitements de diffusion est comprise entre 700 et 755° C; elle est maintenue constante à $\pm$ 1.5° C pendant toute leur durée qui est de 400 h environ.

Les échantillons sont ensuite sectionnés sur un tour parallèlement à l'interface de soudure. On détermine alors la concentration en U^{234} en fonction de la pénétration, en mesurant l'émission α de la face qui a subi le sectionnement (1). A partir des courbes concentration-pénétration

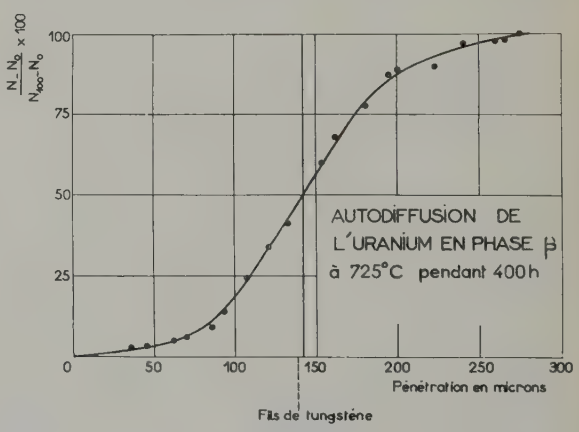

Fig. 1

que l'on peut alors tracer (fig. 1), on calcule les coefficients de diffusion. Ils sont portés dans le tableau ci-dessous:

t (°C)	700	725	740	755
Dcm^{2}sec^{-1}	5.1×10^{-12}	7.9×10^{-12}	1.1×10^{-11}	1.6×10^{-11}

Log D, variant linéairement en fonction de l'inverse de la température absolue ($1/T$), on

détermine l'énergie d'activation Q et le facteur de fréquence D_0 correspondant à l'autodiffusion de l'uranium en phase β.

$$Q = 42\,000 \text{ cal/at g}$$
$$D_0 = 1.35 \times 10^{-2} \text{ cm}^2 \text{ sec}^{-1}.$$

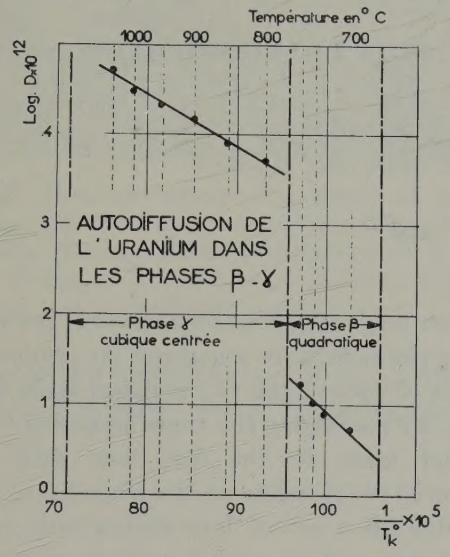

Fig. 2

Si, sur un graphique représentant les variations de log D en fonction de $(1/T)$, on porte les résultats correspondant à la diffusion dans les phases β et γ, on note une discontinuité très brutale à la transformation $\gamma \rightarrow \beta$ (fig. 2): l'énergie d'activation passe de 27 500 cal. (phase γ) à 42 000 cal. (phase β).

La phase β, de structure analogue à la phase σ [3]) des alliages ferreux, présente des liaisons covalentes. L'existence de ces liaisons conduirait à une augmentation de l'énergie de formation des lacunes qui expliquerait l'accroissement brutal de l'énergie d'activation d'autodiffusion observé.

Bibliographie

[1]) Y. Adda et A. Kirianenko, J. Nucl. Mat. **1**, No. 2 (1959) 120–126

[2]) Y. Adda, J. Philibert et H. Faraggi, Rev. Metall. **54** (1957) 597

[3]) W. Hume-Rothery et G. V. Raynor, The Structure of Metals and Alloys. Londres: Institute of Metals (1956)

JOURNAL OF NUCLEAR MATERIALS - 3 (1959) 302–303 - NORTH-HOLLAND PUBLISHING CO., AMSTERDAM

LETTER TO THE EDITOR

HABIT PLANES FOR U_4O_9 PRECIPITATION IN URANIUM DIOXIDE

R. H. TUXWORTH and W. EVANS

Atomic Energy of Canada Ltd., Chalk River, Ont., Canada

Received 3 August 1959

Metallographic examination of fused uranium oxide with a composition $UO_{2.08}$ showed the presence of a second phase which had precipitated in a Widmanstätten structure along four well defined planes in the matrix (fig. 1). An X-ray powder pattern showed that the matrix was UO_2 and the second phase was U_4O_9.

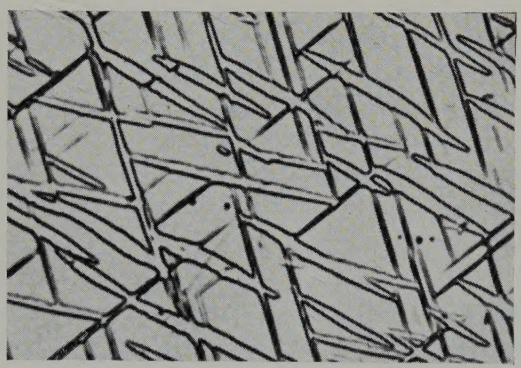

Fig. 1. Photomicrograph of a sample of fused uranium oxide having a composition of $UO_{2.08}$ showing Widmanstätten precipitation of U_4O_9 in a UO_2 matrix. Etched in a 9:1 mixture of 30 % hydrogen peroxide and concentrated sulphuric acid. × 1000

A coarse grained sample was mounted in bakelite and two surfaces at 90° to each other were metallographically polished and etched to reveal both the grain boundaries and the second phase. A typical grain at the intersection of the two polished surfaces was selected for micrographic and X-ray examination. The angles between the edge of intersection of the polished surfaces and each of the four traces of the second phase platelets were measured on photomicrographs of each of the two polished faces of this grain. By combining the angle measured for one platelet trace on the first face with those measured for platelets on the second face, there was defined a set of four planes only one of which was real. A similar procedure with the other three traces on the first face gave a total of four sets of four planes, the poles of which are shown on a stereographic projection, fig. 2.

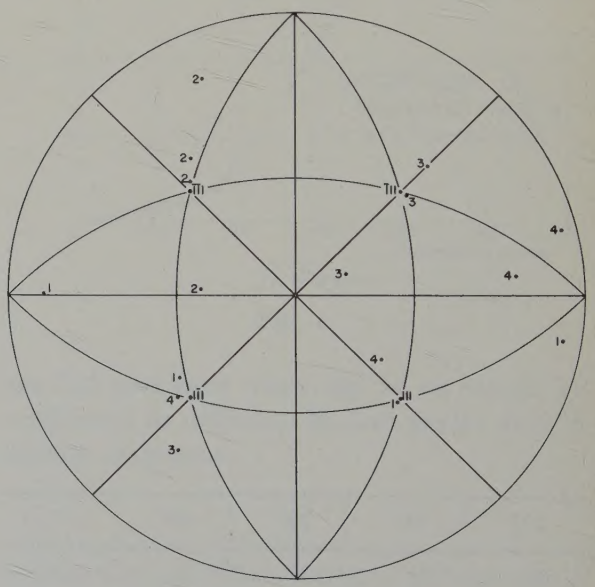

Fig. 2. Stereographic projection of the poles of the 16 possible U_4O_9 habit planes on the (001) standard projection of the UO_2 matrix.

Fig. 3. Photomicrograph of a sample of sintered uranium oxide having a composition of $UO_{2.11}$ showing the same Widmanstätten precipitation of U_4O_9 in UO_2. Etched in a 9:1 mixture of 30 % hydrogen peroxide and concentrated sulphuric acid. × 1000

The poles are numbered to indicate to which of the four sets they belong. The projection was constructed so that it was the standard (001) projection of the UO_2 matrix whose orientation was determined by the Laue back-reflection technique. It remained to choose the one plane of each set which was real. From fig. 2 the most logical choice for the habit planes of the U_4O_9 platelets in the UO_2 matrix was the form (111). The procedure was repeated for another grain with the same result.

The same Widmanstätten structure has also been observed (fig. 3) in a sintered uranium dioxide pellet that had been oxidized for 16 hours at 900° C in a static helium and air mixture to a composition of $UO_{2.11}$. After oxidation the sample had been annealed for four hours at 900° C in pure helium and slowly cooled to room temperature.

NEWS ITEM

La Société Française de Métallurgie organise, avec le concours du Commissariat à l'Energie Atomique, un

SYMPOSIUM INTERNATIONAL SUR LA METALLURGIE DU PLUTONIUM

qui se tiendra à Grenoble, du 19 au 22 Avril 1960.

Pour tous renseignements concernant l'inscription ou la présentation de mémoires à ce symposium, prière de s'adresser à:

Société Française de Métallurgie
25, *rue de Clichy*
Paris

ou à:

E. Grison
Centre d'Etudes Nucléaires de
Fontenay-aux-Roses (*Seine*)

4th INTERNATIONAL SYMPOSIUM ON THE REACTIVITY OF SOLIDS to be held in Amsterdam from May 30th to June 4th, 1960

During the third symposium on the reactivity of solids at Madrid, it was decided to hold the fourth symposium in 1960 in the Netherlands.

This symposium will be held in Amsterdam between 30th May and 4th June 1960. The "Koninklijke Nederlandse Chemische Vereniging" (Royal Netherlands Chemical Society) and the "Nederlandse Natuurkundige Vereniging" (Netherlands Physical Society) have placed the organization of this symposium in the hands of the "Nederlandse Keramische Vereniging" (Netherlands Ceramic Society), a division of these two societies.

The organizing committee consists of:

Prof. Dr. J. H. de Boer (president), Prof. Dr. M. J. Druyvesteyn, Ir A. A. H. Gaster, Prof. Dr. H. Gerding, Dr. E. W. Gorter, Dr. G. H. Jonker, Dr. O. Drexler, Dr. K. J. Keller, Prof. Dr. C. H. MacGillavry, Prof. Dr. G. W. Rathenau, Dr. G. C. A. Schuit, Dr. E. J. W. Verwey, P. Zwietering, Ir G. van Gijn (secretary).

The preceding three symposia, held at Paris in 1948, Gotheborg in 1952 and Madrid in 1956 have brought together chemists, physicists, mineralogists, ceramists and metallurgists from many countries to discuss scientific problems related to the reactivity of solids. The subject matter at Gotheborg and Madrid was divided among the following sections:

1. reactivity of solids, theory
2. minerals and mineral reactions
3. measuring methods
4. catalyst and catalysis
5. cement and cement minerals
6. ceramics and refractories
7. glass
8. metallurgy
9. powder metallurgy

The organizing committee wishes again to bring together the scientists who work on the subjects listed above. In view of the considerable advances made in the theoretical knowledge of reactions in the solid state, it is deemed advantageous, however, to adhere less rigidly to a distinction, according to technologies, as above. Instead, it is intended:

to stress the mechanism and kinetics of reactions in the solid state, such as:

chemical reactions between solids;
transformation of solids into solids of a different chemical composition;
precipitation in the solid phase;
recrystallization of solid chemical compounds;
etc.

to accentuate the factors influencing reactivity, and
to discuss the technical consequences of reactivity.

A division as to these various aspects is now under consideration.

The general trend of the symposium should be the study of mobility of ions, atoms and molecules in inorganic and organic solids and the changes which are caused by the movements of these constituents.

It is hoped that in this way again an intensive exchange of scientific ideas is obtained between workers in the different technological fields.
The secretariat is located at:

Technische Hogeschool Eindhoven,
Insulindelaan 2, Eindhoven

Prof. Dr. J. H. de Boer, *president*
Ir G. van Gijn, *secretary*